

# **Towards Synthetic Molecular Motors Interfaced by AFM**

Dissertation an der Fakultät für Physik  
der Ludwig-Maximilians-Universität  
München

Thorsten Hugel  
aus Konstanz

München, 4. Oktober 2002

**Cover:** *The image shows the setup for the single-molecule optomechanical cycle while a flash (1 ms) from our flashlamp (with the 420 nm filter) is traversing the object slide (the light is coupled into the slide from the upper left and can be seen to leave the slide on the lower right). [Image: Daniela Fischer]*

Erster Gutachter:

Prof. Dr. Hermann Gaub

Zweiter Gutachter:

Prof. Dr. Wolfgang Zinth

Tag der mündlichen Prüfung:

3. Februar 2003

*"What would be the utility of such machines? Who knows? ... I can't see exactly what would happen, but I can hardly doubt that when we have some control of the arrangement of things on a small scale we will get an enormously greater range of possible properties that substances can have, and of different things that we can do."*

Richard P. Feynman <sup>[1]</sup>

# Content

<b>1. Abstract.....</b>	<b>1</b>
<b>2. Introduction .....</b>	<b>3</b>
<b>3. Materials and Methods.....</b>	<b>5</b>
3.1. Polyvinylamine (PVA).....	5
3.2. Polypentapeptides .....	6
3.3. Polyazopeptides .....	8
3.4. Covalent Attachment Scheme .....	9
3.5. Coupling of Light into the AFM Experiment.....	9
<b>4. Theory .....</b>	<b>11</b>
4.1. Statistical Mechanics for Single Molecule Force Spectroscopy.....	11
4.1.1. Thermodynamic Boundary Conditions .....	11
4.1.2. Statistical Mechanics of Polymer Chains.....	11
4.1.3. The Freely-Jointed Chain (FJC) Model.....	12
4.1.4. The Worm-Like Chain (WLC) Model .....	14
4.2. Polyelectrolytes.....	18
4.2.1. Basic Parameters .....	18
4.2.2. OSF-Theory .....	19
4.2.3. Force Dependent Persistence Length.....	20
4.3. Force Induced Bond Rupture.....	21
4.3.1. Single Bond Exposed to an External Force.....	22
4.3.2. Multiple Bonds in Parallel.....	25
4.3.3. Multiple Bonds in Series .....	26
4.4. Polyelectrolyte Adsorption and Desorption .....	27
4.5. Transitions and Energy Conversion within Single Molecules .....	30
4.5.1. Hydration Water.....	31
4.5.2. Inverse Temperature Transition .....	32
4.5.3. Optically Induced Transitions.....	34
4.5.4. Optomechanical Transition in Azobenzene.....	36
<b>5. Polyelectrolytes .....</b>	<b>40</b>
5.1. Elasticity of Polyvinylamine .....	40
5.2. Desorption of Polyvinylamine from Solid Substrates.....	42
<b>6. Polypeptides: Inverse Temperature Transition .....</b>	<b>45</b>
<b>7. Polyazopeptides: Optomechanical Transition.....</b>	<b>50</b>
7.1. Covalent Attachment and Optical Coupling.....	50
7.2. Mechanical Characterization of the Polyazopeptide.....	53
7.3. Reversible Optical Switching at Low Force.....	54
7.4. Reversible Optical Switching at High Force .....	55
7.5. Optomechanical Cycle .....	56

<b>8. Discussion</b> .....	<b>58</b>
8.1. Polyelectrolytes.....	58
8.1.1. <i>Elasticity of Polyvinylamine</i> .....	58
8.1.2. <i>Desorption of Polyvinylamine from Solid Substrates</i> .....	60
8.2. Polypentapeptides: Inverse Temperature Transition .....	65
8.3. Polyazopeptides: Optomechanical Transition .....	67
8.3.1. <i>Length Change</i> .....	67
8.3.2. <i>Mechanical Stability</i> .....	68
8.3.3. <i>Optomechanical Cycles, Molecular Machines and Motors</i> .....	69
<b>9. Outlook</b> .....	<b>72</b>
<b>10. Apendices</b> .....	<b>74</b>
10.1. Details of the Coupling Chemistry.....	74
10.1.1. <i>Surface Preparations</i> .....	74
10.1.2. <i>Coupling of the Molecules</i> .....	75
10.2. Details of the Instrumental Setup.....	77
10.3. Data Aquisition .....	78
10.4. Calibration of Spring Constants.....	79
10.5. Abbreviations.....	80
<b>11. Literature</b> .....	<b>81</b>

# 1. Abstract

Molecular machines are at the ultimate limit of miniaturization. Living organisms provide a variety of examples for such molecular machines, but in order to utilize and to control them, they need to be interfaced with the macroscopic world. On the other hand, there are synthetic molecular machines. Some have been interfaced already [2] [3] [4] [5] but usually in high vacuum at very low temperatures, which is clearly not desirable for technical applications. In this thesis, AFM-based single molecule force spectroscopy (SMFS) was utilized to investigate the mechanical change in single synthetic molecules upon environmental changes (external stimuli) in liquid environment at room temperature. The molecules are either from theory or from bulk experiments supposed to be able to convert such an external stimulus into mechanical work, which is a prerequisite for molecular motors. Three different types of molecules and various external energy inputs were investigated which led to the realization of a light driven synthetic molecular machine:

- Polyelectrolytes should, by OSF-theory, change their persistence length (and therefore the overall length at a constant force) with the Debye screening length of the solvent (which is manipulated by the salt concentration). Therefore, the elasticity of the polyelectrolyte polyvinylamine, which could be covalently attached to the substrate and the AFM tip, was investigated in dependence on the salt concentration. It was found that the dependence of persistence length on salt concentration is much smaller than expected from OSF-theory, [6] which made this system less attractive for a molecular machine, but led to new theoretical insights. [7] [8]
- The adhesive properties of polyelectrolytes onto charged solid supports in aqueous solution are a subject of current research in industry and academia. A manipulation of polymer – substrate adhesion, e. g. at an AFM tip, could lead to a molecular 'grab and release' device. Therefore, the desorption force of single polyvinylamine-molecules from solid supports was investigated. Polyvinylamine was physisorbed to a glass substrate and covalently attached to the cantilever. Then, the charge-charge interaction was manipulated by variation in salt concentration and polymer charge. While this has not led to a single molecule device yet, it gave new insights into the desorption of polyelectrolytes from charged substrates. [6] [9] The measurements performed here revealed that van der Waals forces and other non-covalent chemical interactions such as hydrogen and coordinative bonds can by far outweigh the electrostatic coulomb force (namely at short distances), and are therefore a more promising candidate for the tuning of adhesion forces. [10]

- Elastin-based polypeptides have proven various kinds of energy conversion in cross-linked bulk samples. <sup>[11]</sup> The mechanism is based on a hydrophobic folding transition, which can be manipulated by temperature, salt, pH, electrochemistry, and/or by the composition (hydrophobicity) of the polymers. The difference between the folded and random state could be detected and investigated here at the level of individual polymer chains and characterized by the force-extension traces of the two polypeptides (GVGVP)<sub>nx251</sub> and (GVGIP)<sub>nx260</sub>. Because of their different hydrophobicity their folding temperatures lie above and below room temperature, respectively. With the polypeptide (GVGIP)<sub>nx260</sub> the folded state was investigated extensively. All observations support the conjecture, that intermolecular aggregation dominates intramolecular aggregation. This is further supported by the finding that neither a change in temperature nor the treatment with sodium dodecyl sulfate or guanidinium hydrochloride could force any of the two polypeptides from the folded to the random state or vice versa within an experiment, which in turn would be a prerequisite for a polypeptide based molecular motor.
- The most successful approach to building an AFM-interfaced molecular machine was in taking advantage of reversible configurational changes in azobenzene polymer molecules upon irradiation with light. Azobenzene can be driven from a shorter 'cis' to a longer 'trans' configuration by illumination with  $\lambda = 420$  nm light and vice versa by  $\lambda = 365$  nm. <sup>[12]</sup> In order to utilize azobenzene, a setup had to be developed and built, which allows for the coupling of light into the AFM experiment. Total internal reflection geometry was necessary to avoid any artifacts due to direct effects of the light on the cantilever. A polypeptide chain with multiple functional azobenzene units was covalently fixed to both, a gold coated cantilever and a flint glass substrate. In the force-extension traces lengthening as well as shortening of the polyazopeptide was observed even under an applied external force. <sup>[13]</sup> This is not only a proof of principle for the first single molecule motor interfaced to the macroscopic world, but also generates discussion concerning potential energy landscapes under external force.

## 2. Introduction

Our organism is very rich in molecular devices, machines and motors.<sup>1</sup> The processive motors myosin and kinesin move muscles or transport loads by the hydrolysis of ATP, while the enzyme RNA polymerase transcribes a DNA template into mRNA by drawing energy from the nucleotide condensation reaction. Other examples are the rotary motor F1-ATPase, which again by the hydrolysis of ATP acts as a proton pump, or the retinal component of rhodopsin, which by the absorption of light undergoes photoisomerization accompanied by a change in the conformation of opsin. [15] [16] [17] [18] It is a particularly fascinating goal to mimic such functions for the realization of artificial 'smart' materials, i.e. new functional polymers performing specific tasks. This often involves a specific response to an external stimulus, i. e. an energy conversion from one form to another. [19]

That synthetic materials are capable of many energy conversions has been demonstrated with cross-linked polypeptides in bulk. [19] [11] On the single molecule level, rotaxans and catenans have shown considerable energy conversion potential, [18] but the most extensively investigated system, that can be reversibly switched by light, is azobenzene. [12] Despite the extensive work on these systems it had not yet been possible to read out the mechanical change directly on a single addressed molecule.

An established method to measure minute mechanical changes is the atomic force microscope (AFM). [20] [21] [22] Fundamental intramolecular and intermolecular interactions have been studied directly at the molecular level with an AFM. [23] [24] [25] [9] This is usually achieved by the investigation of force-extension traces, i. e. the measurement of the force that a molecule applies to the cantilever when being extended. The measurements can be performed in many kinds of solvents, which allows the testing of environmental effects (e. g. changes in salt, temperature, pH) on the force extension traces. If the molecule is only physisorbed to the AFM cantilever or the substrate, it is likely to detach by the perturbations imposed while changing the solvent. Even with DNA, which is known to stick very well to gold substrates, there are only few experiments known, where the solvent was exchanged with a molecule staying attached. [26] But with a covalent attachment of the molecule to both the AFM cantilever and the substrate, the direct impact of an external stimulus (change in environment) should be detectable on a single molecule, which is the prerequisite for a molecular machine. In addition, a covalent attachment allows to probe a molecule for hours.

---

<sup>1</sup> There are numerous definitions for a machine. [14] Here, the expression 'machine' shall refer to a device that converts energy from one form into another in a cyclic way. The specific machine, which converts a 'fuel' into mechanical work in repeated cycles, shall be termed 'motor'.

Therefore, each of the investigated molecules has functional groups to allow for covalent chemical coupling. A concept of a single molecule motor, the investigated molecules and the corresponding external stimuli are depicted in Figure 2.1.

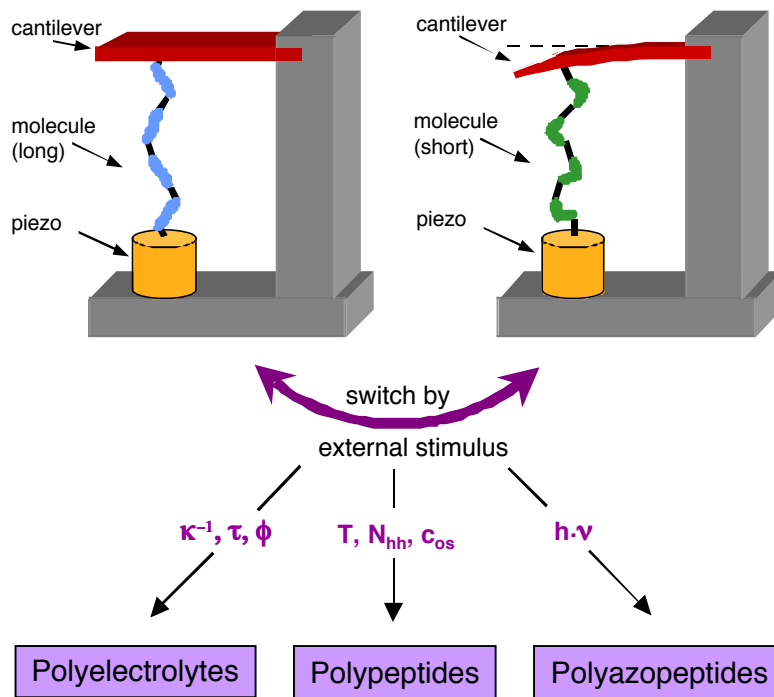


**Figure 2.1:**

*For three different molecules (polyelectrolytes, polypeptides, polyazopeptides) the switching from a long (blue) to a short (green) conformation was investigated with many different external stimuli: the concentration of ions ( $\kappa^{-1}$ ), the line charge density ( $\tau$ ), the surface potential ( $\phi$ ), the temperature ( $T$ ), the hydrophobicity ( $N_{hh}$ ), the concentration of organic solutes ( $c_{os}$ ), and light ( $h\nu$ ).*

Polyvinylamines are promising candidates for a variety of molecular machines - they are supposed to considerably change their stiffness and adsorption properties with the concentration of salt (described by the Debye screening length,  $\kappa^{-1}$ ), the line charge density,  $\tau$ , and the surface potential,  $\phi$ , [27] [28] [29] while their amino side groups allow for a covalent attachment to functional cantilevers and substrates. This is similar for polypeptides, which undergo an inverse temperature folding transition that can be manipulated by means of many external parameters, among those are the temperature,  $T$ , the hydrophobicity,  $N_{hh}$ , and the concentration of organic solutes,  $c_{os}$ . Polypeptides can be end-functionalized by various amino acids (e.g. cysteine, lysin) for covalent attachment. [11]

Polyazopeptides change their configuration upon irradiation with light,  $h\nu$ . Light had not yet been used as an external stimulus in SMFS experiments, but is utilized in this thesis (in total internal reflection geometry). With this setup polymers containing the functional azobenzene unit became the most promising candidates for single molecule machines. Such a polyazopeptide could be covalently linked between the AFM cantilever and a flint glass substrate by heterobifunctional chemistry. Irradiating this polymer with light of wavelength of 420 nm or 365 nm (in total internal reflection geometry) resulted in an extension or shortening of the polymer, respectively. This could be detected in the force-extension traces with the AFM, even against an applied force. Finally, optomechanical switching could be done in a cyclic way, which proves the feasibility of a synthetic light driven single-molecule machine. [13] [30]

## 3. Materials and Methods

The development of new experimental tools in the past 15 years enabled the measurement of forces in the pN (and even fN) range, which allows for mechanical experiments with single molecules. Today a number of techniques differing in force- and dynamical ranges are available. The most common of these are magnetic beads, [31] optical tweezers, [32] glass microneedles, [33] the biomembrane force probe (BFP), [34] and atomic force microscopy (AFM). [20] [21] [24] [25] [9] This technical advancement has made single molecule force spectroscopy a widely used tool for the structural and functional investigation of biomolecules in their native environment. Within the accessible force window, the whole force spectrum from entropic forces at several femtonewton (fN) [31] to the rupture of covalent bonds at a few nanonewton (nN) [35] has now been investigated at the molecular level.

As the use of the atomic force microscope (AFM) in force spectroscopy has emerged from the study of biopolymers, many of the basic aspects of the development and application of this technique are related to the application of force measurements in the study of biopolymers and other biologically relevant systems. [24] [25] [36] In contrast, the focus of this work is the application and extension of single molecule atomic force microscopy to synthetic materials and their manipulation by external 'non mechanical' stimuli, especially with light. In the following the investigated molecules, the principle of the covalent chemical attachment of the molecules and the coupling of light into the AFM experiment is depicted.

### 3.1. Polyvinylamine (PVA)

The polyvinylamines were synthesized by partial hydrolysis of poly-N-vinylformamide, such that the fraction of amino groups in the polymer chains could be controlled by synthesis. The samples were provided by Dr. Andreas Pfau from the Polymer Research Division, BASF-AG, Ludwigshafen, Germany. In Figure 3.1, the molecular structure of the PVA polymers, their degree of hydrolysis,  $x$ , as determined by stoichiometric control (and checked by NMR), as well as the line charge density,  $\tau$ , are shown. The average molecular weight of the polymers as estimated from the K-value<sup>2</sup> and light scattering was  $M_w \approx 500,000 \text{ g}\cdot\text{mol}^{-1}$ , this corresponds to an average degree of polymerization,  $N_w \approx 12,000$ , which gives an average contour length of the polymers,  $L_{\text{avg}} \approx 3 \text{ }\mu\text{m}$ . The provided high viscous solutions contained about 10 % PVA and 10% negatively charged low molecular weight organic acids and salts from the hydrolysis of the charged amino groups. In the following the specimen will be named by the rounded value for the degree of hydrolysis (Figure 3.1):

---

<sup>2</sup> The K-value is an empiric value which defines the molar mass by the viscosity of a solution and is 88 for the used PVA.

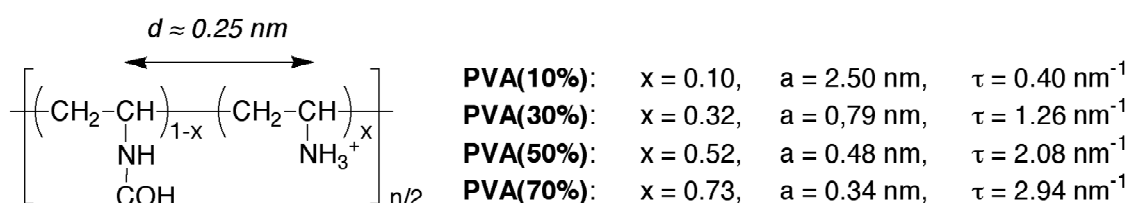


**Figure 3.1:** Molecular structure of polyvinylamines used in SMFS experiments.  $x$  - degree of hydrolysis;  $a$  - distance between neighboring positive charges;  $\tau$  - line charge density.

### 3.2. Polypentapeptides

The investigated elastomers are polymers comprised of repeating peptide sequences. They can be prepared by chemical synthesis (both solution and solid phase) and by recombinant DNA technology (e. g. microbial biosynthesis). [37] The disadvantages of both methods were overcome by first synthesising the polypeptides chemically (which is very expensive and gives low yield) and then using these as a standard for the purification of microbially prepared polymers. Their composition is then exactly defined, which allows for the variation of single amino acids. In the following the standard one letter code for the amino acids is used, i. e.: G - Glycine, V - Valine, P - Proline, I - Isoleucine, C - Cysteine. Figure 3.2 gives the structural formula of the two investigated pentapeptide sequences.

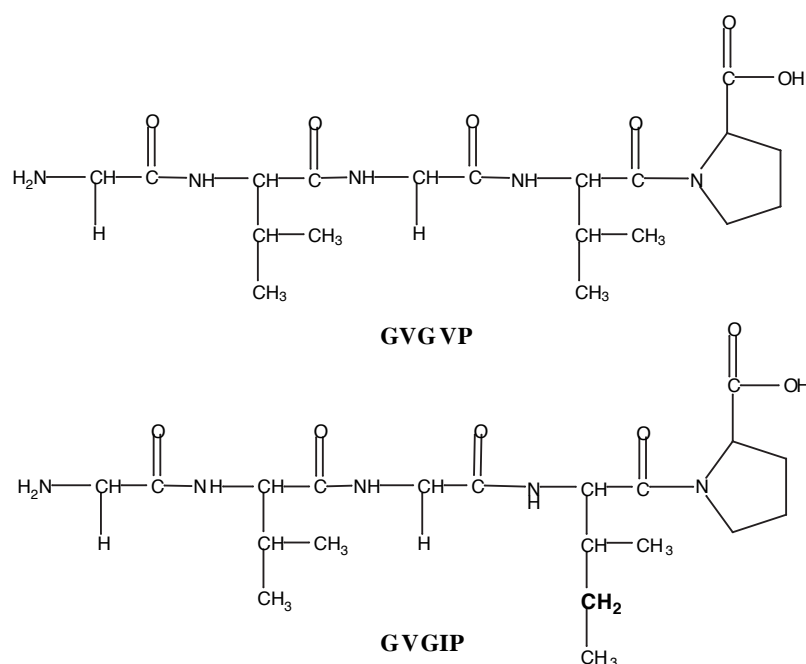


**Figure 3.2:** Structural formulae of the pentapeptides GVGVP and GVGIP.

(GVGVP) is the most prominent repeating sequence in the natural bioelastomer elastin, occurring more than eleven times in a single sequence while (GVGIP) has only one additional  $\text{CH}_2$ -group, which makes it more hydrophobic. The high molecular weight polymers  $(\text{GVGVP})_{n \times 251}$  and  $(\text{GVGIP})_{n \times 260}$  were prepared by means of recombinant DNA technology in a microbial biosynthesis followed by a polymerization. The degree of polymerization,  $n$ , was

not controlled, but kept small ( $n = 1-8$ ). A part of the sample was then terminated by a cysteine residue to allow for covalent attachment to a gold substrate. If not otherwise mentioned, these cysteine terminated samples were used. The samples were produced at Bioelastics Research Limited, Birmingham, USA and provided by Prof. Urry.

**(GVGVP)<sub>251</sub>** is soluble in water below the temperature  $T_t = 25$  °C. On raising the temperature above 25°C it aggregates and undergoes a phase transition to a viscoelastic state which is about 50% peptide and 50% water.

**(GVGIP)<sub>260</sub>** has just one additional CH<sub>2</sub> group per pentamer and undergoes the same kind of phase transition, but with a considerably decreased  $T_t$  of about 12 °C.

The transition temperatures,  $T_t$ , were measured in pure water and PBS by turbidity experiments, which are sensitive to an aggregation of molecules. [38] Their dependence on organic solvents and salts is also given in [38]. Turbidity experiments showed that the influence of the concentration is negligible. But in highly diluted solutions (which cannot be accessed by turbidity experiments),  $T_t$  is supposed to increase significantly. [39]

Further knowledge of the structure of these polypeptides comes from light and electron microscopy. Light microscopy reveals that chemically cross-linked polypeptides have self-assembled into several micron diameter fibers, which are made up of parallel aligned fibrils (as was seen by SEM). These fibrils arise from the association of 5 nm diameter filaments with a supercoiled or twisted substructure, which was seen by TEM and negative staining. It is further assumed that the filaments consist of beta-spirals, where 3 pentamers give a length of about 1 nm, while in the unfolded state an amino acid has a length of about 0.36 nm, which gives a total length of 5.4 nm. This finally leads to the schematic representation given in Figure 3.3. [19]

The solid state of untreated poly(GVGVP) is characterized by an amorphous phase, in which a dense net of hydrogen bonds is established. Thermal treatment (above  $T_t$ ) transforms this metastable phase to a more stable state (with a certain loss of hydrogen bonds) which is still non-crystalline. [40]

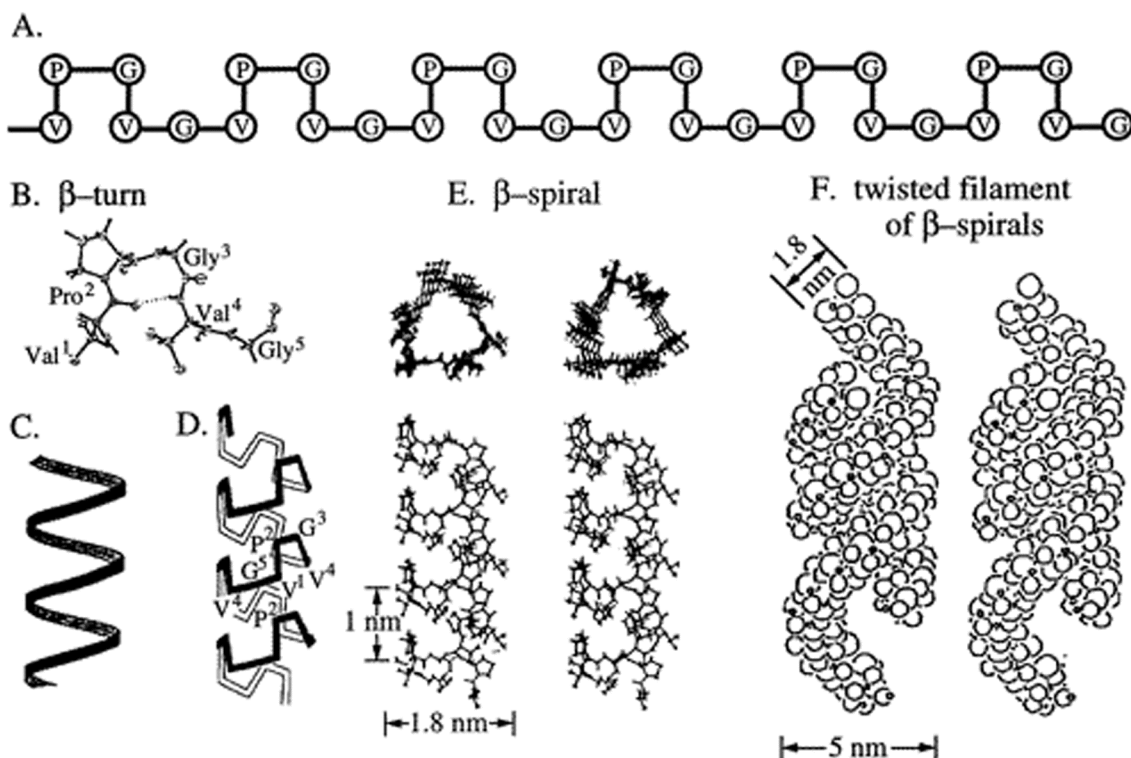


**Figure 3.3:** (A) Schematic representation of the polypeptide chain with the P-G sequence inserting a repeating  $\beta$ -turn. (B) The repeating  $\beta$ -turn, as obtained from the crystal structure of  $\text{cyclo}(\text{GVGVP})_3$ . (C and D) Helical representations of the repeating pentamer structure without and with showing the  $\beta$ -turns positioned as spacers between the turns of the helix. (E) Detailed plots in stereo (cross-eye viewing) of the helical structure of  $\text{poly}(\text{GVGVP})$ , called a  $\beta$ -spiral. (F) Association of  $\beta$ -spirals in space filling united residue representation giving rise to the twisted filament, or supercoiled, structures. (Adapted from [11]).

### 3.3. Polyazopeptides

The synthesis of the investigated azopeptides was done by Dr. Anna Cattani in the group of Prof. Moroder (Max-Planck-Institut für Biochemie, Martinsried, Germany). It was directed by the desire to maximize the potential length change upon irradiation, the need for a sufficiently long chain to be investigated by SMFS and the need to chemically attach the polymer both to the AFM tip and the glass substrate.

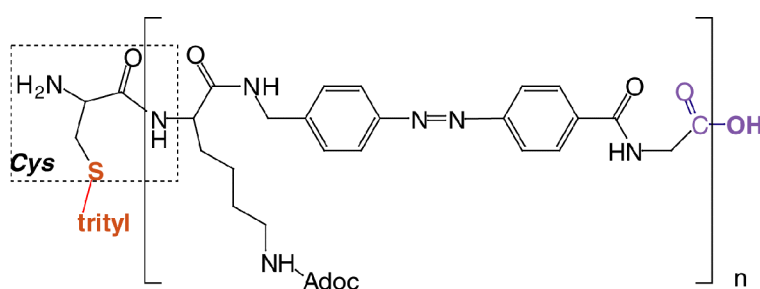


**Figure 3.4:** Structural formula of the investigated poly(azopeptide),  $n \sim 20$ .

The polymer is shown in Figure 3.4, it is a polypeptide with multiple azobenzene moieties incorporated in the backbone. For the incorporation of multiple azobenzene moieties into a linear polymer a sequential polypeptide approach based on polycondensation of tripeptide monomers containing (4-aminomethyl)phenylazobenzoic acid (AMPB) [41] was selected. Upon thermal relaxation into the all-*trans*-azo configuration, the average contour length of the polymer was estimated at 54 nm. For a more detailed description of the synthesis see [30]. The C-terminus is suited to form a peptide bond to an amino-modified surface while the N-terminus was extended with a trityl protected cysteine. This allowed for a heterobifunctional attachment of the polyazopeptide to the AFM tip and the substrate

### 3.4. Covalent Attachment Scheme

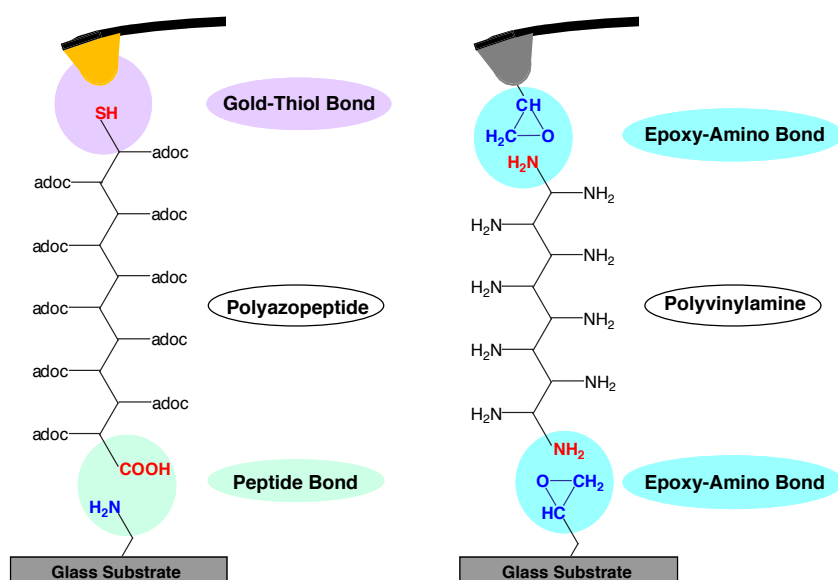


**Figure 3.1:** Schematics of the utilized covalent attachments: Polyazopeptides are coupled via gold-thiol and carboxy-amino chemistry (left). Polyvinylamines are coupled via Epoxy-Amino chemistry (right).

Three covalent attachment mechanism were used for the investigated polymers. They are depicted in Figure 3.5 and described in detail in Section 10.1.

### 3.5. Coupling of Light into the AFM Experiment

The light to excite the azobenzenes units in the polyazopeptide molecule is coupled into a flint glass microscope slide in total internal reflection (TIR) geometry (Figure 3.6). A single molecule is covalently attached between cantilever and substrate and excited in the evanescent field of the flint glass (Figure 3.7). For further details see Section 10.2.

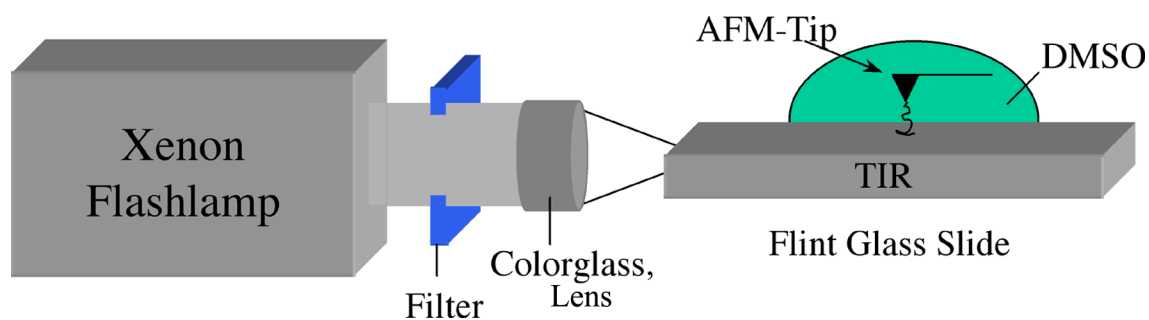


**Figure 3.6:** Schematics of the modified AFM with optical excitation. The light of a Xenon-flashlamp is coupled into a flint glass object slide in total internal reflection (TIR) geometry. The polymer is excited in the evanescent field.

Total internal reflection was of crucial importance to eliminate the deleterious effects of absorption by and thermal heating of the cantilevers. The penetration depth of the evanescent field is about  $\lambda/2\pi \sim 50$  nm. This is short enough to prevent interaction with the cantilever itself and long enough to excite most of the azobenzene units in the polyazopeptide.

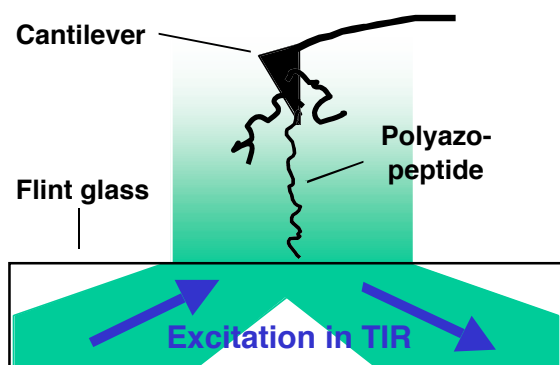


**Figure 3.7:** Schematics of the polyazopeptide in the evanescent field produced by total internal reflection (TIR) in a flint glass slide

## 4. Theory

### 4.1. Statistical Mechanics for Single Molecule Force Spectroscopy

In the following the statistical mechanics of a polymer will be laid out with special emphasis to single molecule force experiments. As the system cantilever-polymer is not a thermodynamically large system the thermodynamic boundary conditions of the single molecule experiment have to be considered first. Based on this, the well-accepted concept of entropic elasticity is summarized, which results in an effective restoring force upon stretching a flexible polymer chain by an external force field as a result of a loss in conformational freedom. However, as the full range from thermal fluctuations to the strength of individual chemical bonds is explored by single molecule force spectroscopy, other elastic contributions have also to be considered, especially in the high force range at several hundred pN.

#### 4.1.1. Thermodynamic Boundary Conditions

In a single molecule stretching experiment fluctuations become non-negligible and the different statistical ensembles are therefore not equivalent. Strictly, neither the Gibbs ensemble (no force fluctuations) nor the Helmholtz ensemble (no distance fluctuations) is correct, and one has to find a proper statistical analysis of a system with constant spring constant. This is given in recent publications by Kreuzer et al., [42] [43] there it is also shown, that for single molecule force experiments in the soft cantilever regime (which applies to the usual experimental conditions) the Gibbs ensemble is a good approximation. Therefore, in the following the Gibbs ensemble is applied.

#### 4.1.2. Statistical Mechanics of Polymer Chains

Polymers have been synthesized since about 150 years, but their structure was long unknown. For many years it was supposed that small molecules form large aggregates. In 1920 Hermann Staudinger recognized, that substances like caoutchouc are built from high molecular weight polymers which are covalently bound and named them "Makromoleküle" (ger.: macromolecules) in 1922. [44]

The theoretical analysis of the properties of single macromolecules is well developed for flexible polymers and will be given in the following. If the length scale is chosen large enough all linear macromolecules can be considered to be flexible. In this limit they adopt a random coil conformation in solution, and Brownian motion causes a permanent fluctuation of the molecule around a mean equilibrium conformation. This problem is closely related to

problems such as random walks or diffusion, and the mean values describing the conformation of such a polymer chain in solution can then be derived by a statistical approach. [45-48] The classical partition function of the system is set up, based on which the probability of configurations with, e.g. the same specified end-end distance,  $R$ , can be deduced.

The discussion is started with the 'classical' entropic contribution at low stretching forces. Assuming a Gaussian distribution for the random polymer coil, [47] [48] this restoring force is strictly proportional to the relative extension of the polymer chain,  $F \sim R/L$  ( $L$  - contour length of the polymer). However, the linear response regime of a stretched Gaussian chain is limited to small extensions (or small forces, respectively). Apparently, the real end-end distance of a polymer chain cannot be larger than its contour length (a restriction not considered in the Gaussian distribution), such that the restoring force must be a non-linear function of  $R/L$ , approaching infinity upon full extension of the polymer chain. The two most prominent and most simple theoretical models which satisfy this boundary condition are the 'freely-jointed chain' (FJC) model [46] and the 'worm-like chain' (WLC) model, [49] which are usually used to describe the measured force-extension profiles of individual polymer chains.

Strictly, a polymer confined between the walls of a surface and an AFM tip is not accurately described by any theoretical model, in which the polymer ends are 'fixed' to an arbitrary point in space. The real confinement to a half space has the effect that the z-component of the polymer's end-end distance,  $\langle R_z \rangle$ , is non-zero under zero force, while in the FJC and the WLC model the force acting on the unconfined polymer chain is exactly zero for  $\langle R_z \rangle = 0$ . Both models therefore fail in the short distance regime of the AFM experiment, in which a compression force would be needed to reach  $\langle R_z \rangle = 0$  (i.e. to bring all polymer end groups to the substrate). This force has not been quantified experimentally for single molecules yet, as other limiting factors such as adsorption and desorption of polymer segments to the surfaces and tip-surface interactions usually dominate the stretching profile at short tip-surface distances.

### 4.1.3. The Freely-Jointed Chain (FJC) Model

In the freely-jointed chain model, a polymer is described as a chain of  $N$  segments of equal length,  $l$ . The segments are freely jointed, i.e. there are no restrictions to their spatial distribution such that each segment can point in every direction with equal probability. This condition is not fulfilled for real polymers, but this restriction does not change the general form of the force-distance relation. Effectively, the freely-jointed chain model can be used with adjusted contour and segment lengths. This effective segment length is also termed Kuhn length,  $l_K$ . The contour length of the polymer chain is then simply given by  $L = N l$ . Generally, the restoring force,  $F$ , as a function of the chain's end-end distance,  $R$ , can be obtained from

the first derivative of the partition function at given end-end distance,  $Z_R$ , i.e.  $F(R) = k_B T \cdot \frac{\partial \ln Z_R}{\partial R}$ . However, in most cases as even for the simple FJC model, it is not possible to derive an analytical expression for  $Z_R$ . Therefore, the stretching energy,  $F \cdot R$ , is introduced as an additional term into the chain's partition function at constant force,  $Z_F$  (Equation 1). For a freely-jointed chain, the partition function at constant force is given by

$$Z_F^{FJC} = \int_{l_1} \dots \int_{l_N} e^{-(E(l_1, \dots, l_N) - F \cdot R)/k_B T} dl_1 \dots dl_N, \quad (1)$$

in which  $l_1, \dots, l_N$  are the bond vectors representing the  $N$  segments of length  $l$ .  $E(l_1, \dots, l_N)$  is the energy of a given set of bond vectors (i.e. conformation), which is a constant for the case of a freely-jointed chain, as there is no interaction between the individual segments. From this, the mean end-end distance,  $R$ , can be calculated as a function of the external stretching force,  $F$ ,

$$R = k_B T \cdot \frac{\partial \ln Z_F}{\partial F}. \quad (2)$$

The force-distance profile,  $F(R)$ , is given by the inverse function. Introducing Equation 1 into Equation 2, and for the stretching force acting along the z-axis, the mean extension along the z-axis,  $R_z$ , is obtained as a function of the applied force by

$$R_z = N \cdot l \cdot \left[ \coth\left(\frac{F \cdot l}{k_B T}\right) - \frac{k_B T}{F \cdot l} \right] = N \cdot l \cdot \mathcal{L}\left(\frac{F \cdot l}{k_B T}\right). \quad (3)$$

$\mathcal{L}(x) = \coth(x) - x^{-1}$  is the Langevin function, and the average force acting in z-direction is given by the inverse of Equation 3.

The Langevin function approximates  $x/3$  for small  $x$  and  $(1-1/x)$  for large  $x$ , which yields the following approximations for  $R_z$ :

$$R_z \cong \begin{cases} \frac{Nl^2 F}{3k_B T} & \frac{Fl}{k_B T} \ll 1 \\ Nl\left(1 - \frac{k_B T}{Fl}\right) & \frac{Fl}{k_B T} \gg 1 \end{cases}. \quad (4)$$

The behavior for small  $F$  is therefore equivalent to an ideal spring with spring constant

$$k = 3 \frac{k_B T}{R_e^2}. \quad (5)$$

Here,  $R_e$  is the average end-end distance without an applied force ( $R_e^2 = N l^2$ ).

The two adjustable fit parameters in this model are the segment length,  $l$ , and the number of segments,  $N$ . As the stretching force is still a function of the chain's relative extension, i.e.  $F \sim f(R_z/L)$ , all force traces originating from different polymer chains of identical structure will superimpose when scaled to the same contour length. The only relevant fit parameter in the freely-jointed chain model is therefore the segment length,  $l$ , which is a measure of the flexibility of the random coil. It may coincidentally agree with the length of a structural monomer unit or the length of a C-C-bond, typically the values for flexible polymers in good solvents are 0.3 - 0.6 nm. [50] [51] [52]

To this point, this model just accounts for the entropic elasticity of the chain's backbone, which implies a fixed contour length,  $L$ . This assumption does not hold in the higher force regime probed in the AFM experiment, which reaches up to nanonewton forces where even covalent bond rupture can be observed. Before chemical bonds break, the deformation of bond angles and the stretching of covalent bonds will result in an effective increase of the segment length. Therefore, enthalpic contributions to the restoring force of the polymer chain have to be considered. In the simplest approach, it is assumed that the restoring force can be separated into an enthalpic and entropic (conformational) contribution such that the extensibility of the segments can be considered as an additional Hookean term,  $F_H$ , which scales linearly with the relative extension. With  $F_H = K_o (R_z/L)$ , the distance-force relation becomes<sup>3</sup>

$$R_z = N \cdot l \cdot L \left( \frac{F \cdot l}{k_B T} \right) + \frac{N \cdot l}{K_o} \cdot F. \quad (6)$$

This introduces an additional parameter  $K_o$ , the (normalized) segment elasticity, which is the inverse of the normalized compliance of the polymer chain, thus a measure for its extensibility.

#### 4.1.4. The Worm-Like Chain (WLC) Model

All approaches to describe a semiflexible chain have in common the concept of a persistence length. The persistence length should be a measure of stiffness, but exactly how this is measured is a matter of definition, and there are plenty of definitions (for an overview see [53]). To give an instructive definition of a persistence length,  $L_p$ , and its relation to the bending modulus,  $\kappa$ , of a rod the approach given by Netz in his lecture on polymer physics 2002 at the LMU München (based on [54]) is laid out in the following. A further advantage of this approach is, that it leads to the definition of the persistence length, which is the starting point for the OSF-theory for charged chains treated in Section 4.2.2.

---

<sup>3</sup> To be exact, the Hookean term would have to be included into the partition function and  $R_z$  again calculated, but this is a more involved calculation which was e.g. done by R. R. Netz (private note) and gives no marked change in the fit trace.

The chain is described by a continuous trace with a bending modulus,  $\kappa$  ( Figure 4.1).

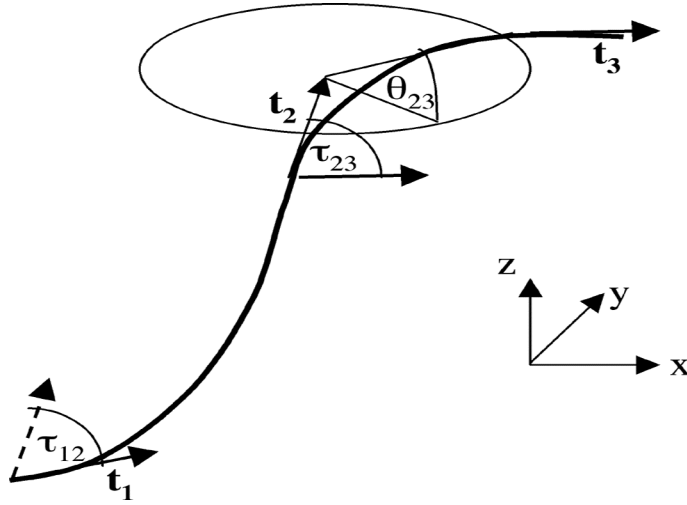


**Figure 4.1:**  
Sketch of a polymer  
worm-like chain  
and the relevant  
parameters.

The variables are defined as ( $\langle \mathbf{a}, \mathbf{b} \rangle$  is the angle between the two vectors  $\mathbf{a}$  and  $\mathbf{b}$ ):

$$\begin{aligned}\tau_{12} &= \angle(\mathbf{t}_1, \mathbf{t}_2) \\ \tau_{23} &= \angle(\mathbf{t}_2, \mathbf{t}_3)\end{aligned}$$

$\theta_{23}$ : torsion angle between plane of  $\mathbf{t}_1, \mathbf{t}_2$  and  $\mathbf{t}_3$ ,

$$\mathbf{t}_2 = \begin{pmatrix} 0 \\ 0 \\ 1 \end{pmatrix}, \quad \mathbf{t}_1 = \begin{pmatrix} \sin \tau_{12} \\ 0 \\ \cos \tau_{12} \end{pmatrix}, \quad \mathbf{t}_3 = \begin{pmatrix} \cos \theta_{23} \sin \tau_{23} \\ \sin \theta_{23} \sin \tau_{23} \\ \cos \tau_{23} \end{pmatrix},$$

the expectation value for the vector product  $\mathbf{t}_1 \mathbf{t}_3$  is given by

$$\langle \mathbf{t}_1 \mathbf{t}_3 \rangle = \langle \sin \tau_{12} \sin \tau_{23} \cos \theta_{23} \rangle + \langle \cos \tau_{12} \cos \tau_{23} \rangle. \quad (7)$$

As  $\mathbf{t}_1$  and  $\mathbf{t}_3$  are just coupled by an intermediate point (Markov chain) the angles  $\theta_{23}$  and  $\tau_{12}$  are decoupled:

$$\langle \mathbf{t}_1 \mathbf{t}_3 \rangle = \langle \sin \tau_{12} \rangle \langle \sin \tau_{23} \rangle \langle \cos \theta_{23} \rangle + \langle \cos \tau_{12} \rangle \langle \cos \tau_{23} \rangle, \quad (8)$$

and as the rotation around  $\theta_{23}$  is free:  $\langle \cos \theta_{23} \rangle = 0$ .

Further the expectation value of two distant tangent vectors equals their product

$$\langle \mathbf{t}_1 \mathbf{t}_3 \rangle = \langle \mathbf{t}_1 \mathbf{t}_2 \rangle \langle \mathbf{t}_2 \mathbf{t}_3 \rangle, \quad (9)$$

and therefore in general

$$\langle \cos[\tau(s_1 + s_2)] \rangle = \langle \cos[\tau(s_1)] \rangle \langle \cos[\tau(s_2)] \rangle, \quad (10)$$

with  $s_1$ : contourlength between  $\mathbf{t}_1$  and  $\mathbf{t}_2$ ,  
and  $s_2$ : contourlength between  $\mathbf{t}_2$  and  $\mathbf{t}_3$ .

The only function which guarantees this is the exponential, therefore

$$\langle \mathbf{t}(0) \mathbf{t}(s) \rangle = e^{-s/L_p}, \quad (11)$$

with the persistence length,  $L_p$ .

To give the persistence length a physical meaning, it is in the following related to the bending modulus,  $\kappa$ . The bending energy of a thin rod with length  $L$  is given by Landau and Lifschitz [55]

$$\chi = \frac{\kappa}{2} \int_0^L ds \left( \frac{d\mathbf{t}(s)}{ds} \right)^2. \quad (12)$$

An arbitrary trace can be approximated in a point by a circle of radius  $R$ . The absolute value of the bending vector is from differential geometry equal to  $1/R$ :  $|d\mathbf{t}/ds|=1/R=\tau/L$ . Therefore,

$$\chi = \frac{\kappa}{2} L \left( \frac{\tau}{L} \right)^2 = \frac{\kappa \tau^2}{2L}. \quad (13)$$

From the equipartition theorem every quadratic degree of freedom contributes  $1/2 k_B T$  of internal energy, which yields one  $k_B T$  for the bending energy of the stiff rod (two free angles):

$$\langle \chi \rangle = k_B T = \langle \frac{\kappa \tau^2}{2L} \rangle \Rightarrow \langle \tau^2 \rangle = \frac{2L}{\kappa} k_B T. \quad (14)$$

On the other hand is Equation 11 for  $s \ll L_p$  to first order<sup>4</sup>

$$\begin{aligned} \langle 1 - \frac{\tau^2}{2} \rangle &\approx 1 - s/L_p \\ \Rightarrow \langle \tau^2(s) \rangle &\approx 2s/L_p \end{aligned} \quad (15)$$

Combined with Equation 14 this yields the following relation between the persistence length,  $L_p$ , and the bending modulus of a rod,  $\kappa$ :

$$L_p = \kappa / k_B T. \quad (16)$$

The problem of a semiflexible chain under tension is analytically not exact solvable. First numerical approaches by Fixman and Kovac, [56] as well as analytical approaches by Kovac and Crabb [57] started from a freely rotating chain. They introduced harmonic bending potentials for the orientation of two neighboring chains and the extension of a single segment. Then they took the limit  $N \rightarrow \infty$ ,  $L_p \rightarrow 0$ ,  $\cos(\theta) \rightarrow 1$ . Several years later Marko and Siggia

<sup>4</sup> The restriction  $s \ll L_p$  is not necessary, if the problem is approached by field theory. [56]

[58] [59] introduced an interpolating formula for the WLC-model. It is usually used to describe semiflexible polymers and was extended by Wang et al. [60] to include a (normalized) segment elasticity,  $K_0$ :

$$F = \frac{k_B T}{L_p} \cdot \left[ \frac{R_z}{L} - \frac{F}{K_0} + \frac{1}{4(1 - R_z/L + F/K_0)^2} - \frac{1}{4} \right] \quad (17)$$

It reproduces the exact behavior of their numerically calculated solution [59] for large ( $F > 20$  pN) and small ( $F < 1$  pN) forces while the deviations in the intermediate range are up to 10%. An improvement to this formula is given by Bouchiat et al. [61] They subtracted the Maro-Siggia interpolation formula from the exact numerical solution of the WLC model and expressed the residuals as a seventh-order polynomial. This results in less than 0.01 % deviation from the exact WLC model. But as the WLC-model itself has some shortcomings for AFM experiments, not the deviation from the model, but the model itself probably imposes the biggest error.

Stimulated by the finding that especially in the high force range the WLC-model does not fit the data well, Livadaru et al. [8] performed extensive transfer-matrix calculations for the force-response of a freely-rotating chain model<sup>5</sup> as a function of varying bond angle (and thus varying persistence length,  $L_p$ ) and chain length,  $L$ . The results are not published yet, but submitted to *Macromolecules* and discussed in Section 8.1. They showed a crossover from the WLC to the discrete-chain (DC) behavior, which occurs at a force  $F \sim L_p / b^2 k_B T$  ( $\sim 57$  pN for a carbon backbone with bond length  $b \sim 0.15$  nm) and is thus probed in the performed AFM-experiments. This crossover is due to the fact that at increasing forces the dominant chain fluctuations probe progressively smaller length scales and above the crossover force become sensitive to the discrete nature of the semiflexible chain.

The persistence length in the limit of stiff bonds follows from the discretization of the WLC model. In this DC regime the stretching response shows a different force dependence than in the WLC regime,

$$\text{WLC:} \quad \frac{R_z}{L} = 1 - \left( \frac{4F L_p}{k_B T} \right)^{-0.5}, \quad (18)$$

$$\text{DC:} \quad \frac{R_z}{L} = 1 - \left( \frac{F L_p}{c k_B T} \right)^{-1}. \quad (19)$$

The DC behavior is similar to the behavior of a FJC, but not equal, as the architectural details of the chain are contained in the constant  $c$ . A simple heuristic function for the force-distance relation to fit experimental data is given by ( $F_{\text{WLC}}[x] = 3/4 - 1/x + x^2/4$ )

---

<sup>5</sup> And also elastically jointed chain model, which should be applicable to stiff biopolymers and is not further discussed here.

$$\frac{R_Z}{L} = 1 - \left\{ \left( F_{WLC}^{-1} \left[ \frac{F L_P}{k_B T} \right] \right)^\beta + \left( \frac{c F b}{k_B T} \right)^\beta \right\}^{-1/\beta} + F/\gamma. \quad (20)$$

In the following it shall be called WLC\_DC-fit. To present, only the parameters for a carbon backbone are calculated:  $b \sim 0.15$  nm;  $L_P \sim 0,76 b$ ;  $\beta \sim 2$ ;  $c \sim 2$ ;  $\gamma \sim 28000$  pN. [8]

## 4.2. Polyelectrolytes

Polyelectrolytes are macromolecules carrying covalently bound anionic or cationic groups, and low-molecular weight 'counterions' securing for electroneutrality. They are of central importance in nature and in industrial applications. For instance the conformation as well as the adhesive behavior of proteins are governed to a significant extent by electrostatic interactions. [62] [63] Due to their unique adsorption properties at interfaces, synthetic polyelectrolytes are used in many industrial areas, for example in paper, textile, petrol, cosmetics and chemical industry. These and other applications are treated in the book by Dautzenberg. [64]

In addition to the acid or base strength of the ionic sites, the average distance between adjacent charges,  $a$ , (or the line charge density  $\tau=1/a$ ) is an important parameter. It can be controlled by polymerizing the heteropolymer from charged and neutral groups as units. This fixes the charge distribution along the chain during the polymerization. It is usually quantified by the degree of hydrolysis, i. e. the fraction of charged groups.

The theoretical treatment of polyelectrolyte chains is much more involved, because the electrostatic interactions are long-ranged. There are different models and therefore different definitions for the electrostatic persistence length,  $L_{p,e}$ . In the following the OSF-theory and a recent theory including stretching and bending fluctuations are summarized. The OSF-theory is often applied, but based on the WLC model it neglects some fluctuations in the system. Several experiments show, that this is an oversimplified model, which does not describe a charged polymer chain under stress satisfactorily. [59] [6] The below discussed recent theory [7] includes fluctuations, which results in the experimentally observed force dependent persistence length.

### 4.2.1. Basic Parameters

The **Bjerrum Length** is the distance, at which the electrostatic interaction of two unit charges,  $e$ , in a solvent without counter ions equals the thermal energy,  $k_B T$ ,

$$l_B = \frac{e^2}{4\pi\epsilon\epsilon_0 k_B T}. \quad (21)$$

$l_B$  is about 0.71 nm in water at room temperature. The presence of ions screens the electrostatic potential of a polymer chain considerably. An estimate for the range of the coulomb potential in the presence of counter ions in the solvent is given by the **Debye Length**,  $\kappa^{-1}$ . For monovalent ions it is given by

$$\kappa^{-1} = \lambda_{DH} = \left( \frac{8\pi c_S e^2}{\epsilon k_B T} \right)^{-\frac{1}{2}}, \quad (22)$$

with the concentration of the monovalent ions,  $c_S$ , and the dielectric constant,  $\epsilon$ , of the solvent (for water:  $\epsilon \approx 80$ ). Additional factors for multivalent ions are given in [65]. For  $r > \lambda_{DH}$  the typical electrostatic potential (proportional to  $r^{-1}$ ) is screened and given by  $r^{-1} \exp(-r/\lambda_{DH})$ . This approximation is valid at distances larger than the **Gouy-Chapman Length**,

$$\lambda = \frac{2k_B T \epsilon}{e^2 \sigma} = \frac{1}{2\pi \sigma l_B}. \quad (23)$$

The Gouy-Chapman length corresponds to the distance of a single ion from a charged wall at which its bare interaction with the wall is on the order of  $k_B T$ .

#### 4.2.2. OSF-Theory

According to the OSF-theory, which was established independently by Odijk, [27] Skolnick and Fixman, [28] the bending rigidity of a polyelectrolyte chain is increased as its like-charged segments electrostatically repel each other. This favors a stretched chain conformation, which can be described in the rod-limit by an electrostatic contribution,  $L_{el}$ , which adds to the bare elastic persistence length,  $L_o$ , of the polyelectrolyte so that overall,

$$L_{OSF} = L_o + L_{el}. \quad (24)$$

For the electrostatic persistence length,  $L_{el}$ , they found a simple power law for the dependency on concentration of monovalent ions,  $c_S$  (represented by the Debye screening length,  $\kappa^{-1} \sim c_S^{-1/2}$ ), and the polymer charge density: [27]

$$L_{el} = l_B \kappa^{-2} \tau^2 / 4. \quad (25)$$

However, at high charge densities, there is a limit for the line charge density as counterion condensation reduces the average distance between two charges along the chain to the Bjerrum length,  $l_B$ . [66] In this 'Manning-limit', the effective line charge density becomes one charge per Bjerrum length,  $\tau = l_B^{-1}$ , and Equation 25 reduces to

$$L_{el} = \kappa^{-2} / 4 l_B. \quad (26)$$

Small angle static light-scattering experiments [67] and magnetic birefringence measurements [68] confirmed this behavior for rather stiff chains and polyelectrolytes with high charge density. For flexible chains there is a discrepancy among existing theories, simulations and experiments. Netz and Orland [69] as well as Dobrynin et al. [70] give many examples for publications that show quadratic, linear, or even sublinear dependence of the electrostatic persistence length from the Debye screening length. Netz and Orland themselves show in their variational theory that previous variational calculations were too restrictive and in releasing this constraint find agreement with the predictions by Odijk (for rigid polymers) and Khokhlov [71] ( who predicted a quadratic dependence on the screening length for flexible polymers).

### 4.2.3. Force Dependent Persistence Length

The concept of a static persistence length, as given in the OSF-theory, breaks down in single molecule force experiments on semiflexible polymers where bending and stretching fluctuations become non negligible. Barrat and Joanny [72] showed that  $L_{OSF}$  depends on the scale of the bending fluctuations, leading to a softening of the charged chain for bending wavelengths smaller than the screening length. This results in an effective decrease of  $L_{OSF}$  for large applied forces (as in AFM experiments), which has qualitatively been predicted theoretically and verified by experiments several years ago by Marko and Siggia. [59] Recently Netz [7] calculated the stretching response of a single charged semiflexible polymer in the limit of large tensile forces considering the effects of (i) the coupling of bending and elongational fluctuations, (ii) the electrostatic contribution to the bending and elongational energies, and (iii) nonlinear bare elastic elongational energies. For a linear elasticity, i. e. an ideal spring model with spring constant  $\gamma$  for the stretching energy, the stretching response is given by <sup>6</sup>

$$\frac{R_Z}{L} = 1 + \frac{g + F}{\gamma} - \frac{1 + (g + 2F)/\gamma}{2\sqrt{l_{eff}F(1 + (g + F)/\gamma)}}. \quad (27)$$

Here,  $F$  is the external force acting on the chain,  $L$  the contour length and  $R_Z$  the end-to-end distance of the chain.

The linear stretching constant  $g$ , which can be interpreted as an intrinsic force which pushes the monomers apart, is given by (in units of  $k_B T$ )

$$g = \frac{l_B q^2}{a^2} \left( \kappa a \frac{e^{-\kappa a}}{1 - e^{-\kappa a}} - \ln(1 - e^{-\kappa a}) \right). \quad (28)$$

Where  $a$  denotes the distance between charges of valency  $q$ .

---

<sup>6</sup> For a general formula see [7].

As the persistence length in stretching experiments on single molecules is defined by the force acting on the molecule, the effective persistence length,  $l_{\text{eff}}$ , becomes force dependent and is defined by

$$\langle t_{\perp}^2 \rangle = (f^* l_{\text{eff}})^{-1/2}, \quad (29)$$

here,  $\langle t_{\perp}^2 \rangle$  is the expectation value of the perpendicular tangent vector component and  $f^* = F \left( 1 + \frac{g + F}{\gamma} \right)$  the normalized force (for linear elasticity).

This results in a scale dependent electrostatic persistence length, and shows a softening as the pulling force increases. A heuristic expression for the rescaled effective persistence length is given as [7]

$$\frac{l_{\text{eff}} - L_0}{L_{\text{OSF}}} = \frac{1}{1 + \left( \frac{f^*}{L_0 \kappa^2} \right)^{0.58}}, \quad (30)$$

where  $L_0$  is the bare persistence length, and  $L_{\text{OSF}}$  the electrostatic persistence length (given by the OSF-theory). This shows, that in the 'high force' regime, the effective persistence length,  $l_{\text{eff}}$ , of the polymer is reduced to its bare elastic contribution,  $L_0$ .

The force at which this crossover occurs is  $f^* = L_0 \kappa^2$ . For synthetic polyelectrolytes ( $L_0 \sim 1$  nm)  $f^* k_{\text{B}}T \sim 4$  pN for  $c_{\text{S}} = 100$  mM and  $f^* k_{\text{B}}T \sim 40$  fN for  $c_{\text{S}} = 1$  mM. For DNA, with  $L_0 \sim 30$  nm, this results in a crossover force of more than 120 pN at physiological salt concentration.

These findings are qualitatively consistent with the above mentioned theoretical and experimental considerations and are supported by recent experimental evidence obtained in single molecule force measurements on synthetic polyelectrolytes. [52] [73] [6] They are further discussed in Section 8.1.

### 4.3. Force Induced Bond Rupture

The first experiments reporting rupture forces of single bonds were performed at fixed pulling velocities and spring constants.[74] [50] It is now generally accepted, that the rupture force of an isolated bond is not only dependent on the shape of the unbinding potential and the temperature, but also on the force loading rate: any non-covalent bond will fail under any level of pulling force if held for sufficient time. [75] [76] Therefore, with the bond dissociation process being a non-equilibrium dynamical process, the bond strengths (as well as strengths of adhesion) can be expected to be time- and loading rate dependent properties. This has been shown in several experiments, most striking employing the biomembrane force probe technique by which the applied force-loading rate was varied over six orders of magnitude. [77] Dynamic force spectroscopy thus not only allows the determination of the unbinding

forces at the molecular level, but also explores wide regions of the energy landscapes of ligand-receptor bonds, and thus can reveal a detailed picture of the binding potential. [78] [79] [80]

In the following a short summary of the models used to describe force induced single bond rupture is given. Systems with many bonds in parallel show various behavior, especially for the dependence of the net rupture force on the number of bonds in parallel.

### 4.3.1. Single Bond Exposed to an External Force

The first theoretical Equation to describe chemical reactions was the Van't Hoff - Arrhenius Law [81], which describes the exponential dependence of the reaction rate from temperature. It was then realized that escape from a state of local stability can happen only via noise-assisted hopping events. The theory of Brownian motion was therefore the starting point for the following two theories. They give the rate of escape from the states of local stability along a preferential path over the confining barrier via a saddle point in the energy surface under the assumption that the diffusion current is constant in space :

- Eyring and others derived a rate formula dependent on quantities that are available from the underlying potential surface. This theory is commonly known as the **Transition State theory**, when the concept of a point of no return (i. e. no trajectory that passes the transition state returns) is introduced (an extensive review is given by Hänggi [82]).
- **Kramers theory** [83] is based on Brownian motion dynamics driven by thermal forces,  $F$ , which in turn are connected with the temperature,  $T$ , and the damping,  $\zeta$ , via the fluctuation-dissipation theorem [82]

$$\langle F^2 \rangle \Delta t \sim k_B T \zeta . \quad (31)$$

Equation 31 is derived under the assumption of overdamped motions, where  $v = F / \zeta$ . [84]

Both theories give the lifetime of a bond with an energy barrier  $\Delta V_u^\ddagger$  in the absence of an external force as

$$\tau_o = \frac{1}{k_o} = \frac{1}{\nu_o} \cdot e^{+\Delta V_u^\ddagger / k_B T} . \quad (32)$$

In the transition state theory the pre-factor  $\nu_o$  is the natural vibration frequency of the bond, which is of the order of  $\nu_o \approx 5 \cdot 10^{13} \text{ s}^{-1}$  for C-C bonds. Neglecting any damping effects, the corresponding activation barriers / relaxation times would be  $35 k_B T / 30$  seconds,  $40 k_B T / 1.3$  hours or  $50 k_B T / >3$  years.

In Kramers theory the attempt frequency (or inverse diffusion time),  $\nu_o = D/l_c l_{ts}$ , is governed by viscous damping ( $D = k_B T / \zeta$ ) and two length scales. The length  $l_c$  is the thermal spread

defined by the rise in energy local to the bound state and  $l_{ts}$  is the energy-weighted width of the barrier defined by the drop in energy local to the transition state. In harmonic approximation they are derived from local curvatures of the energy landscape. [85] [86]

The additional potential energy due to an applied constant stretching force along the conformational coordinate effectively reduces the intermolecular potential by  $-F \cdot (z - z_0)$  as shown in Figure 4.2. The lifetime of the bond under the influence of a stretching force is given by the 'Bell equation' [75]

$$\tau_F = \frac{1}{\nu_o} \cdot e^{+(\Delta V_u^\ddagger - F\Delta z_u) / k_B T} = \tau_o \cdot e^{-F\Delta z_u / k_B T}, \quad (33)$$

where  $\Delta z_u$  denotes the length of the unbinding path.

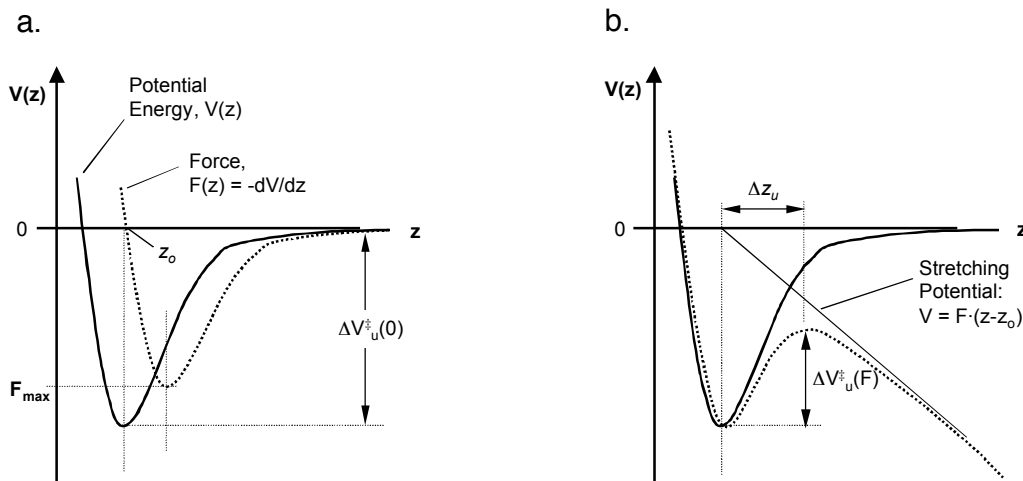


**Figure 4.2:** Potential energy profile of a single molecular bond. a) The equilibrium force,  $F(z)$ , is given by the first derivative (dotted curve) of the interaction potential,  $V(z)$ .  $z_0$  is the equilibrium distance of the two binding partners,  $F_{max}$  is the maximum unbinding force, and  $\Delta V_u^\ddagger$  is the activation barrier for unbinding b) As an effect of an applied mechanical force,  $F$ , the activation barrier in the dotted curve is lowered by the mechanical stretching energy,  $F \cdot (z - z_0)$ . (Adapted from [9]).

This simple model correctly predicts that the rate of bond rupture increases with the applied force, and that bond rupture forces are dependent on the intrinsic lifetime of the bond, the temperature, and on the measurement time. It is only valid if the potential energy landscape under the applied force is the sum of the original potential and the (linear) potential by the applied force with fixed unbinding length and unbinding path. Equation 33 also does not account for the stochastic nature of single bond rupture, and the model can not predict the actual distributions of measured bond strengths around the average value as they are experimentally observed. These statistical fluctuations arise from random fluctuations of the system in its equilibrium state and have to be distinguished from the previously discussed time-dependence of the average value.

In Bell's theory, all features of the energy landscape are put into one parameter - the unbinding length,  $\Delta z_u$ . To overcome this limitation, Evans (reviewed in [76]) introduced a different model for the description of bond rupture under an external force, which is based on Kramer's theory. The general solution is

$$\tau_F = \tau_o g(F) \cdot e^{-F\Delta z_u / k_B T}. \quad (34)$$

The dimensionless function  $g(F)$  describes the shift of the potential minimum and the energy maximum along the path. It is still assumed that all possible reaction paths are focused onto one by the application of an external force. Therefore, the energy landscape can be sketched one-dimensionally along the reaction coordinate.

From the transition rate  $k = 1 / \tau_F$ , the distribution of rupture forces in a stretching experiment, in which the force is increased, can be derived:

Neglecting the on-rates, the probability  $P_b(t)$  that a bond existing at time 0 is still there at time  $t$  is given by

$$\frac{dP_b(t)}{dt} = -k[F(t)]P_b(t). \quad (35)$$

Assuming that the force increases linearly in time,  $F(t) = \dot{F}(t) \cdot t$ , the time can be replaced by the force

$$\frac{dP_b(F)}{dF} = -\frac{k(F)}{\dot{F}} P_b(F). \quad (36)$$

A solution of this equation is

$$P_b(F) = \exp\left[-\frac{1}{\dot{F}} \int_0^F dF' k[F']\right]. \quad (37)$$

The probability distribution for rupture forces  $dP_b/dF$  is given by

$$\frac{dP_b(F)}{dF} = -\frac{k(F)}{A\dot{F}} \exp\left[-\frac{1}{\dot{F}} \int_0^F dF' k[F']\right], \quad (38)$$

'A' is a constant to normalize the distribution.

The probability for bond dissociation at a given force,  $F$ , is therefore the product of a dissociation rate, which increases with force and a function, which decreases exponentially with force. This gives a maximum in the force distribution curve, which increases with the force loading rate,  $\dot{F}$ . The simplest model including spontaneous bond dissociation was proposed by Bell. [75] It assumes that  $k_{off}$  increases exponentially with force

$$k_{off}(F) = k_0 e^{F/F_0}. \quad (39)$$

$k_0$  is the spontaneous dissociation rate, while  $F_0$  describes the properties of the specific bond. With this approach the distribution of rupture forces can be derived, it exhibits a peak at

$$F_{max} = F_0 \ln \left[ \frac{\dot{F}}{k_0 F_0} \right]. \quad (40)$$

This shows that at loading rates below the characteristic rate,  $k_0 F_0$ , spontaneous bond dissociation occurs faster than force application. Therefore, the maximum of the distributions of rupture forces is located at zero force if the rate of force application does not exceed  $k_0 F_0$ . [87]  $F_0$  is often expressed by the width of the unbinding potential,  $\Delta z_u$ :

$$F_0 = \frac{k_B T}{\Delta z_u}. \quad (42)$$

Therefore, the most probable rupture force can also be written as

$$F_{max} = \frac{k_B T}{\Delta z_u} \ln \left( \frac{\dot{F} \cdot \Delta z_u}{k_B T \cdot k_0} \right), \quad (43)$$

i.e. the most probable rupture force,  $F_{max}$ , depends logarithmically on the force loading rate  $\dot{F}$ . The position of the activation barrier,  $z^\ddagger = z_o + \Delta z_u$ , can be determined according to Equation 43 from the slope of the  $F$  vs.  $\ln(\dot{F})$  plot. The relationship between the detachment force and the activation barrier further suggests that dynamic force spectroscopy can be used to reveal even more details of complex potential energy surfaces of intermolecular bonds. Kinetic processes that involve complex molecules such as proteins, nucleic acids or ligand-receptor pairs may exhibit multiple local maxima and minima along the reaction coordinate. In such cases, the plot would exhibit a sequence of lines with different slopes, each one mapping the position of a particular energy barrier in the unbinding path. [76] [77] [80] The extrapolation of the different linear segments to  $F = 0$  will then differ by an amount related to the relative differences in the magnitudes of the individual energy barriers; the absolute values of multiple activation barriers can no longer be calculated directly.

### 4.3.2. Multiple Bonds in Parallel

In a recent theoretical study [88] it was shown that multiple bond rupture may cause a very complicated behavior under dynamic loading. Even as all bonds were assumed to experience the same force the dependence of the net rupture force on the number of bonds did not show an uniform behavior. It was found to be either linear, square root, or logarithmic, depending on the rigidity of the surface anchoring of the investigated polymer, the stiffness of the force probe, the reversibility of the bond and the retraction speed.

### 4.3.3. Multiple Bonds in Series

For multiple bonds in series, each bond contributes an increment in length along the direction of force on unbinding and thus the thermal force scale is lowered, i. e. it takes much less force for cooperative failure of bonds in series than for bonds in parallel. The bonds can be loaded in series or peeled apart like a zipper. If rebinding is neglected, multiple bonds have in both configurations strengths comparable to that of a single-constituent bond. [86]

The shape of the recorded force curve in unbinding experiments of multiple bonds in series strongly depends on the dynamics of the system, ranging from sawtooth patterns to long extended plateaus. This is supported by theoretical considerations,<sup>[89]</sup> which suggest that the shape of the force-extension profile for the continuous desorption of adsorbed (or bound) polymer chains from a solid substrate (Figure 4.3a) depends on the force loading rate. An important parameter determining the peak height is the natural off-rate of the monomer-surface contacts. At pulling rates much faster than the internal dynamics of the probed bonds, each monomer-surface detachment provides a peak of a saw-tooth pattern (Figure 4.3b). As discussed before, the peak heights are reduced for lower pulling rates. For pulling rates much slower than the natural unbinding and rebinding rates this results in a flat plateau of constant force (Figure 4.3c). Typically, unbinding peaks are therefore observed for covalent bonds, [35] but also for most specific ligand-receptor bonds [74] [90] [91] [92] coordination complexes, [93] [94] and for the rupture of protein domains. [23] [95] Accordingly, continuous desorption plateaus of constant force are observed in experiments where the polymer is only very weakly adsorbed or bound via ionic bonds, such as for polyelectrolytes adsorbed to charged substrates [51] [6] [96] and for the unzipping of DNA.[97] In such cases, the on-off-dynamics of individual bonds is typically much faster than the applicable stretching rates (5 - 3000 nm/s). Thus, the continuous unbinding process of several bonds in series is investigated under true equilibrium conditions.

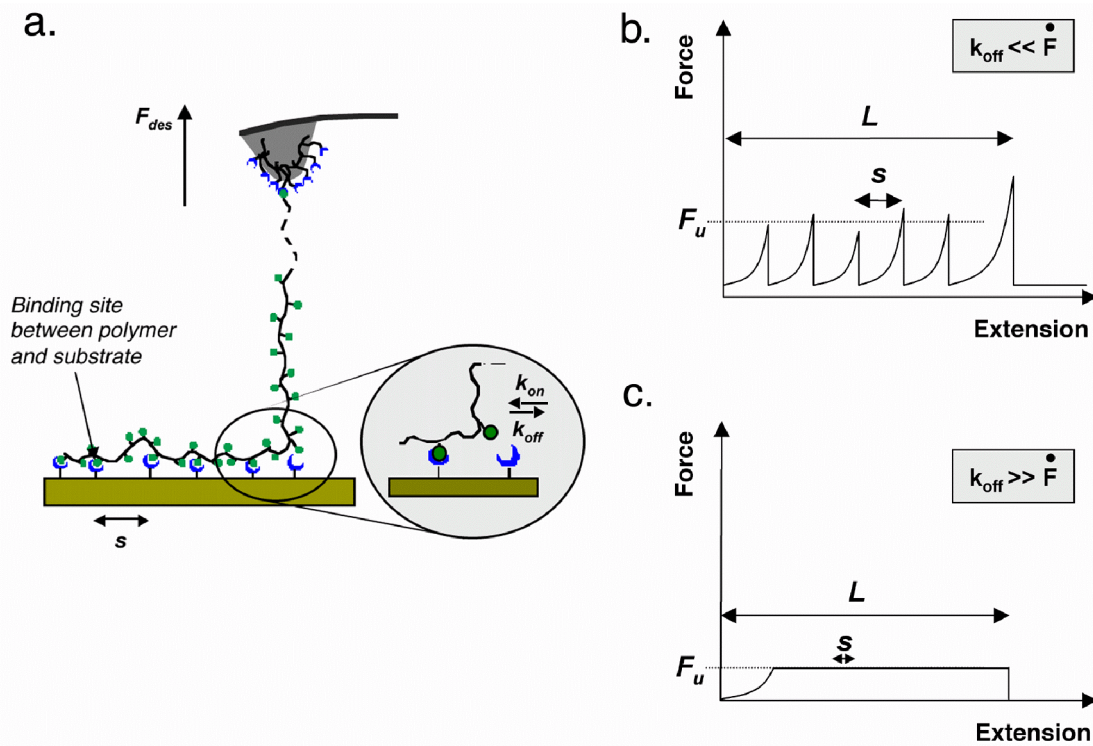


**Figure 4.3:** Schematics for the desorption of polymer chains from solid substrates (a). Depending on the relative magnitudes of the force loading rate,  $\dot{F}$ , and the internal (un-)binding dynamics of the surface attachment sites (bonds), quantified by the intrinsic on- and off-rate constants  $k_{on}$  and  $k_{off}$ , the force-distance profile recorded upon polymer desorption forms a saw-tooth pattern with individual peaks of distance,  $s$ , related to individual bond rupture (b), or plateaus of constant force with lengths related to the lengths,  $L_i$ , of the desorbing polymer chains (c). (Adapted from [9]).

#### 4.4. Polyelectrolyte Adsorption and Desorption

Typical example systems with multiple weak bonds (in parallel) are charged polymers adsorbed onto silica surfaces. The interaction between charged polymers and surfaces has implications for numerous industrial processes, among them the coating of fibers in paper industries, waste-water treatment, mineral processing, and chromatographic separations. Obviously, this is also connected to understanding the physics of charged biomolecules, charged proteins, and nucleic acids.

The theoretical treatment of polyelectrolytes in solution is not very well established because of the delicate interplay between the chain connectivity and the long range nature of electrostatic interactions. [98] This is even more complicated when charged chains in solution are adsorbed to charged surfaces, which is reviewed in [29].

The important parameters are the fraction of charged monomers, the surface charge density, the amount of salt, and in some cases the solution pH. The repulsive electrostatic interaction between monomers leads to an effective stiffening of the chain, which favors the adsorption

of the chain as less entropy is lost, but opposes the formation of a dense adsorption layer close to the surface. Three parts of the adsorbed polymer are distinguished: 'trains' are defined as regions of the polymer chains which are bound to the surface, while 'loops' are unbound regions of the chain in between two such bound trains. Finally, 'tails' are non-adsorbed or free chain ends.

The role of salt is given by the Poisson-Boltzmann equation. It is based on a mean-field calculation, taking the local ion concentration from a Boltzmann distribution

$$\rho_m(r) = c_0 e q e^{-\beta q e \phi(r)} - c_0 e q e^{+\beta q e \phi(r)}, \quad (44)$$

with the valency,  $q$ , of the ions, the elemental charge,  $e$ , the bulk salt concentration,  $c_0$ , the inverse of the thermal energy,  $\beta = (k_B T)^{-1}$ , and the electrostatic surface potential,  $\phi(r)$ .

Combining this Boltzmann equation with the Poisson equation yields

$$\Delta \phi(r) = -\frac{\rho(r)}{\epsilon} = \frac{c_0 e q}{\epsilon} (e^{\beta q e \phi(r)} - e^{-\beta q e \phi(r)}). \quad (45)$$

This equation is exactly solvable only for a planar charged wall: [99]

$$\frac{\phi(r)}{k_B T} = \frac{2}{e} \ln \left( \frac{1 - \gamma e^{-\kappa r}}{1 + \gamma e^{-\kappa r}} \right) \quad (46)$$

The constant  $\gamma$  is determined by the electric surface field, which is proportional to the surface charge density,  $\sigma$ , and the inverse of the Gouy-Chapman length,  $\lambda$ : [99]

$$\left. \frac{e}{k_B T} \frac{d\phi_p(r)}{dr} \right|_{x=0} = \frac{4\gamma\kappa}{1-\gamma^2} = \frac{e\sigma}{\epsilon k_B T} = \frac{2}{\lambda} \quad (47)$$

The value for  $\gamma$  is:

$$\gamma \approx \begin{cases} 1/2\lambda\kappa & \text{for } \lambda\kappa \gg 1 \\ 1 - \lambda\kappa & \text{for } \lambda\kappa \ll 1 \end{cases} \quad (48)$$

The asymptotic behavior of the potential is then: [99]

$$\frac{e\phi(r)}{k_B T} = \begin{cases} -4\gamma e^{-\kappa r} & \text{for } \lambda\kappa \gg 1 \text{ or } r \gg \kappa^{-1} \\ 2\ln\left(\frac{\lambda\kappa}{2}\right) + 2\ln(1+r/\lambda) & \text{for } \lambda\kappa \ll 1 \text{ and } r \ll \kappa^{-1} \end{cases} \quad (49)$$

The first limit corresponds to the Debye-Hückel regime, where the screening length is sufficiently short so that nonlinear effects can be neglected. This result is also obtained by linearizing Equation 45, which results in the Debye-Hückel equation:

$$\Delta \phi(r) = \kappa^2 \phi(r) \quad (50)$$

It is valid if the electrostatic potential acting on an elementary charge is smaller than  $k_B T$ , i.e. for  $\beta e q \phi(r) \ll 1$ . This applies for a wide range of salt concentrations and surface potentials of roughly less than 25 mV. The second limit is the Gouy-Chapman regime, where the Debye-Hückel approximation breaks down close to the charged surface.

With divalent or trivalent ions and surface charge densities of more than  $1 \text{ nm}^{-2}$  the limit of strong coupling is reached. This limit was approached by field-theory [100] and, like the Debye-Hückel approximation, leads to an exponential density profile but with a different density contact value.

At very short distances from the surface **van der Waals interactions** become relevant. They are universal, exist in all systems and their interaction energy is proportional to  $r^{-6}$  at small and intermediate distances of separation (from an Angström to several nm). [101] The following three contributions can be distinguished: [65]

- Keesom interaction (dipole orientation force): This is the Boltzmann-averaged interaction between two permanent dipoles.
- Debye induction force: This is the interaction between one permanent and one induced dipole.
- Dispersion force, also known as London force, charge-fluctuation force, electrodynamic force, and induced-dipole-induced-dipole force: It acts between all atoms and molecules, even totally neutral ones, as it describes the interaction between two induced dipoles. The force is quantum mechanical (in determining the instantaneous, but fluctuating dipole moments of neutral atoms), but still essentially electrostatic - a sort of quantum mechanical polarization force. [65] E.g. for the interaction of two Bohr atoms:  $w(r) = -C/r^6 = -3/4 \alpha_0^2 h\nu / (4\pi\epsilon_0)^2 r^6$ .

Dispersion forces probably are the most important contribution to the total van der Waals force between atoms and molecules, which is unified in the London equation. [65]

Hamaker [102] showed that the attractive van der Waals force is directly proportional to a constant  $A_H$ , since called the Hamaker constant, which depends only on the nature of the material:  $A_H = \pi^2 C \rho \rho'$  ( $\rho$  and  $\rho'$  are the number densities of the two interacting bodies). For example, for a sphere interacting with a surface, the interaction energy is given by  $E_{\text{int}} = -A_H R/6D$ , [65] (for  $D \ll R$ ) where  $R$  is the radius of the sphere and  $D$  the distance between sphere and surface.

There is a huge amount of theoretical and experimental work on the thickness and (charge) density of the adsorbed layer, usually based on the Debye-Hückel approximation (see Borukov, [98] Netz, [103] and references therein). The conformation of an adsorbed polymer

chain is determined by the interplay of enthalpic and entropic terms. Depending on the experimental conditions during the adsorption process, a polyelectrolyte chain may be found to lie perfectly flat and homogenous on the oppositely charged surface so that all charges are located in the energy minimum at the surface. In other cases in which the interaction between the polymer and the substrate is weaker (or screened), the surface-adsorbed polymer may form 'loop' and 'train' configurations at the interface. [65] Most of the polyelectrolyte's charges are then located at a certain distance from the substrate at a higher energy, which is compensated for by a gain in entropy.

The separation of single polyelectrolyte chains by force from a charged substrate in aqueous environment provides useful insight into the molecular mechanism behind the adsorption process. [104] [51] [6] [96] From the desorption experiments performed in this work a simple new model to describe the desorption of single molecules from solid substrates arose and is discussed in Section 8.2.

## 4.5. Transitions and Energy Conversion within Single Molecules

A general definition of a phase transition is, that in the thermodynamic limit the free energy per volume<sup>7</sup> as a function of its order parameters (temperature, magnetic field, etc.) becomes non-analytical. The thermodynamic limit is reached for  $V \rightarrow \infty, N \rightarrow \infty$  and constant intensive parameters. Typical thermodynamic observables like temperature, pressure or free energy, are only well-defined in this limit. Also phase transitions with their singularities in thermodynamic observables strictly only exist with infinitely many degrees of freedom – otherwise long-ranged correlations are not possible. [105] Therefore, most transitions are extensively studied and described in bulk, which is a good approximation for large systems with many degrees of freedom.

The single molecule techniques developed in the past 15 years and recent theoretical advances made it possible to investigate transitions in single molecule systems. Especially interesting are reversible transitions, which can be triggered externally and are accompanied by a considerable change in the mechanical properties; this makes them potential candidates for single molecule machines. In this thesis two such systems are extensively studied on the single molecule level and described in detail: The inverse temperature transition in polypeptides and the optomechanical transition in polyazopeptides. To understand the inverse temperature transition the idea of hydration water is important.

---

<sup>7</sup> Or any other thermodynamic potential, as in the thermodynamic limit all potentials are equivalent.

### 4.5.1. Hydration Water

An overview of the historical knowledge about hydration water is given in [11] starting with the observations by Edsall and Butler in 1935 and 1937 via the explanations of Frank and Evans (1945, "icebergs"), Kauzmann (1959, "hydrophobic bond"), and Teeter (1984, "pentagonal arrangements of water"). The picture of hydration water is still far from being complete. There is agreement about the higher density and greater order of this water, but especially the thickness of the hydration layer is still controversially discussed. Therefore, in the following some recent findings are summarized:

#### a) Thickness

The reported values of the thickness of the hydration layer vary from a few Angström to several nanometers:

- Molecular dynamics simulations [106] explain recent x-ray and neutron solution scattering data on the lysozyme hydration water [107] by a 3 Angström thick first hydration layer.
- Pal et al. [108] state that at a distance of about 0.7 nm essentially all trajectories are bulk-type. They measured the solvation time for the dynamics of hydration at the surface of an enzyme and found that it is more than an order of magnitude slower (38 ps) than in bulk water (1 ps). This is attributed to a dynamic process with two general types of trajectories, those that result from weak interactions with the surface site, giving rise to bulk-type solvation and those that have a stronger interaction, enough to define a rigid water structure with a much slower solvation time.
- Urry et al. [11] measured the microwave dielectric relaxation data. It shows an intense relaxation at about 5 GHz which is attributed to hydrophobic hydration water. The amount of this water (100 and more molecules per pentamer) speaks in favor of a several nanometer thick layer of ordered molecules undergoing a small entropy and heat change in becoming bulk water.
- Interfacial water dielectric-permittivity-profile measurements using atomic force microscopy reveal a thickness of several nm for the hydration layer on mica. [109]

#### b) Density

Svergun et al. [107] combined small-angle x-ray scattering in water with that of neutrons in water and D<sub>2</sub>O. The density of the hydration water was measured to be about 15% higher than in bulk water, mainly because of a geometrical effect caused by the definition of the surface. Two thirds of this effect would therefore even arise if the water density was not at all perturbed by the presence of the protein lysozyme. However, on top of this effect is about a 5% density increase caused by perturbation of the average water structure from bulk water. About half of this density increase arises from shortening of the average water-water distances and the other half arises from an increase in the coordination number.

### c) Effect of Charges

Molecular dynamics simulations <sup>[110]</sup> show that the presence of a charged solute can disrupt the 'hydrophobic contact bond' between two neighboring apolar solutes by forcing them towards a different configuration. This effect is larger for negatively charged solutes, because the hydrogen atoms of the water molecule can reach closer to the solute than the negative oxygen of water in the case of the positive solute. The hydration shells of the negatively charged solute are expected to be hardly compatible with optimal configurations of water molecules around hydrophobic solutes, and to have a disturbing effect on them. This is consistent with MD simulations by Chandra et al.<sup>[111]</sup>, which show that the average number of hydrogen bonds per water molecule decreases with increase of ion concentration.

Bakk et al. <sup>[112]</sup> describe apolar and polar protein hydration data with high accuracy over a broad temperature range (5-125°C). They use an ice-like shell analogy for the hydration of apolar surfaces, which is modeled as an increase number of hydrogen bonds compared with bulk water. The hydration of polar surfaces is modeled as a lack of hydrogen bond compared with bulk water. In addition the dipolar water molecules are supposed to be strongly bound to ionic and polar parts along the protein surface.

Finally, Urry gives a model of the hydrophobic hydration water and its destruction by heat or electric charges (Figure 4.4).

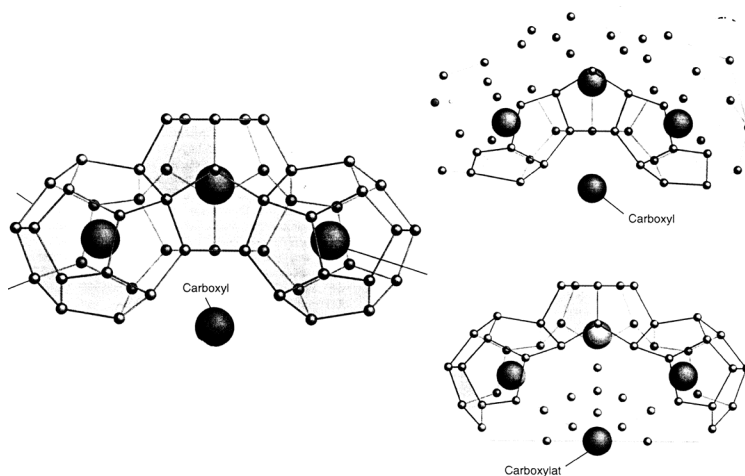


**Figure 4.4:**

*In the vicinity of hydrophobic parts the water molecules are ordered via hydrogen bonds to a pentagonal structure (left). On heating this low energy state is destroyed (top). Charged hydrophilic groups can also destroy the water structure (bottom). (Adapted from [113]).*

### 4.5.2. Inverse Temperature Transition

Most knowledge about the inverse temperature transition was obtained by Urry and coworkers from bulk measurements in aqueous solution with the polypeptide elastin. It was reviewed in <sup>[11]</sup> and is summarized in the following.

The inverse temperature transition is a hydrophobic folding and assembly transition, it occurs when the temperature is raised above a critical onset temperature,  $T_t$ .

This is also observed in polymers with a lower critical solution temperature (LCST) behavior, like e. g. PNIPAM (Poly(N-isopropylacrylamide)). [114] The difference is that the state above  $T_t$  in elastin is an ordered state that still holds a considerably large amount of water, while LCST-polymers undergo a hydrophobic collapse to a random state holding little water (such a state is also finally reached in elastin after denaturation at elevated temperature).

All polymers with the correct balance of apolar and polar moieties including water soluble proteins and protein-based polymers, increase their order in such a hydrophobic folding and assembly transition as the temperature is raised above  $T_t$ . Usually, in warm-blooded animals temperature is not raised to achieve the folding transition, but instead the temperature at which the folding occurs is lowered from above to below physiological temperature in order to drive folding and function. This allows for energy interconversion in between many different forms.

The inverse temperature transition is best described, analyzed, and classified by the temperature  $T_t$  at which the hydrophobic folding and assembly transitions occurs. The Gibbs free energy difference,  $\Delta G$ , of a system is  $\Delta G = \Delta H - T\Delta S$  with the enthalpy,  $H$ , the temperature,  $T$ , and the entropy,  $S$ . At the transition temperature  $T_t$  the change in enthalpy,  $\Delta H$ , equals the change in entropy,  $\Delta S$ , times temperature and the change in Gibbs free energy is zero, which results in

$$T_t = \Delta H / \Delta S. \quad (51)$$

Therefore,  $T_t$  is a relative measure for the amount of water of hydrophobic hydration that changes to bulk water during the transition. For convenience,  $T_t$  is taken as the readily measured temperature for the onset of turbidity, i.e., for the onset of the aggregational phenomenon of the transition on raising the temperature. [11]  $T_t$  of a system can be manipulated mechanically, by pressure, electromagnetic radiation, electrically, chemically or thermally. [11] This mechanism of driving hydrophobic folding and assembly in order to achieve diverse energy outputs, is descriptively called the  $\Delta T_t$ -mechanism. [19]

On raising the temperature of these protein-based polymers in water, the more ordered water surrounding the hydrophobic moieties becomes less ordered bulk water. This positive entropy change is larger in magnitude than the negative entropy change due to the polypeptide part of the system becoming more ordered. Therefore, the  $T_t$ -transition can also be described by the change in the amount of hydrophobic hydration water,  $N_{hh}$ . An example is given in Figure 4.5, where  $N_{hh}$  of poly(GVGVP) is shown in comparison to the slightly more hydrophobic poly(GVGIP).

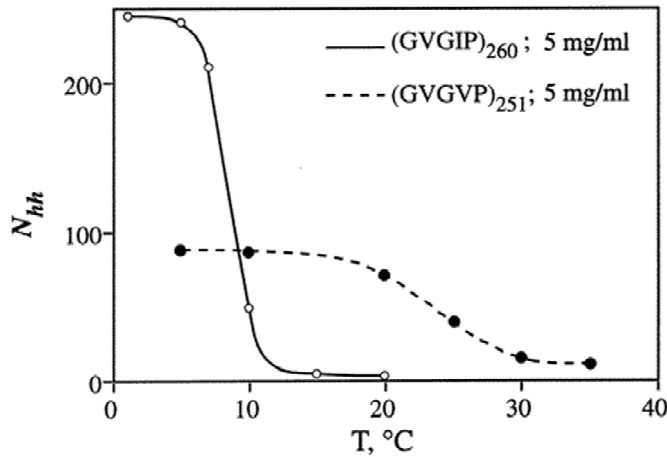


**Figure 4.5:**

*Amount of water of hydrophobic hydration  $N_{hh}$  for poly(GVGVP) and poly(GVGIP). (Adapted from [11]).*

This transition can be used to define a  $T_t$ -based hydrophobicity scale. [19]

### 4.5.3. Optically Induced Transitions

Photons have been proposed as an ideal primary energy source for the design of synthetic molecular machines, because their application is fast, well controlled, and clean, i.e. it does not result in byproducts if used moderately. [115] Especially reversible transformations in chemical species induced by photoexcitation, have attracted much attention owing to their high potential for application into various optoelectronic devices, such as optical memory, photooptical switching, and display. [12] [116-119] In this section the basic parameters and coefficients for the interaction of electromagnetic waves with matter are given:

#### Absorption Coefficient $\alpha$

The intensity  $I(\nu, z)$  of a electromagnetic wave with frequency  $\omega$  crossing a medium in  $z$ -direction is given by the Lambert absorption law [120]

$$I(\nu, z) = I(\nu, 0) \cdot e^{-\alpha(\nu)z}. \quad (52)$$

The frequency dependent absorption coefficient,  $\alpha(\nu)$ , gives the reciprocal distance, at which the intensity,  $I(\nu, z)$ , is reduced to  $I(\nu, 0)/e$ . As the absorption is basically determined by the number of absorbing atoms or molecules in the beam, Beer found that  $\alpha(\nu)$  is linearly dependent on the concentration. [120]

#### Extinction Coefficient $\epsilon$

The intensity of radiation in a medium can decrease because of two reasons. The radiation can be absorbed, i.e. converted into another form of energy, or it can be scattered. Both absorption and scattering together are called extinction. The extinction coefficient in principle is defined like the absorption coefficient, but care has to be taken with the units, as  $\epsilon$  is defined as  $\log(I_0/I) = \epsilon c z$ . [121] Therefore the linear dependence on the concentration  $c$  is not included in

the extinction coefficient, decadic instead of the natural logarithm is used and  $\epsilon$  is defined per mole of a material and not per molecule. It is the interaction cross-section which a mole of a material has for absorption and scattering. The units are:  $[\text{M}^{-1}\text{cm}^{-1}] = [\text{mol}^{-1}\text{cm}^{-1}\text{ liter}]$ . [122]

For the (4-amino)phenylazobenzoic acid (AMPB) peptide in DMSO averaged values for the extinction coefficient are: [122]

trans ( $\sim 369$  nm,  $\pi\pi^*$ ):  $3 \cdot 10^4 \text{ M}^{-1} \text{ cm}^{-1}$ ,

cis ( $\sim 449$  nm,  $n\pi^*$ ):  $3 \cdot 10^3 \text{ M}^{-1} \text{ cm}^{-1}$ .

Where  $\pi\pi^*$  describes excitation from a binding to an unbinding  $\pi$  orbital, while  $n\pi^*$  is the excitation from a  $\sigma$  to an unbinding  $\pi$  orbital.

### Quantum Yield $\eta$

The original definition of the quantum yield comes from the photoeffect, where it is defined as  $\eta = n_e/n_p$  with the number of photons interacting with the medium,  $n_p$  and the number of photoelectrons,  $n_e$ . [120] Here, in the case of an optically induced transition,

it is defined as 
$$\eta = \frac{\text{number of switching events}}{\text{number of absorbed photons}}$$

where a switching event is either a transition from the cis to the trans state of the azobenzene or from the trans to the cis state. Values for the photoisomerization of azobenzene in various solvents (n-hexan, ethanol, acetonitrile) are: [12] [123]

for trans  $\rightarrow$  cis in  $\pi\pi^*$ :  $\eta_{t-c} = 0.1 - 0.2$ ,

and cis  $\rightarrow$  trans in  $n\pi^*$ :  $\eta_{c-t} = 0.45 - 0.68$ .

### Interaction Cross-section $\sigma$

The original definition of the interaction cross-section comes from scattering theory, where it is defined as the surface area around an atom, through which a particle has to pass in order to be scattered by a detectable angle. [124] In the case of optical excitations, it is the surface area around a molecule, where a transmitted photon excites this molecule. It is given in terms of the extinction coefficient,  $\epsilon$ , and Avogadro's number,  $N_A$ , by

$$\sigma = 2.3 \epsilon / N_A. \quad (53)$$

#### 4.5.4. Optomechanical Transition in Azobenzene

An extensively studied photoinduced molecular process is the trans-cis (or E-Z-) configurational transition of double bonds, such as found in the stilbene or the azobenzene moiety. The isomerization between the more extended (trans) and the shorter (cis) configurations of azobenzene is reversibly triggered at two different wavelengths of light, and thus allows various applications as a light triggered switch. [125] [12] It has been the basis for the first artificial examples of light-driven ion transport through membranes, [126] and has since been frequently used for synthetic photoresponsive systems regulating the geometry and function of biomolecules [127] [128] [129] and organic materials, [118] [16, 119, 130] as well as supramolecular complexes. [131-133]

In addition, the reversible geometrical change (lengthening and shortening) of the azobenzene chromophore upon photoisomerization may result in significant photomechanical effects, which has been demonstrated for azobenzene polymers in bulk. [134-139] The ability to convert optical excitation energy into molecular motion thus makes photochromic molecules such as azobenzene highly promising for the development of synthetic molecular level machines. Such light triggered morphological changes are already utilized by our body, e.g. when rhodopsin absorbs light, its retinal component undergoes photoisomerization accompanied by a change in conformation of opsin. This light-induced conformational change is a trigger which excites the nerve cells of the rods of the retina. [15] [16]

Optomechanical transitions are still under investigation and there is no complete conclusive picture yet. Therefore, the following might be restricted to the azobenzene system, which is the best investigated optomechanical single molecule system.

Azobenzene exists in a cis or a trans configuration which can be selectively excited as the absorption spectrum in the visible and near UV is determined by low lying ( $n\pi^*$ ) bands between  $\lambda = 380$  nm and  $\lambda = 520$  nm and the ( $\pi\pi^*$ ) bands at 330 nm (trans) and  $\lambda = 275$  nm (cis) (Figure 4.6). The first excited states equilibrate with about equal probability to the cis and trans state. From studies performed on azobenzene [12] as well as on peptides containing the AMPB moiety [122] [140] it is known that cis / trans photoisomerization of the azobenzene unit is reversible upon irradiation at  $\lambda = 365$  nm and  $\lambda = 450$  nm, respectively. However, because of the spectral overlap of the excitations of *cis*- and *trans*-azobenzene isomers, complete photoisomerization upon optical pumping is not possible. The maximum populations that are typically obtained in azobenzene-containing peptides are 70% to 80 % of the *trans*- and *cis*-azobenzene isomer. [141]

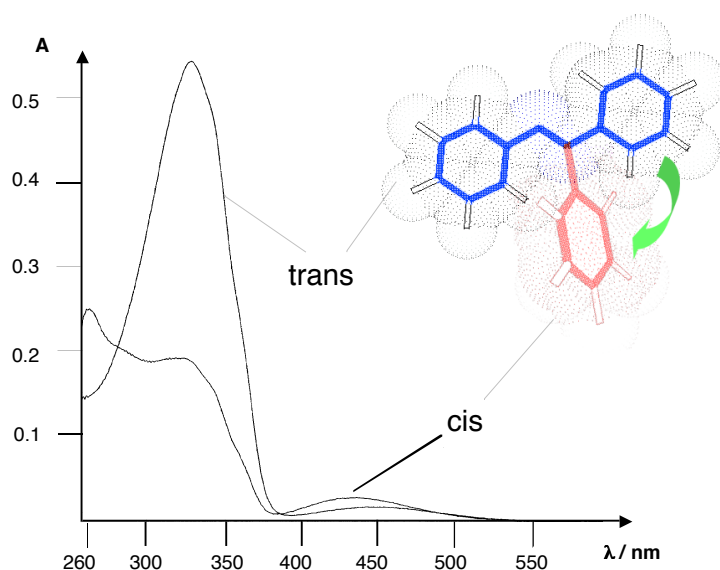


**Figure 4.6:**  
*UV-Vis spectrum of the azobenzene tripeptide monomers containing (4-aminomethyl) phenylazobenzoic acid (AMPB) in the saturated trans and cis state.*

The length difference in the end-end distance of a single azobenzene unit between the cis and the trans states,  $\Delta l$ , was calculated in ab initio quantum mechanical calculations using the INSIGHT II software package:  $l_{\text{trans}} \approx 1.9$  nm,  $l_{\text{cis}} \approx 1.65$  nm, and therefore  $\Delta l \approx 0.25$  nm. Thus, assuming a symmetric potential the unbinding length,  $\Delta z^* \approx 0.13$  nm. As described above, the spectral overlap of the excitations of cis and trans configurations limits the photochemical switching of polyazopeptides to shifting the average configurational populations between the two limits  $\sim 80\%$  trans and  $\sim 75\%$  cis state. [122] From this, we may give an average monomer length in the polymer's saturated trans state as  $\langle l_{\text{trans}} \rangle \approx 1.85$  nm and in the saturated cis state,  $\langle l_{\text{cis}} \rangle \approx 1.71$  nm, which corresponds to an average contraction of  $\langle \Delta l \rangle \approx 0.14$  nm per monomer.

A simplified one dimensional energy scheme along the inversion pathway is given in Figure 4.7. The relevant configurational coordinate is the bond angle,  $\phi_{\text{NNC}}$ , which changes from about  $-60^\circ$  to about  $+60^\circ$ .  $S_0$  is the singulett electronic ground state and  $S_x$  an excited state. At 365 nm ( $\pi\pi^*$ ) the molecule is excited into the second excited state  $S_2$ , from where it relaxes to the ground state via the first excited state  $S_1$ . At 420 nm ( $n\pi^*$ ) the molecule is directly excited to the first excited state.

For AMPB peptides in DMSO an activation energy barrier for thermal re-isomerization from the cis- to the trans-isomer of  $\Delta G^* = 44 \pm 2$   $k_B T$  has been determined. [122] The experimentally determined lifetime of the *cis*-azo configuration at 301 K is 120 h. [122]

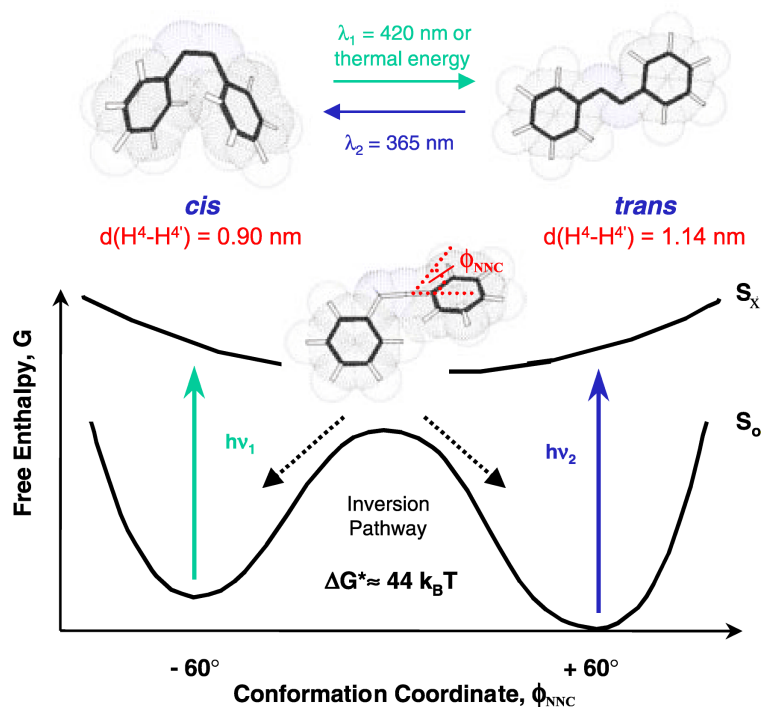


**Figure 4.7:** Schematics of the potential energy landscape of azobenzene along the inversion pathway (see text for further details).

Further knowledge about the azobenzene system comes from femtosecond spectroscopy measurements, which are performed in the groups of Zinth and Wachtveitl. In these experiments absorbance changes in dependence on the delay time between the 'pump' and 'probe' pulse are measured. In addition, the dependence on the wavelength is probed. The decay of the absorbance change with time is then described by (multiple) exponentials. The decay times of these exponentials are called components. For the photoproduct formation of azobenzene depending on the solvent and the direction of the isomerization a dominant component of several hundred femtoseconds, and weak components of a few picoseconds and about 10 picoseconds are found (the last component is assigned to the cooling of the 'hot' ground state). [142] [123] Experiments with cyclic azopeptides (one azobenzene unit and eight amino acids) revealed that substantial conformational transitions in this compound proceed on the time scale of 50 ps. [143] These results demonstrate that the photoisomerization in azobenzene and probably also conformational transitions in the utilized polyazopeptide occur on time scales which cannot be resolved in a single molecule force experiment.<sup>8</sup>

The pathway of the photoisomerization is still under discussion. Dependent on the excitation wavelength two different pathways are proposed: [123] For an excitation in  $n\pi^*$  an inversion mechanism and for an excitation in  $\pi\pi^*$  a rotation around the N-N axis are assumed. Potential energy curves of the ground state and the first two excited states of azobenzene along the inversion pathway were calculated 1982 by Monti et al. [144] and along the rotation pathway 1984 by Rau. [145] A schematic representation of these calculated potential energy surfaces is

<sup>8</sup> The resonance frequencies of the used cantilevers were below three kHz in DMSO.

---

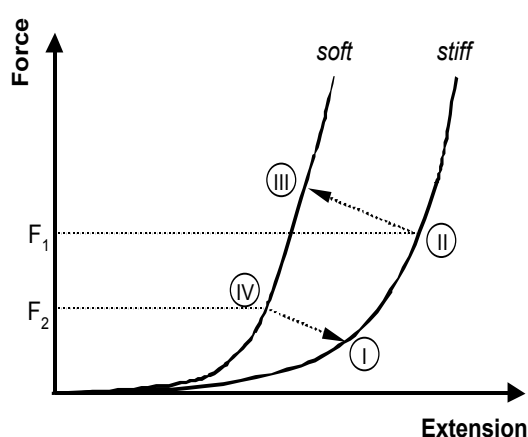
given in [12] [142] [123]. Newer calculations including an applied mechanical force are just being performed and discussed by R. Netz and H. Grubmüller in response to the measurements performed in this thesis.

## 5. Polyelectrolytes

### 5.1. Elasticity of Polyvinylamine

The experiments on the elasticity of polyelectrolytes were driven by two aims:

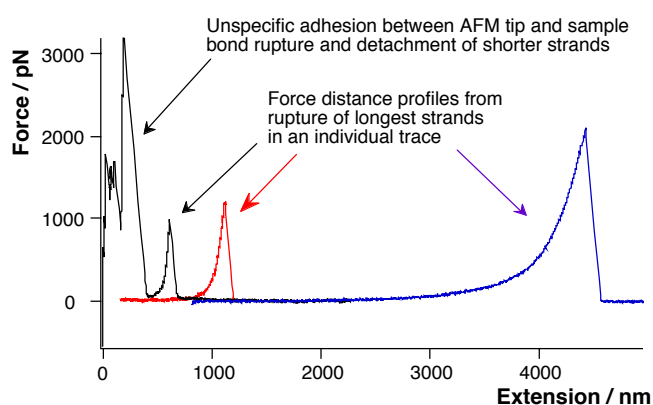
- As mentioned in Section 4.1 and 4.2, the theoretical description of force-extension traces on single (charged) polymers was and is still under discussion. The single molecule data on polyvinylamine with varying line charge density should prove or falsify theories and inspire new theoretical approaches.
- Switching the persistence length and segment elasticity of a polyelectrolyte by changing the electrolyte concentration could be the basis for a single molecule machine as depicted in Figure 5.1. From OSF-theory the polyelectrolyte stiffness should change considerably upon changing the electrolyte concentration (Debye-length  $\kappa^{-1}$ ).



**Figure 5.1:**

*Schematics of a force-extension trace of a single polyelectrolyte in an extended 'stiff' and a coiled 'soft' state. The polymer is in an extended state (e. g. low salt) and stretched from I to II. Then on lowering the salt concentration, the system should be driven from state II to III (if  $F_1$  is not too high). The succeeding relaxation of the polymer brings it to state IV, from where an increase in salt concentration could bring the polymer back to state I.*

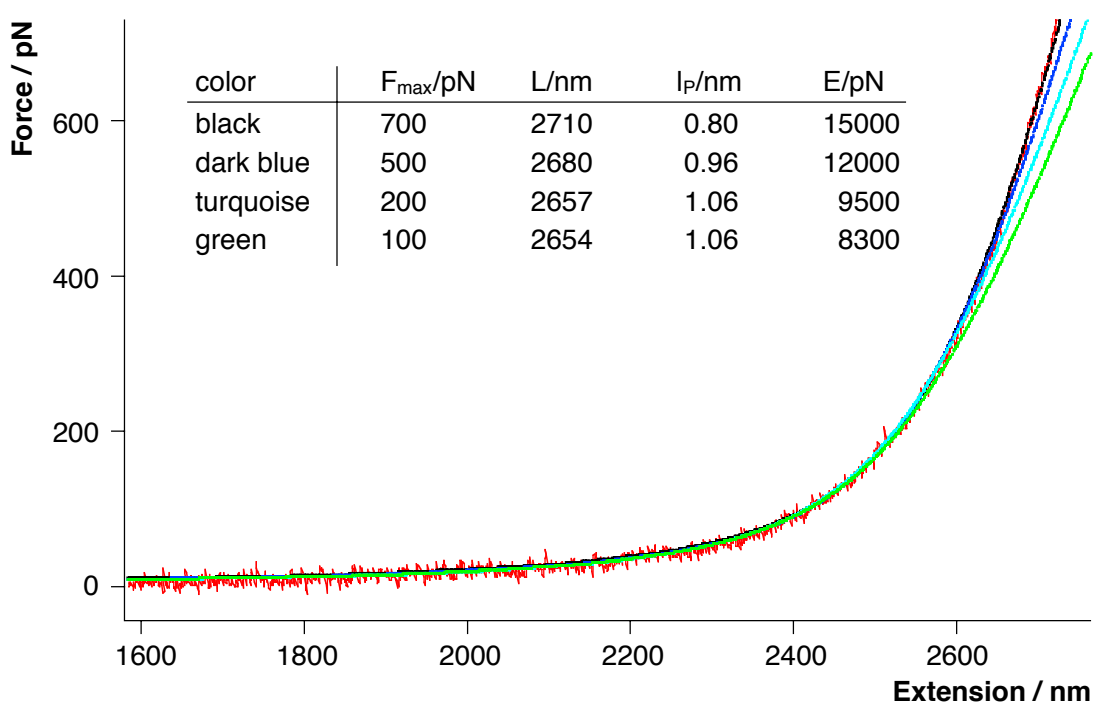
Many force-extension traces at various salt concentrations were obtained on the polyvinylamine specimen. In Figure 5.2 some examples are given.



**Figure 5.2:**

*Elastic behavior of PVA(50%) covalently fixed between glass substrate and AFM tip. Three typical traces of individual strands of different contour length are shown. At short distances, the profiles are dominated by a strong adhesive forces which is only illustrated in the black trace. (Adapted from [6]).*

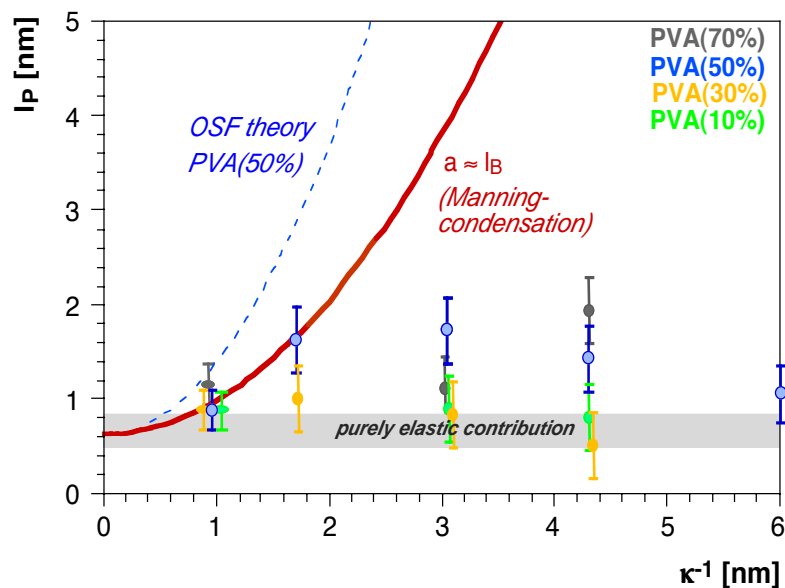
To identify single strand rupture, the extension for all traces measured at equal conditions was set to  $z_{\text{rel}} = 1$  at a force of 200 pN. A clear straight rupture was an additional criteria for a single polymer strand. Some single-molecule traces were then fit with the FJC and the WLC-model. They both did not fit the PVA-traces satisfying over the whole force range. The parameters varied sometimes by more than 50% when the fit-range was varied. In Figure 5.3 four WLC-fits to a single trace are shown.<sup>9</sup> The only difference is the maximum force to which the WLC-formula was fit. It can be seen, that no parameter stays constant, that the elasticity varies by almost 100% and also the persistence length varies by more than 20%. A shift in the baseline (zero force) by one or two pN (which is the uncertainty there) gives an additional error of about 20%. For short molecules the uncertainty in the zero extension also affects the parameters considerably.



**Figure 5.3:** *WLC-fits to PVA(50%) at 40 mM NaCl. The four WLC-fits were performed to different maximum forces ( $F_{\text{max}}$ ). The obtained parameters contour length ( $L$ ), persistence length ( $l_p$ ) and elasticity ( $E$ ) are given in the figure.*

In order to obtain at least roughly consistent values, all fits were performed to a force of 200 pN at as many traces as possible. In Figure 5.4 the measured persistence length,  $l_p$ , for different polyvinylamines in dependence on the Debye screening length,  $\kappa^{-1}$ , is given. For PVA(50%), the measurement could be performed with a single cantilever on one day. Therefore, for this polymer the dependence of the persistence length on the Debye screening length calculated from OSF-theory with (bold line) and without (dotted line) Manning condensation is given for comparison. For less charged polymers the theoretical curve is less steep (but still quadratic).

<sup>9</sup> The FJC usually fitted the data less well, therefore consistently the WLC-fit was utilized.

**Figure 5.4:**

*Dependence of the persistence length,  $l_P$ , of polyvinylamine (as obtained from WLC fits) on the Debye screening length,  $\kappa^{-1}$ .*

*Theoretical predictions according to OSF theory are shown for PVA(50%) as dotted and solid curves. The solid curve corresponds to the 'Manning limit' considering counterion condensation ( $a \approx l_B$ ).*

The measurements show no strong dependence of the persistence length on the Debye screening length and the line charge density. For the measurement on PVA(50%) the persistence length first increases with decreasing salt concentration (i.e. increasing  $\kappa^{-1}$ ) and approaches then a constant value – or even decreases. The other PVAs have a higher systematic error, as different cantilever and substrates had to be used for each data point. Their behavior is not as pronounced, but in principle PVA(10%) and PVA(30%) show a similar behavior. For the highly charged PVA(70%) there is too few data to give a firm statement, but it clearly also does not show the behavior predicted by OSF-theory.

## 5.2. Desorption of Polyvinylamine from Solid Substrates

The potential of the AFM technique to measure the desorption forces of individual polymer chains from supporting substrates has been demonstrated recently for polyelectrolytes and polysiloxanes on quartz. [104] [51] [6] [96] However, the exact interpretation of the molecular interactions governing polymer desorption is often not straightforward, and several contributions add to the overall interaction forces probed in AFM experiments. [6] [9] In addition a better understanding of the manipulation of adhesion / desorption properties are a prerequisite for the development of many future molecular devices.

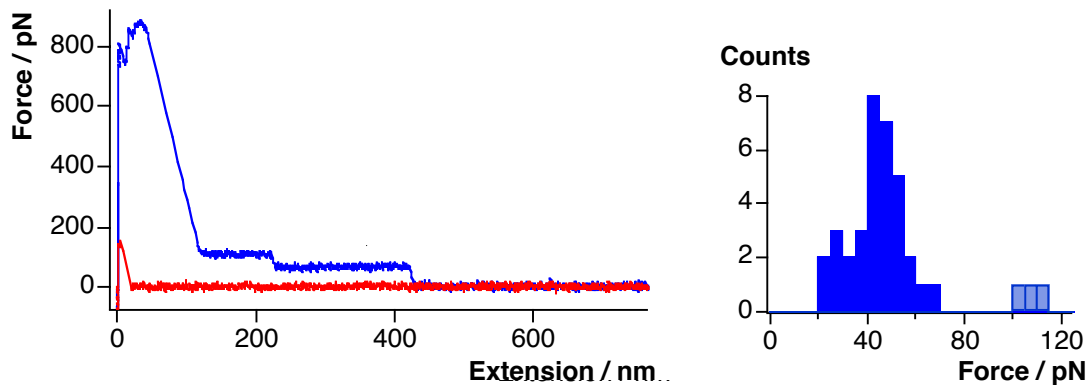
With the investigated polyvinylamines, three relevant parameters concerning the coulomb interaction of a single polymer chain with a solid substrate could be varied:

- Varying the salt concentration allows adjusting the Debye screening length,  $\kappa^{-1}$ .
- The different polyvinylamines allow for variations in the line charge density,  $\tau$ .

- Different substrates allow for the variation of surface properties like the surface charge density,  $\sigma$ , and the van der Waals interaction.

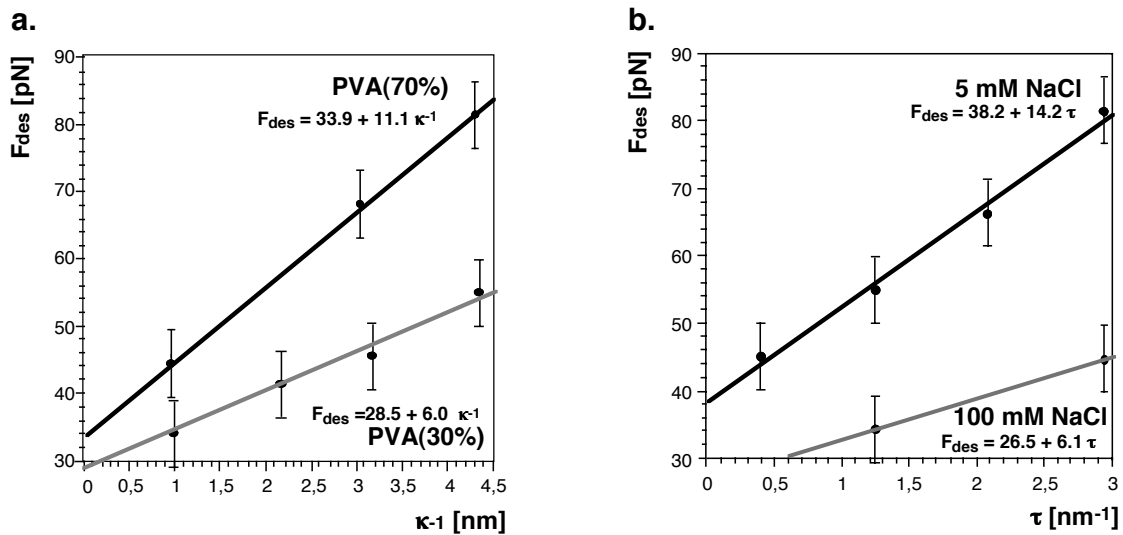
The force-extension traces of molecules physisorbed to the substrate and covalently linked to the cantilever show unspecific adhesion (Section 10.3), little rupture peaks and plateaus of constant force. The plateaus of constant force had about the same height within one experiment and varied with the conditions of the experiment (salt, line charge density, surface), therefore they were investigated in detail.

Figure 5.5 shows an example of a force-extension trace with two plateaus of PVA(30%) in 20 mM NaCl. On the right the histogram of the plateau heights under these conditions is shown.



**Figure 5.5:** Force-distance profile measured upon desorbing PVA(30%) chains in aqueous solution (20 mM NaCl) from a glass substrate (left). Histogram of the plateau heights, the three bright blue counts are interpreted as double plateaus and therefore not considered for data analysis (right).

In Figure 5.6a the dependence of the plateau heights on the Debye length is shown for PVA(30%) and PVA(70%). It can be fit with a linear behavior and a slope of 11.1 pN/nm and 6.0 pN/nm for PVA(70%) and PVA(30%), respectively. In addition by the extrapolation to very high salt ( $\kappa^{-1} = 0$ ) a 'zero charge' contribution  $F_0 \approx 33$  pN is obtained. To check this 'zero charge' value, measurements with the least charged PVA(10%) on hydrophobized (uncharged) silica in PBS were performed and an average plateau height of  $F_{\text{des}} \sim 35$  pN was obtained. In Figure 5.6b the experimental data for the dependence of the plateau height on the line charge density,  $\tau$ , of polyvinylamine in 5 mM and 100 mM NaCl solution is given. The data can again be fit by a linear increase in the average plateau height with the line charge density and a 'zero charge' contribution.



**Figure 5.6:** Dependence of the desorption force  $F_{des}$  from the Debye screening length,  $\kappa^{-1}$ , (a) and from the line charge density,  $\tau$  (b).

Preliminary experiments with molecules covalently coupled to the cantilever prior to the experiment showed less unspecific adhesion and rupture peaks, i.e. more plateaus. In addition, longer plateaus were observed on average. But the cantilever could only be used for some minutes, because after this time no plateaus were observed any more. This problem was solved in the Diploma thesis by Jöstl. <sup>[10]</sup>

## 6. Polypeptides: Inverse Temperature Transition

As described in Section 4.5 polypeptides can promote many kinds of energy conversion, which were extensively investigated in aqueous environment. Despite all these findings, there are many open questions, which were addressed by single molecule force spectroscopy in a cooperation with Prof. Urry:

- What is the form of the folded or aggregated state?
- What is the origin of elasticity in these systems?
- Can these molecules be utilized as single molecule machines, like depicted in Figure 6.1?

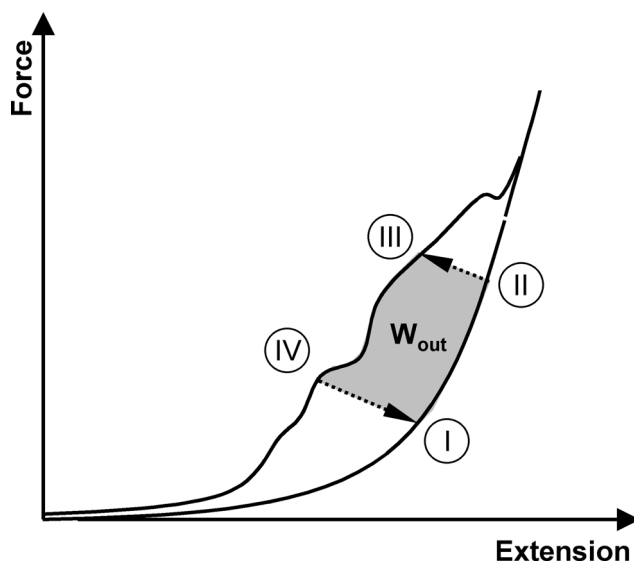


**Figure 6.1:**

*Schematic representation of a polypeptide utilized as a single molecule machine. If it were possible to switch a single peptide by an external stimulus from the folded to the unfolded state at low force (IV  $\rightarrow$  I) and back to the folded state at high force (II  $\rightarrow$  III) a molecular machine would be realized.*

In order to check the (covalent) coupling of the polypeptides to the gold substrate and cantilever, the distribution of rupture length for the polypeptides with terminal cysteines was evaluated for several hundred ruptures. There was no evidence for ruptures at multiples of the length of a (GVGVP)<sub>251</sub> unit (about 460 nm), which would be expected if the molecules were attached at the two cysteine ends. From the many traces taken on polypeptides with and without terminal cysteines the following summary of observations can be given: The (GVGVP)<sub>251</sub> with the cysteines seems to stick a little better onto gold than the molecules without. Nevertheless, even high rupture forces do not show considerably more events at lengths around multiples of 460 nm. In addition, very few events reflected the strength of a covalent gold-thiol bond,<sup>10</sup> but some stuck well enough to investigate the elasticity of single polypeptides in the way described in Section 10.3.

<sup>10</sup> Some experiments were performed with trityl protected cysteines in DMSO. The cysteine was deprotected in proximity to the gold coated cantilever, which was successfully utilized for the azobenzene system (Chapter 7). Some very high rupture forces (>1nN) were observed, but the distribution of the corresponding rupture length also does not show clear evidence for an attachment at the two ends.

In Figure 6.2, force-extension traces of single  $(\text{GVGVP})_{\text{nx}251}$  molecules with different lengths (left) are scaled to one unit length at a force of 200 pN (right). Within the noise, the traces lie on top of each other and can be fit with the WLC-model. As mentioned above the model does not describe the whole force range in a single molecule force experiment well, therefore two fits were performed, one in the low force regime up to 150 pN and one in the higher force regime. The values for the persistence length are 0.4 nm and 0.6 nm, respectively (with an elasticity of 15000 pN). [113]

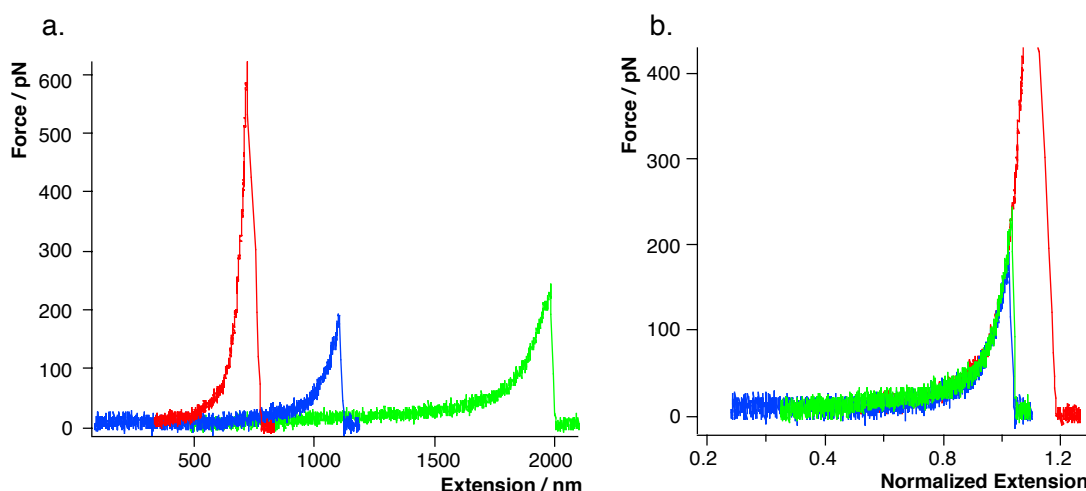


**Figure 6.2:** *a) Single-chain force-extension curves for  $(\text{GVGVP})_{\text{nx}251}$  with different length from different experiments. b) When the length at 200 pN is scaled to one, the traces scale well within the noise level.*

Figure 6.3 shows force-extension traces taken with Olympus Bio-Levers at different pulling velocities. Up to pulling velocities of  $7 \mu\text{m/s}$  (green trace) no considerable viscous drag was observed, i.e. for small and intermediate pulling velocities the force-traces of  $(\text{GVGVP})_{\text{nx}251}$  are perfectly reversible: the forward and backward traces superimpose and they are smooth (no kinks or bumps).

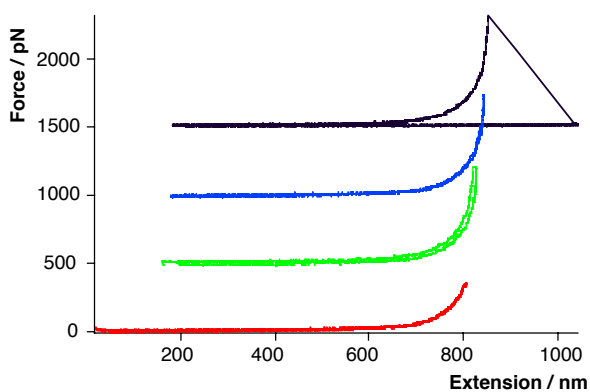


**Figure 6.3:** *Single-chain force-extension curves for  $(\text{GVGVP})_{\text{nx}251}$  at room temperature. Successive traces from bottom to top are offset by 500 pN. Different pulling velocities were applied: red 177 nm/s; green 7000 nm/s; blue 1770 nm/s; black 177 nm/s.*

For  $(\text{GVGIP})_{\text{nx}260}$  room temperature is above  $T_t$  and the behavior is much different. As can be seen in Figure 6.4a there is quite a considerable amount of hysteresis in an extension-relaxation cycle and the extension trace shows features reminiscent of unfolding events. In

contrast, experiments at low polypeptide concentration (Figure 6.4b) and at temperatures below  $T_t$  (Figure 6.7) show some perfectly reversible traces. From these reversible experiments persistence lengths of  $L_p \sim 0.5$  nm and  $L_p \sim 0.7$  nm were found in the low and high force regime, respectively (with an elasticity of 15000 pN like above).

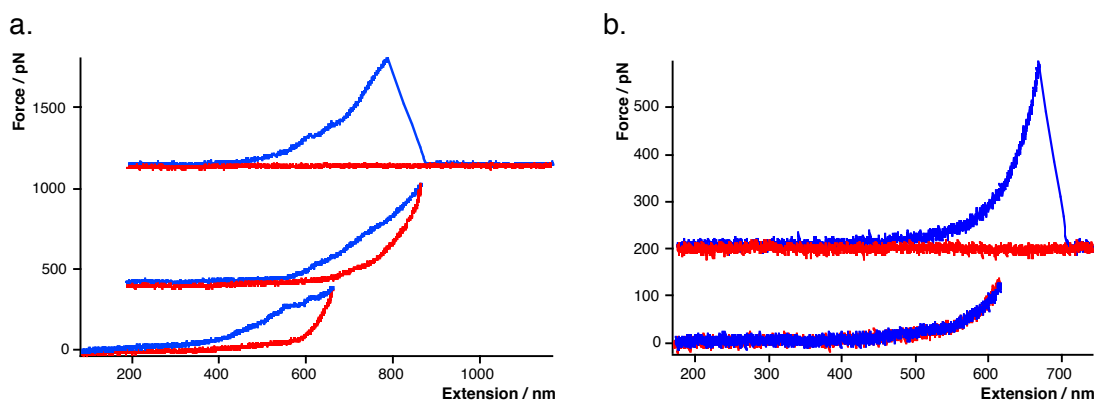


**Figure 6.4:** Force-extension traces for  $(GVGIP)_{nx260}$  taken at room temperature. Successive traces are offset from bottom to top. Extension traces are blue, retraction traces are red. a) Concentration of the adsorbed solution 0.5 mg/ml. b) Concentration 0.05 mg/ml, which results in roughly one attached molecules in 100 scans and sometimes reversible force-extension trace as shown here.

A detailed investigation revealed additional features in the force-extension traces of  $(GVGIP)_{nx260}$  at room temperature, which were neither observed in  $(GVGVP)_{nx251}$  at room temperature nor in  $(GVGIP)_{nx260}$  at a temperature below  $T_t$ :

- In continuous force-extension traces (where all parameters are kept fixed) the peptide becomes longer and longer, i.e. the force-extension traces seem to creep or slip. This is depicted in Figure 6.5 for different pulling velocities and stretching forces. The traces are corrected for piezo- and deflection drift.

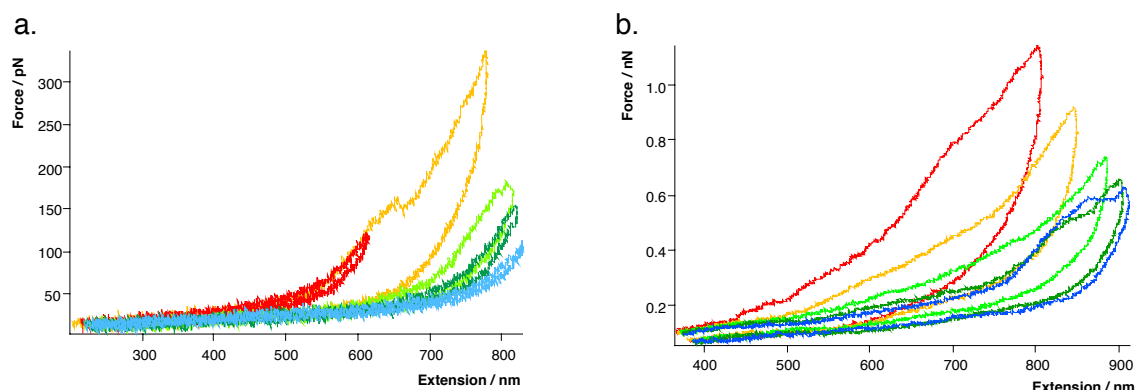


**Figure 6.5:** a) Consecutive scans (continuous pulls – every second scan is shown): red, yellow, bright green, dark green, blue. All parameters were held constant, pulling velocity about  $1.4 \mu\text{m/s}$ . b) Same as (a) for higher forces and slower scans ( $\sim 700 \text{ nm/s}$ ).

- In the relaxation trace for  $(\text{GVGIP})_{\text{nx}260}$  a change in shape dependent on the pulling velocity (and therefore relaxation rate) is observed (Figure 6.6b). At slow pulling velocities the traces do not relax completely. The pulling velocity was changed in every second trace (one out of the two traces taken at equal speed is shown) in different steps forward and backward, so that any time effect can be excluded.

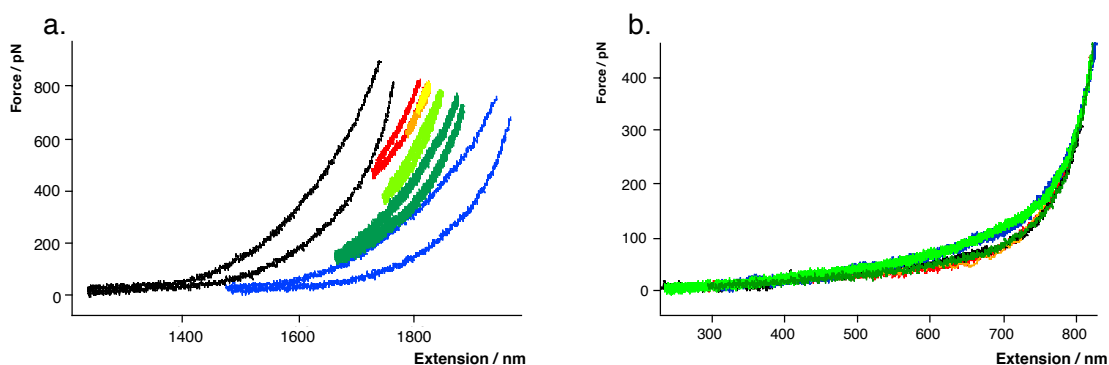


**Figure 6.6:** *a) Consecutive relaxation–extension traces (black, red, orange, yellow, bright green, dark green, blue) varying the force in the relaxed state. b) Relaxation traces at different relaxation velocities. Traces are taken in the following order with the pulling velocity in brackets: black (1.4  $\mu\text{m/s}$ ), red (0.9  $\mu\text{m/s}$ ), orange (14.0  $\mu\text{m/s}$ ), bright green (0.1  $\mu\text{m/s}$ ), dark green (1.5  $\mu\text{m/s}$ ), blue (0.1  $\mu\text{m/s}$ ).*

- In addition, the experiment depicted in Fig 6.6a shows force traces of a molecule, that is held at considerably high force (600–800 pN) and from there relaxed to a certain force and stretched again. It can be seen that the hysteresis builds within less than a second even at forces of several hundred pN.

All these complex features observed in  $(\text{GVGIP})_{\text{nx}260}$  at room temperature (hysteresis, creep, transition) disappeared when the polymer was measured at 11°C (below its  $T_t$ ). For the measurements on  $(\text{GVGIP})_{\text{nx}260}$  below its  $T_t$  the whole room was cooled and equilibrated to 11°C overnight. The system then was very stable and good force-extension traces without hysteresis were obtained (Figure 6.7). Heating the room back to 21 °C did not change the shape of the force-extension traces.

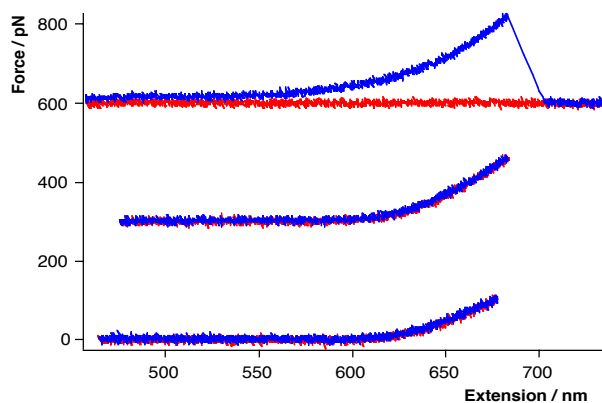


**Figure 6.7:** *Force-extension traces of  $(\text{GVGIP})_{\text{nx}260}$  taken at 11°C, which is below  $T_t$  for this composite. Reversible traces are obtained.*

Organic solutes were found to change  $T_t$  in aqueous environment, a concentration dependence is given in [19]. Sodium dodecyl sulfate (SDS) for example raises  $T_t$  for some ten degrees at concentrations of less than 0.1 M. Guanidinium chloride (GC) at 1 M concentration rise  $T_t$  for a few degree. These two organic solutes were employed to raise  $T_t$  of  $(\text{GVGIP})_{n \times 260}$  above room temperature and with this to prevent hydrophobic folding and hysteresis. SDS, even at concentrations as low as 0.01 M, prevented the molecules from sticking properly to the cantilever, which does not allow for a firm statement in favor of or against hysteresis in the force traces. GC, even at concentrations as high as 1 M, did not make the hysteresis in the force-extension traces disappear.

## 7. Polyazopeptides: Optomechanical Transition

This chapter summarizes the experiments which led to the single-molecule optomechanical cycle, i. e. the demonstration of reversible shortening and lengthening of an azopeptide under high and low force (Figure 7.1). The functional azobenzene unit was chosen, because it is the currently best investigated system that can be switched reversibly by light. Light will probably be the fuel for future single molecule machines <sup>[18]</sup> as it has a very fast response time, is suitable for most ambients, can easily be addressed and has no waste problem. Most experiments were done together with Dr. Nolan Holland.<sup>11</sup>

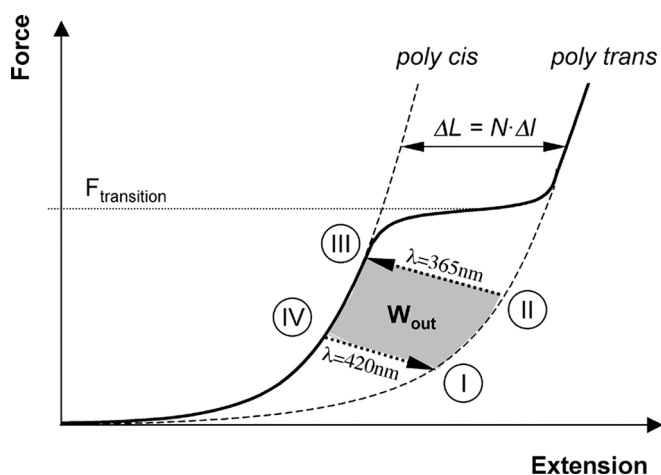


**Figure 7.1:** Schematics of a force-extension traces of a polyazopeptide in its cis and trans state. A single-molecule optomechanical cycle could be realized by extending the azopeptide in its trans state (I->II), then shortening it with  $\lambda=365\text{ nm}$  light (II->III), relaxing it (III->IV) and finally lengthen it again with  $\lambda=420\text{ nm}$  light (IV->I):

### 7.1. Covalent Attachment and Optical Coupling

The formation of a covalent bond between the C-terminus of the polyazopeptide and the aminofunctionalized flintglass within the experiment (sometimes after seconds, sometimes after hours) was reflected by forces in the nanonewton range that could be applied without bond rupture. <sup>[35]</sup> This allowed to stretch and release a single molecule hundreds of times or to hold it with a force of several hundred piconewtons for minutes. Short strands of (non-specifically) bound polymer were ruptured until a single, more than 30 nm long, covalently-bound strand remained. Such a polymer could be irradiated and stretched many times before rupture. Only when the force applied in the experiment rose above 500 pN, the stability of the polymer attachment was observed to decrease substantially. If one considers the occurrence of mechanical noise and the addition of mechanical energy to the system from the light pulse, this is not surprising. Nonetheless, with care an individual chain could be kept attached for more than one hour of continuous measurements (including stretching to several hundred piconewton).

<sup>11</sup> Present address: Department of Physiology and Biophysics, Case Western Reserve University, Cleveland, USA.

In order to correct for tiny drifts in the deflection as well as the piezopath signal, the data was streamed continuously at rates as high as 5 kHz on an additional computer as described in Section 10.3. The drift in the piezo- and deflection-signal was usually corrected by subtracting a straight line. An example for typical experimental raw data is given in Figure 7.2. The data is streamed for ten minutes, and the flashes can be observed as vertical lines in the data. At least three indentation traces per data stream (usually 10 minutes) were taken to correct for drift in the piezopath. Prior to and after the flashes five to ten stretching - relaxation cycles were taken, these were averaged after correcting the drift in the deflection signal. Data was then transformed by the usual procedure into force-extension data.

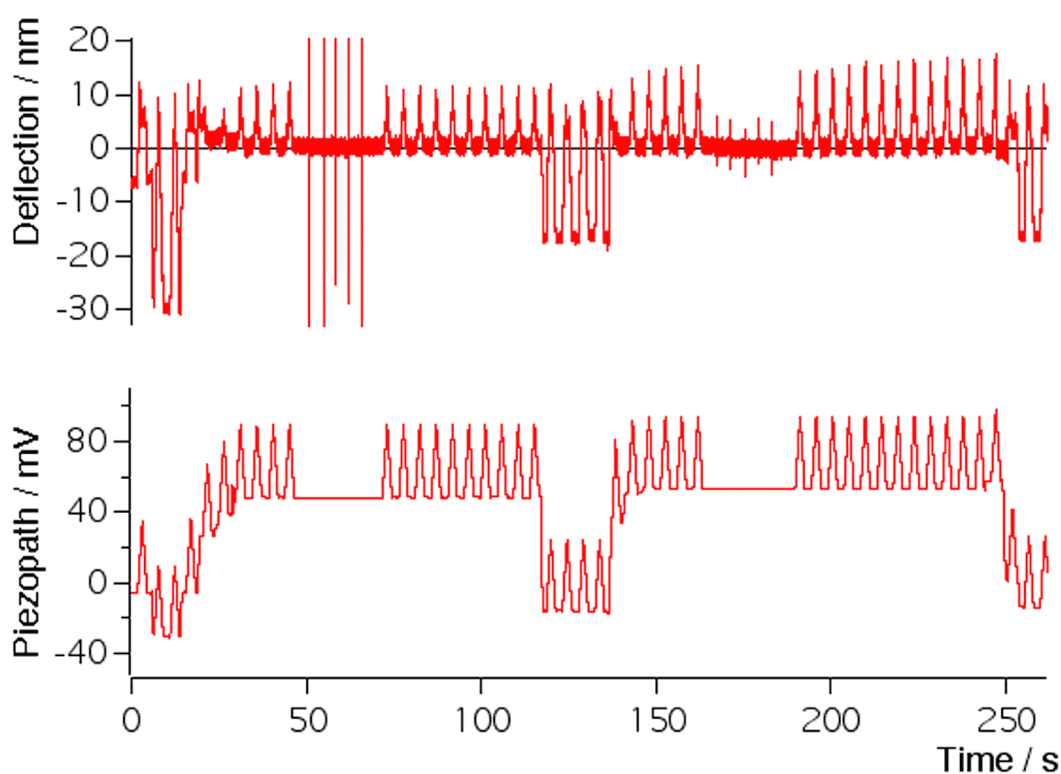


**Figure 7.2:** *Experimental data continuously streamed for 250 s. The upper trace is the deflection data, while the lower shows the output of the strain gauge. The big vertical lines in the deflection data are the  $\lambda=420$  nm pulses and the small (at  $\sim 180$  s) are the  $\lambda=365$  nm pulses.*

Various controls were performed to exclude artifacts which might arise from several sources, including solvent effects and cantilever response to excitation light. First, the effect of a light pulse on the deflection signal in the absence of any polymer molecule was analyzed. Direct illumination of the sample resulted in such a strong interaction with the cantilever, that the resulting cantilever deflection (corresponding to several nanonewtons of force) results in a rupture of the attached polymer. Total internal reflection geometry (Section 3.5) reduced the interactions below the noise level, because with the given length of the cantilever tip of several microns, the penetration depth of the evanescent field is short enough to prevent interaction with the cantilever itself. Therefore, we did not observe crosstalk if the cantilever

was not in contact with the surface, except a spike of 1 ms duration which was visible at all distances from the surface. It turned out, that this is stray light during the pulse which directly reaches the photodiode detecting the cantilever position and does not correspond to any cantilever motion.

However, we observed further crosstalk in the deflection signal from the flashes when a molecule was attached between the cantilever and the substrate (Figure 7.3):

Sometimes a small deflection which decays back to equilibrium on a time scale of seconds was observed (Figure 7.3a). This is the case, when the light is not well coupled into the sample slide. It is believed to be caused by light energy being absorbed by the cantilever resulting in a thermal bimorph effect. It could be reduced below the thermal noise level by shielding all light that is not coupled into the flint glass and adjusting the optics prior to each experiment (Figure 7.3c and 7.3e). Acoustic and vibrational noise from the flash lamp was observed as a damped oscillation in the deflection-time signal starting a few milliseconds after the light pulse (speed of sound) and lasting several hundred milliseconds (Figure 7.3b). By acoustically and vibrationally decoupling the lamp from the AFM and using new electrodes in the lamp, this artifact could be reduced below the thermal noise level (Figure 7.3d and 7.3f).

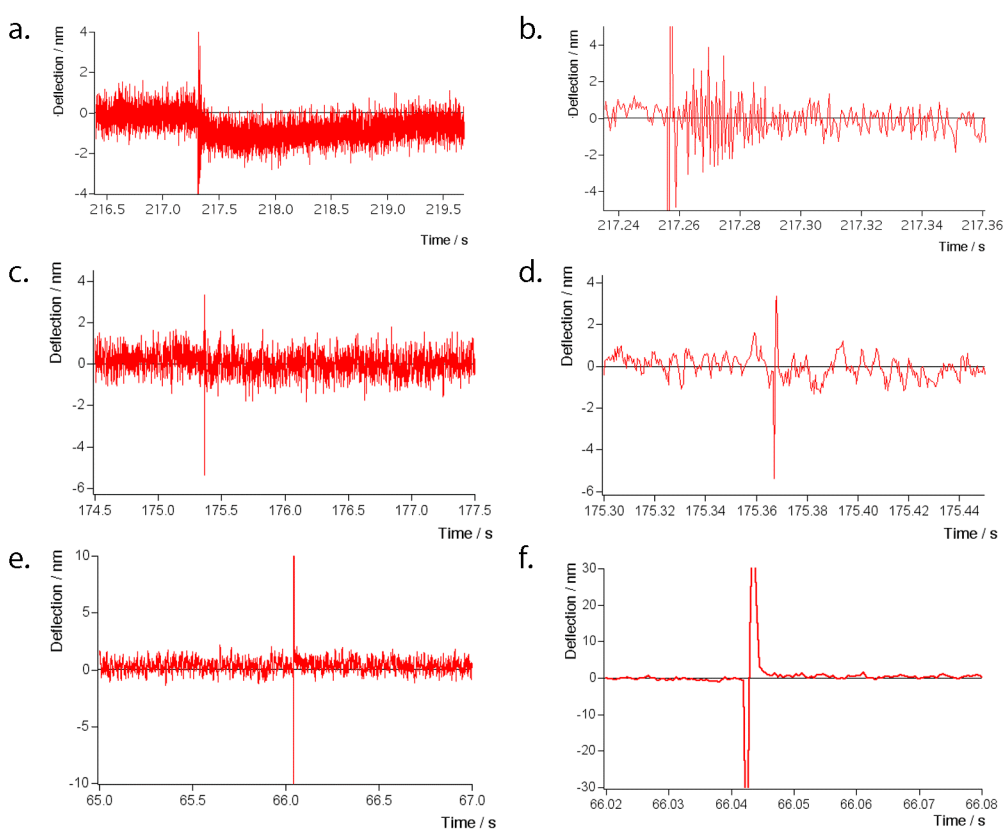


**Figure 7.3:** Analysis of artifacts from the interaction of the flashes with the cantilever at different time scales. a) thermal interaction, b) stray light and sound interaction before the optimization of the setup. c),d) Interaction with the  $\lambda = 365$  nm pulses and e),f) interaction with the  $\lambda = 420$  nm pulses at different time scales after optimizing the setup.

With the optimized experimental setup the flash in the deflection signal should and did only appear as a 1 ms duration spike like shown in Figure 7.3c and 7.3d for the  $\lambda=365$  nm flashes and in Figure 7.3e and 7.3f for the  $\lambda=420$  nm flashes.

To fully exclude artifacts resulting from the irradiation, more control measurements were performed on polysaccharides, which do not contain photochromic molecular units. No measurable effects were observed in the force-extension curves of these polymers (Figure 7.4).

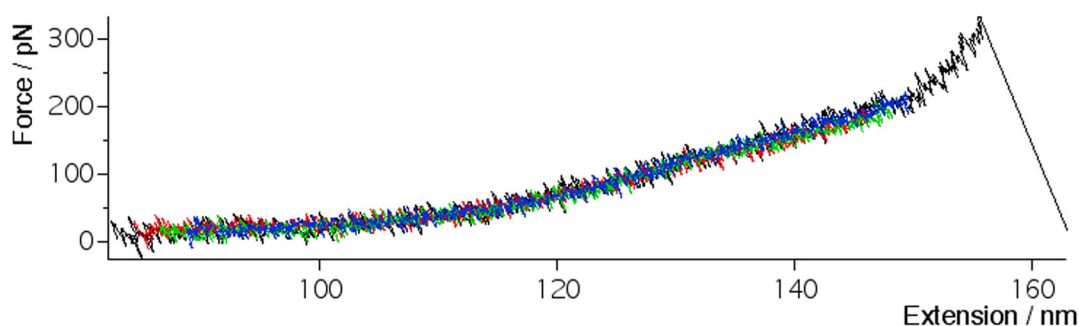


**Figure 7.4:** *Force-extension traces on a single polysaccharide molecule that contains no azobenzene units (in DMSO). Between the red and green trace six  $\lambda=365$  nm pulses were applied, between the green and blue trace six  $\lambda=420$  nm pulses were applied. The black trace shows the final pull revealing the rupture of the molecule.*

## 7.2. Mechanical Characterization of the Polyazopeptide

The characteristic shape of a single azobenzene containing polypeptide was established by taking many force spectra of several individual chains. Figure 7.5a shows a force-extension plot of a polyazopeptide in the cis-state (after irradiation with at least five  $\lambda=365$  nm pulses) and Figure 7.5b in the trans-state (after irradiation with at least five  $\lambda=420$  nm pulses). Even at forces up to 1000 pN the force-extension traces of both configurations show ideal polymer elasticity, there are no hints of any force induced transition visible. Therefore, the cis-trans isomerization of polyazopeptides is only identified by its relative length change upon optical irradiation.

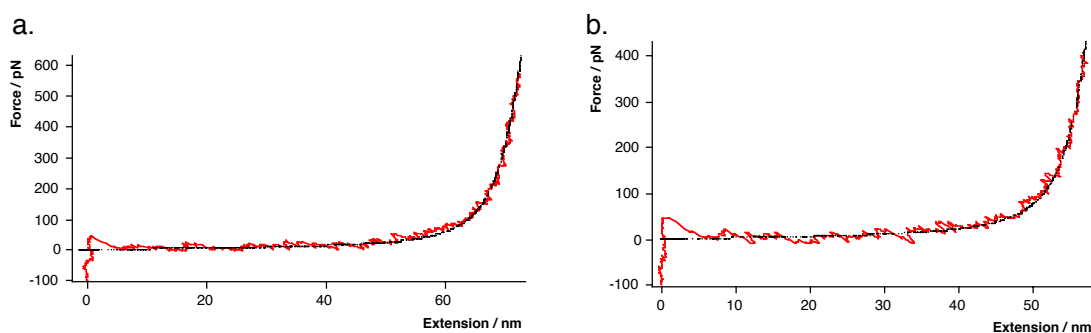


**Figure 7.5:** Force-extension trace for different single polyazopeptides in the *cis* (a) and *trans* (b) state with the corresponding WLC fits. Parameters are  $L_p = 0.5$  nm and  $K_o = 20000$  pN,  $L_{cis} = 75$  nm and  $L_{trans} = 60$  nm.

The shape of the force-extension traces deviates slightly from the WLC fits as can be seen in Figure 7.5. Nevertheless, if the persistence length,  $L_p$ , and the elasticity,  $K_o$ , are held constant, and the fit is performed in the same force range, it gives a good measure for relative length changes. From the two force traces in Figure 7.5 it can be seen, that  $L_p = 0.5$  nm and  $K_o = 20000$  pN give reasonable fits to the polyazopeptide traces in both configurational states. These values were kept constant through all experiments and only the lengths were fitted. For the particular polymer molecules shown in Figure 7.5, contour lengths of  $L_{cis} = 75$  nm and  $L_{trans} = 60$  nm were obtained, respectively. Note, that the deviation from the average length (54 nm) is due to the molecular weight distribution of the material and further enhanced by the overestimation of the contour length from the WLC fit (Section 8.1).

### 7.3. Reversible Optical Switching at Low Force

Figure 7.6 shows typical data obtained in a single molecule force experiment during which optical excitation was coupled into the sample. The traces shown are extracted from data streams of cantilever deflection versus time (three traces are averaged).

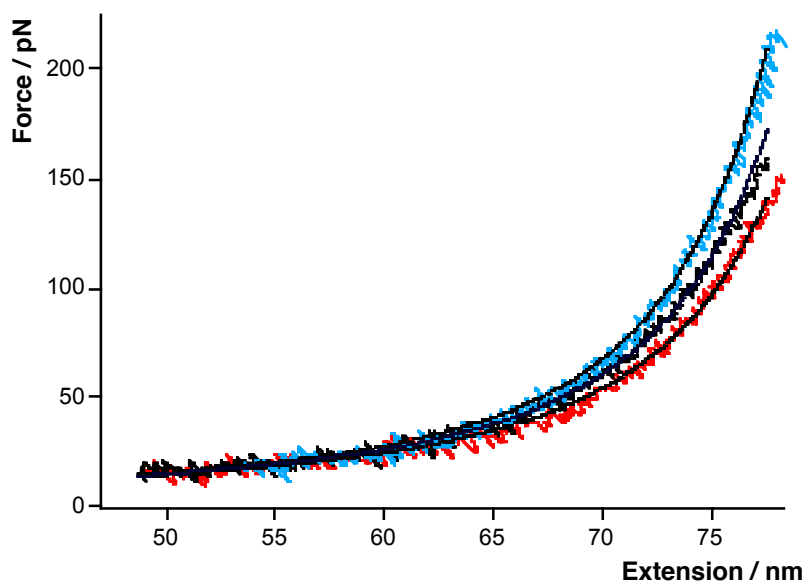


**Figure 7.6:** Switching azopeptides at low force. The traces show the molecule in the undefined configurational mixed state (black), in the extended state after five  $\lambda=420$  nm pulses (red) and in the shortened state after five further pulses with  $\lambda=365$  nm (blue).

The effect of the light pulses on a single azobenzene polymer can be observed by comparing the force-extension traces extracted prior to and after irradiation of the sample. At the beginning of the experiment, the polymer sample assumed an undefined configurationally mixed state owing to the absorbed ambient radiation. The black trace in Figure 7.6 shows a force-extension trace of the polymer in this initial mixed state. After five pulses of  $\lambda=420$  nm light, the polymer chain was lengthened (red trace), and then shortened by irradiation with five pulses of  $\lambda=365$  nm light (blue trace). Such lengthening and shortening could be repeated several times before the polymer or its attachment to tip or substrate ruptured. To obtain a maximal length change several flashes were applied, which drove the system into an equilibrium state. We observed that three maximal energy flashes usually were enough to reach such a photochemical equilibrium.

Repeated measurements of a particular state of the same polyazopeptide molecule (i.e. no optical excitation between successive measurements) resulted in identical force-extension curves (within the thermal noise level), even when the time span between successive measurements was several minutes. The drift stability of the experimental set-up is therefore sufficient to ensure the accurate determination of contour lengths of different polymer configurations based on the WLC fit as described above. A contour length,  $L_{\text{cis}} = 83.7$ , was obtained by fitting the shortest trace in Figure 7.6. The difference in contour length ( $\Delta L$ ) between the short and long state was measured to be 2.8 nm, which corresponds to a relative length change ( $\Delta L/L_{\text{trans}}$ ) of  $\sim 3\%$ .

#### 7.4. Reversible Optical Switching at High Force

Further experiments were carried out to test whether the length of the azobenzene units could be optically switched while holding the polymer under tension. Under this condition, optical switching is of particular interest, as the contraction of a polymer chain against an external force may be employed to perform optomechanical energy conversion with a single-molecule. Figure 7.7 shows the results of one such experiment.

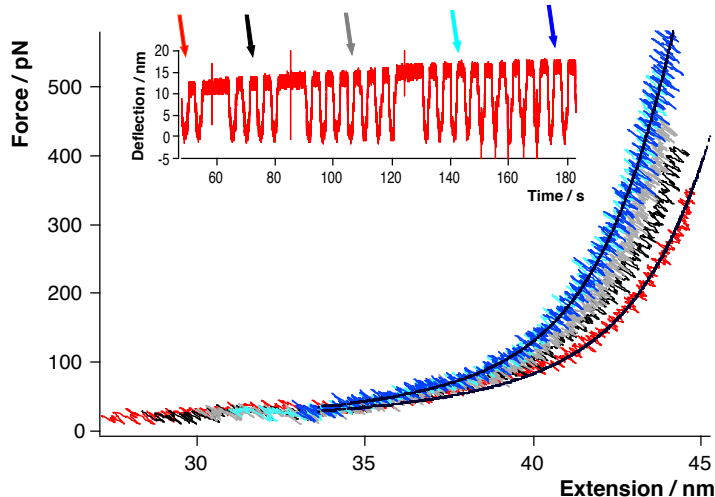


**Figure 7.7:**

*Shortening of an azopeptide against an applied mechanical force. Successive force-extension traces, which demonstrate the switching against an external force. The insert gives the deflection vs. time data with the colored arrows indicating where the traces were taken. The red vertical lines are the  $\lambda=365$  nm pulses.*

Prior to the experiment, the system was driven into the longest state with five consecutive flashes at  $\lambda = 420$  nm. The red trace reveals that in this state the polymer's contour length is 47.7 nm. The molecule was stretched to a force of about 350 pN and a single  $\lambda = 365$  nm pulse at constant tip-sample separation resulted in a shortening by about 1.0 nm, as measured from the black trace. A further pulse resulted in an additional shortening by 0.4 nm (grey trace). The last pulse at high force resulted in an additional shortening of 0.6 nm (bright blue trace). Since five additional  $\lambda = 365$  nm pulses at low force did not result in measurable further shortening (dark blue trace), the polymer was assumed to be in the saturated cis-state. The relative length change observed here against an applied force corresponds well with the value found for switching at low force ( $\Delta L/L_{\text{trans}} \sim 3\%$ ).

Only at very high forces (about 800 pN) hints for a suppression of the optical switching were found. However, due to the limited stability of polymer-surface attachment at high forces, few data at these high forces could be taken up to now. The highest force at which contraction of polymer was definitely observed was 400 pN.

## 7.5. Optomechanical Cycle

Finally, an optomechanical cycle was performed on a single molecule as depicted in Figure 7.1. The smoothed experimental data for an counter-clockwise cycle on a single polyazopeptide molecule is shown in Figure 7.8a. An individual polyazopeptide is first lengthened by five  $\lambda = 420$  nm pulses at a force of 80 pN (I) and then expanded mechanically to a restoring force of 200 pN (II). Then five pulses at  $\lambda = 365$  nm were applied resulting in a contraction of the polymer against the external force (III). Then the force on the polymer was reduced to 85 pN (IV). Finally, the cycle was completed by applying five pulses at  $\lambda = 420$  nm resulting in an optical expansion of the molecule to its original length. The insert shows the corresponding deflection vs. time data, the three flashes can be seen in the green part. The mechanical work performed during the cycle in Figure 7.8a, which is given by the area enclosed by the cycle, is  $W \approx 5 \cdot 10^{-20}$  J. In Figure 7.8b a clockwise cycle was performed, with a different molecule.

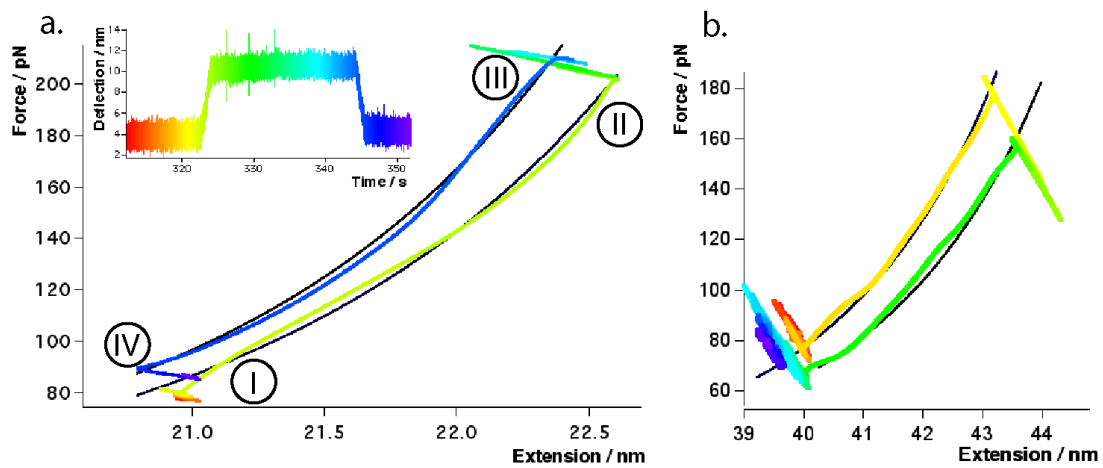


**Figure 7.8:** *Single-molecule optomechanical cycles. a) The azopeptide is lengthened at low force and shortened at high force (counter-clockwise), the included WLC-fits (black traces) yield contour length of 24.8 nm and 24.5 nm, respectively. The inserts show the deflection vs. time data for the cycle. b) The cycle on this molecule is performed clockwise, the length increases from 47.9 nm to 48.8 nm.*

## 8. Discussion

### 8.1. Polyelectrolytes

#### 8.1.1. Elasticity of Polyvinylamine

The investigated dependence of the persistence length on the Debye screening length and the line charge density shows a clear deviation from the usually used OSF-theory. By OSF-theory the electrostatic persistence length should add to the purely elastic contribution and below the Manning limit depend quadratic on the line charge density and the Debye screening length (Equation 25). This is clearly not observed here (Figure 5.4) and can by no means only be explained by the uncertainties in the fitting process (see below). In addition the data is in qualitative agreement with earlier measurements on the salt-dependence of DNA elasticity by Smith et al. using magnetic beads, [31] as well as with recent observations on the synthetic polyelectrolyte poly(methacrylic acid) employing the AFM technique. [52]

The obtained data is still not good enough to instead propose a different relationship between  $\kappa, \tau$  and  $L_p$ . This is mainly due to the above mentioned uncertainties in the fitting process. Qualitatively the observations speak in favor of the recent theory given in Section 4.2.3, with a force dependent persistence length. As can be seen in Figure 8.1a, a fit with Equation 27 (PE-fit) still deviates from the measured force-extension trace, but represents the shape (especially in the high force range) better than the WLC fit.

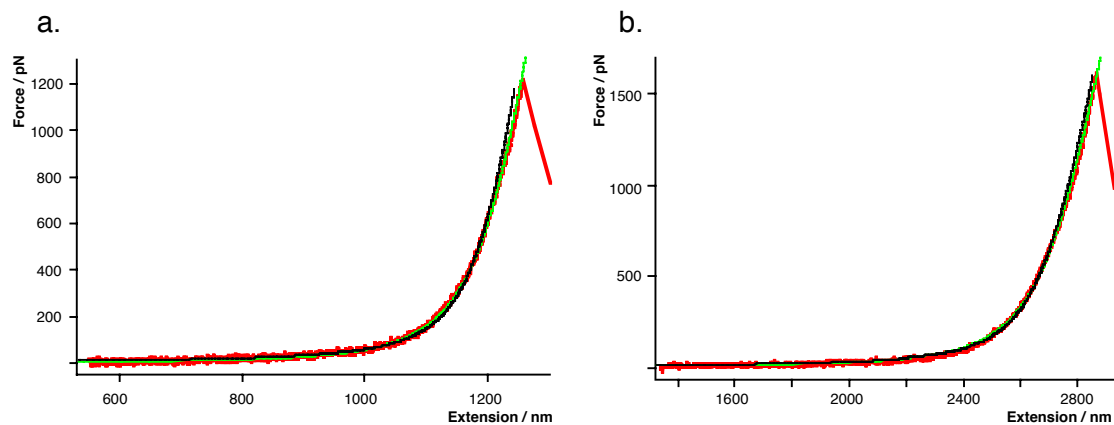


**Figure 8.1:** Comparison of WLC-fits (black) and PE-fits (green) for PVA(50%) in 10 mM NaCl (a) and 40 mM NaCl (b). An elasticity  $E=28000$  pN was used, the obtained fit-parameters are:  
 (a) WLC:  $L=1244$  nm,  $L_p=0.5$  nm, PE:  $L=1275$  nm,  $L_0=1.5$  nm,  
 (b) WLC:  $L=2797$  nm,  $L_p=0.5$  nm, PE:  $L=2841$  nm,  $L_0=2.0$  nm,

A further step towards a better theoretical description of AFM force-extension traces was just recently done by Livadaru et al.[8] They performed extensive transfer-matrix calculations for the force-response of a freely-rotating chain model, which led to Equation 20. To present,

only the parameters for a (uncharged) carbon backbone are calculated, therefore the weakly charged PVA(30%) in 100 mM salt is used to compare this WLC\_DC-fit to the WLC-fit. When the rupture force is high enough and a harmonic potential is assumed for bond deformation, the length of the polymer can be determined from an extrapolation of the linear stretching regime at high force (green trace in Figure 8.2). Then no fit-parameter is needed for the WLC\_DC-fit at all, while the WLC-fit still has the persistence length as fit-parameter. Nevertheless, Figure 8.2 shows that the WLC\_DC-fit represents the data better and that the WLC-fit considerably overestimates the contour length.

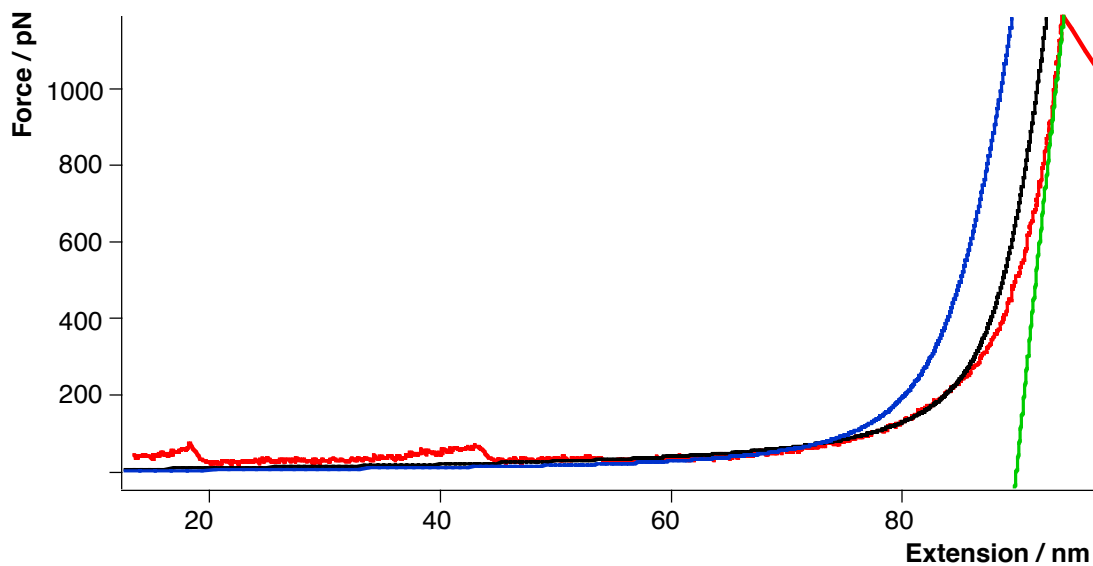


**Figure 8.2:** Comparison of WLC and WLC\_DC fits for PVA(30%) in 100 mM NaCl. The green trace extrapolates the high force regime to a contour length of 90 nm. With the calculated parameters given in the text, the black trace is obtained from a WLC\_DC fit (without any fit-parameter). The blue trace gives the WLC-fit with a persistence length of 0.4 nm.

These preliminary results demonstrate, that the discrete nature and architecture of the chain, stretching and bending fluctuations, and the segment elasticity cannot be neglected if the elasticity of a stretched polymer is to be described. Especially the architecture of the chain will become much more important, when more complex chains are investigated. For example, from bulk measurements in polypeptides it is conjectured, that the internal dynamics of a polymer chain ('rocking') may contribute significantly to the entropic elasticity. [146] [147] [11] Nevertheless, to describe experimental data perfectly, one or two fit parameter are necessary, and if the above discussed limitations are kept in mind the WLC-models is still useful to quantify the elastic behavior of individual polymer chains.

Finally, it is important to note that a quantitative comparison of the obtained persistence lengths with other experimental methods is not straightforward as they are based on different models and obtained in different regimes. The most striking difference is, that these methods

(e. g. light scattering, x-ray scattering or neutron scattering) measure at basically zero force, while in the stretching experiments, the polymers are almost completely stretched in the range where the fits are performed. In addition, X-ray or neutron scattering experiments are usually performed above the overlap concentration and then fitted / simulated by scattering functions, [148] which makes it even more difficult to relate the obtained values to the persistence length from single molecule force experiments.

### 8.1.2. Desorption of Polyvinylamine from Solid Substrates

The plateaus of constant force observed in the desorption experiments are interpreted like shown in Figure 8.3. In the range from 0 nm to 100 nm, there are many chains and the cantilever itself interacting with the substrate. Then at the first plateau, two polymer chains are simultaneously desorbed from the substrate. When the plateau force drops to half of its height, one chain detaches completely from the substrate. Finally at the last step, the remaining polymer detaches.

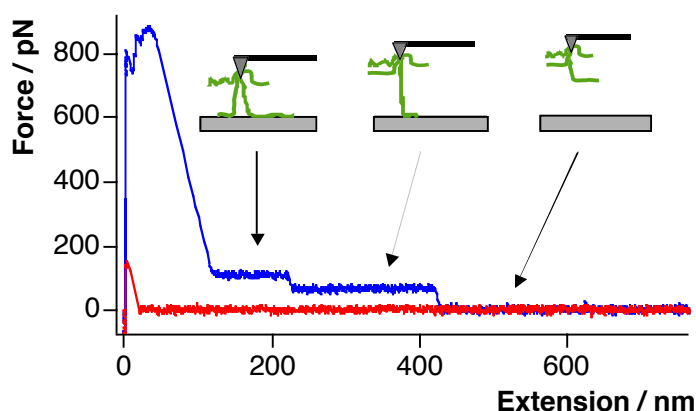


**Figure 8.3:**  
*Force-distance profile measured upon desorbing PVA(30%) chains in aqueous solution (20 mM NaCl) from a glass substrate and interpretation of the observed plateaus.*

The measured linear dependence of the plateau force on the Debye screening length led to the following theoretical model, which could be confirmed by the linear dependence of the desorption force on the line charge density (Figure 5.6):

As indicated above, the dissociation rate of ionic bonds between the positively charged amino groups of the polymer and the negatively charged surface sites is much faster than the pulling rate applied in our experiments. Thus, on the time scale of the experiment, the polyelectrolyte chain can be considered as a string of constant charge<sup>12</sup> continuously desorbing from the charged substrate against the attractive potential of the surface. The coulomb contribution to the force that needs to be applied in order to induce this continuous desorption can be

<sup>12</sup> A polyelectrolyte can be considered as a chain of individual charges separated by a certain distance,  $a$ , or as a string of constant charge density  $\tau = 1/a$  ( $a$  now represents the length of a segment of unit charge). Both approaches are equivalent so that for our qualitative discussion we will treat all charges individually, whereas in the mathematical description a constant charge density will be used for convenience.

described as follows: The electrostatic potential,  $V^{\text{el}}(z)$ , of the substrate in electrolyte buffer is taken in the Debye-Hückel approximation (Equation 49) [149]

$$V^{\text{el}}(z) / k_{\text{B}}T = 4\pi l_{\text{B}} \sigma \kappa^{-1} e^{-\kappa z}. \quad (54)$$

Upon desorption of one polymer segment of length  $a$ , the entire polymer chain is moved against the electrostatic surface potential, i.e. the separation of each charged segment from the substrate is increased by the distance  $a$ . No transition barriers need to be overcome along the 'electrostatic unbinding pathway' during which the charged species has to overcome the restoring force

$$F(z) = dV^{\text{el}} / dz = -(4\pi l_{\text{B}} k_{\text{B}} T) \sigma e^{-\kappa z}. \quad (55)$$

If no covalent bonds need to be broken at the substrate surface (e.g. deprotonation of acidic groups) and other stronger binding interactions 'pinning' the polymer segments to the surface can be neglected, the removal of the ions from the substrate is a continuous equilibrium process which gives rise to the typical plateau curves shown in Figure 8.3.<sup>13</sup>

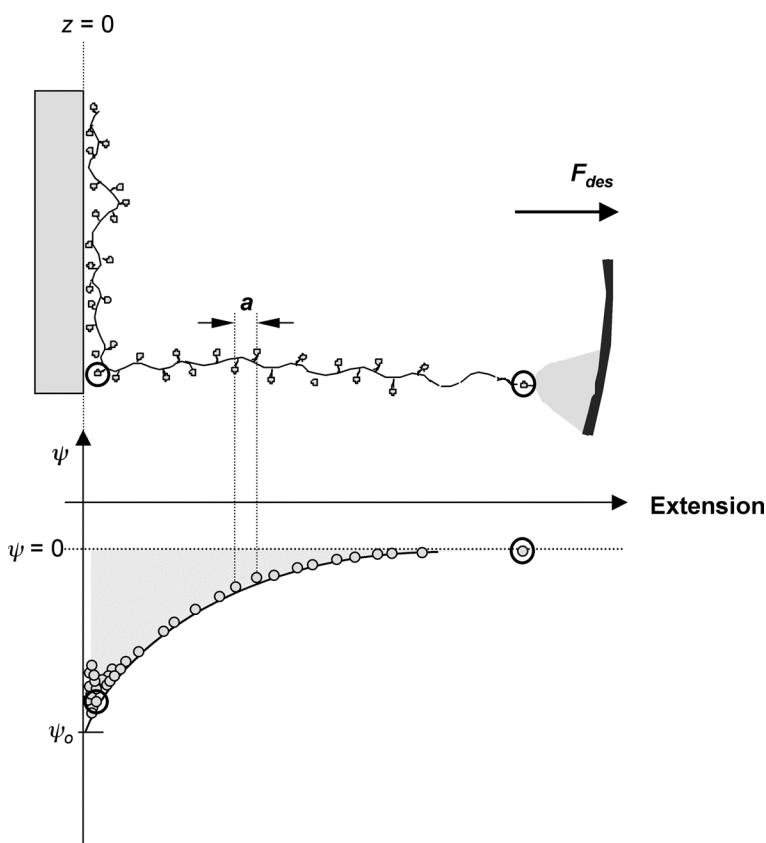


**Figure 8.4:**

*Representation of the desorption process of a single polyelectrolyte chain with discrete positive charges of intermediate distance,  $a$ , from a negatively charged substrate with screened electrostatic potential  $\Psi(z)$  in aqueous solution. The black circles highlight the position of individual charges at  $z=0$  and  $z=\infty$  and their corresponding position in the electrostatic potential. (Adapted from [9]).*

<sup>13</sup> The small restoring force experienced by the single charges upon taking their infinitesimal steps along the broad exponential 'unbinding' pathway would hardly be detectable by AFM. However, as will be seen below the integration over all charges along a polymer chain will give rise to a detectable desorption force in the range of several ten piconewton.

The desorption of a polyelectrolyte chain against the attractive electrostatic potential of the substrate can therefore be described by a series of charges subsequently moving up the exponential curve in Figure 8.4. One charge after the other is removed from the pool of charges at  $z = 0$  until eventually the chain-end fully detaches from the substrate, upon which the desorption force of the chain vanishes. The coulomb force acting on a desorbing polymer chain can be calculated by integrating  $F(z)$  over the entire chain, i.e. from  $z = 0$ <sup>14</sup> to  $z = \infty$ . The desorption force is then found to linearly dependent on the surface charge density, on the Debye screening length, and on the polymer charge density: [9]

$$F_{des}^{el} = 4\pi l_B k_B T \sigma \tau \int_{z=0}^{\infty} e^{-\kappa z} dz = (4\pi l_B k_B T) \cdot \sigma \cdot \tau \cdot \kappa^{-1}. \quad (56)$$

Note that this result is equivalent to the transfer of one infinitesimal chain segment carrying the charge density  $\tau$  from  $z = 0$  to  $z = \infty$  with the rest of the chain staying in place. Somewhat more detailed derivations yield a similar linear relationship between the desorption force and the line charge density and the Debye length for strong fields. For weaker fields more complicated expressions have been derived. [104] The result is also consistent with the adsorption energy of a cylinder on a charged plane. [103]

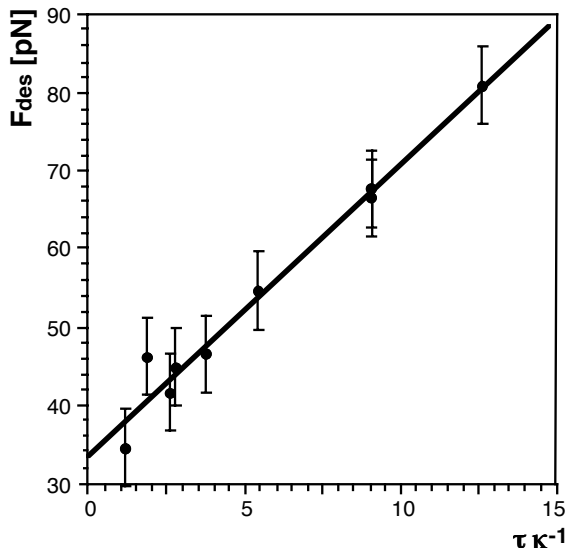
Thus, the linear dependence of the desorption force on the Debye length,  $\kappa^{-1}$ , (for constant polymer charge) as well as on the line charge density,  $\tau$ , (for constant electrolyte concentration) is explained. To a first approximation, the electrostatic force,  $F_{des}^{el}$ , is then the only additive term dependent on  $\sigma$ ,  $\tau$  and  $\kappa$ , such that

$$F_{des} = F_0 + (4\pi l_B k_B T \sigma) \kappa^{-1} \tau. \quad (57)$$

The surface charge density,  $\sigma_{SiO_x}$ , of the silica substrates used in the experiments can be extracted from the slope of the  $F_{des}^{el}$  vs.  $(\tau \kappa^{-1})$  plot given in Figure 8.5 and is measured as  $\sigma_{SiO_x} \approx 0.1 \text{ nm}^{-2}$ .

---

<sup>14</sup> The chain is not in contact with the surface but at a distance  $D$ , therefore the result is only valid for  $\kappa D < 1$ , which is given at our experimental conditions.

**Figure 8.5:**

Dependence of the desorption force,  $F_{des}$ , on the product of Debye screening length,  $\kappa^{-1}$ , and polymer line charge density,  $\tau$ . From this the surface charge density and the 'zero force' contribution can directly be obtained.

The electrostatic surface potentials can be obtained, under the assumption that the surface charge is independent of the salt concentration, by  $(F_{des}-F_o) = V(0)\cdot\tau = \psi_o\cdot\tau$ , i.e.

$$\psi_o = F_{el}/\tau = (4\pi l_B k_B T \sigma) \kappa^{-1}. \quad (58)$$

According to this simple model, the surface potential of the silica substrate is thus given by the slope of the linear fit to the experimental data in Figure 5.6, such that e.g. for 5 mM NaCl:  $\psi_o(\text{silica}) = -14.2 \text{ pN}\cdot\text{nm}\cdot(\text{unit charge})^{-1} \approx -88 \text{ mV}$ .

The determined surface potential is in good agreement with values reported in the literature. [65] [150] And agrees especially well with zeta potential measurements by Radmacher [151] (Figure 8.6).

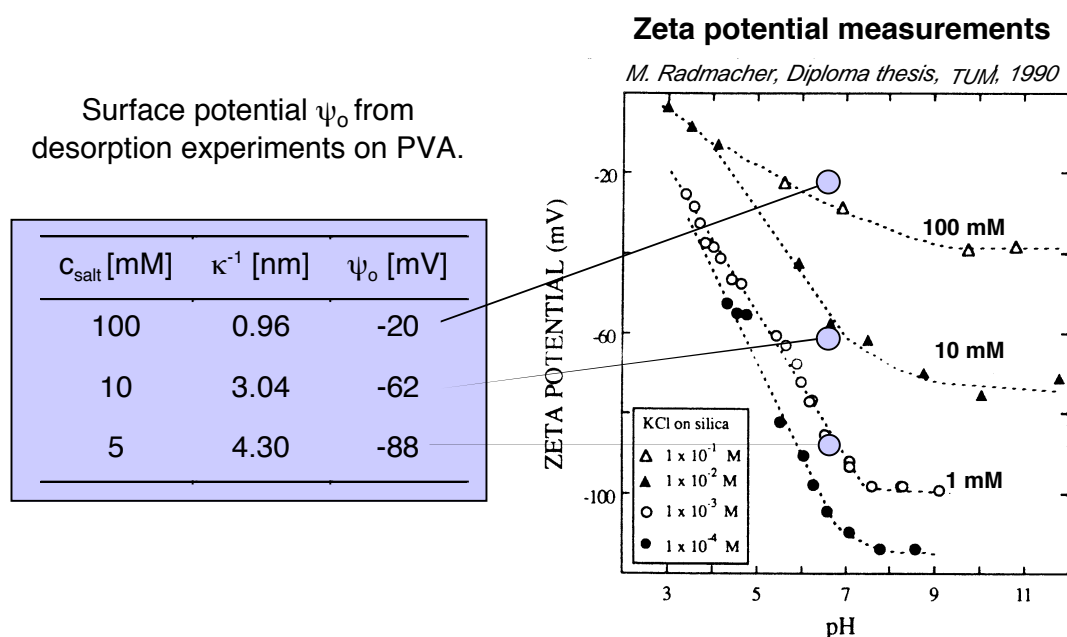


**Figure 8.6:** Comparison of the surface potential for silica determined by desorption experiments with zeta potential measurements.

The net charge of glass surfaces with an area per charge of  $27 \text{ nm}^2$  in 1 mM NaCl reported by Poptoshev et al.<sup>[152]</sup> is in qualitative agreement with the above obtained values. They also report a small dependence on the salt concentration, i. e. a reduced area per charge with increasing salt concentration, which brings this value even closer to the here obtained result (for 5 – 100 mM NaCl).

Probably Equation 57 still is an approximation, because glass surfaces have some special properties which are not explicitly included. One problem might be, that the charge at the glass-water interface originates from dissociation of the surface silanol groups which leads to a diffuse charge distribution. This might also be the reason why glass surfaces as well as adsorbed polyelectrolytes are capable of charge regulation, i.e. both can regulate their charge in such a way that the net charge of the surface and the adsorbed layer becomes small.<sup>[152]</sup>

Nevertheless, also single molecule desorption measurements by Jöstl<sup>[10]</sup> on mica and calcite support the above interpretation. Jöstl managed to link polyelectrolyte chains covalently to the cantilever tip<sup>[153]</sup><sup>[96]</sup> and to stabilize this tip such that measurements with one tip (and therefore the same few molecules) were possible for days.<sup>15</sup> With this setup he obtained plateaus which were on average cleaner and longer than in the measurements reported here. This is probably due to the very clean substrates (mica was freshly cleaved prior to each experiment and calcite is a self-cleaning substrate). On mica he found an electrostatic contribution with a linear dependence on  $\tau\kappa^{-1}$  similar to the measurements reported here on glass. The 'zero charge' contribution was little higher ( $F_0=46 \text{ pN}$ ). The plateau heights on calcite did almost show no  $\tau\kappa^{-1}$  dependence, this is consistent with the almost uncharged surface of calcite at the investigated pH and the strong shielding due to the dissolved  $\text{Ca}^{2+}$  ions. In contrast, the 'zero charge' contribution was considerably higher ( $F_0=70 \text{ pN}$ ).

Still under discussion is the origin of this additive 'zero charge' contribution,  $F_0$ , to the overall desorption force. Most likely it is caused by van der Waals interactions, which in many geometrical configurations are quantified by the Hamaker constant  $A_H$ .<sup>16</sup> It is difficult to directly derive the Hamaker constant from the desorption measurements, because too many parameter are not exactly known for the probed polymers. For example, if it is approximated by a sphere on a surface, the radius of this sphere,  $R$ , and the distance between sphere and surface,  $D$ , are not known. But it is straightforward to relate the Hamaker constant of any surface to the one of mica,<sup>17</sup> if it is assumed, that the van der Waals contributions are additive and that the polymers have on average the same distance from the substrate. The ratio of the

<sup>15</sup> The cantilever was silanized with epoxy-silan, and polyvinylamine was covalently bound to the cantilever. Then the epoxy groups that did not react with the polyvinylamine were saturated with ammonium to prevent multiple bonding of the chains to the tip and leave long enough dangling ends.

<sup>16</sup> It is interesting to note, that this force ( $\sim 35 \text{ pN}$ ) corresponds to an energy of  $\sim 1 k_B T$  acting over the distance of 0.12 nm, which are typical energies and lengths for van der Waals bonds.<sup>[36]</sup>

<sup>17</sup> The Hamaker constant for mica was measured with different methods and in different surroundings, e.g. in water by the SFA:  $2 \cdot 10^{-20} \text{ J}$ <sup>[65]</sup> and calculated by full Lifshitz:  $1.34 \cdot 10^{-20} \text{ J}$ <sup>[101]</sup>

two 'zero charge' contributions,  $F_0$ , corresponds then to the ratio of the Hamaker constants, if the surfaces are probed with the same cantilever and molecule. This is also supported by the above mentioned measurements by Jöstl, [10] he found that the ratio of the Hamaker constants for mica and calcite is about the same as the ratio of the constant force contributions,  $F_0$ .

## 8.2. Polypentapeptides: Inverse Temperature Transition

The force-extension traces for  $(\text{GVGVP})_{\text{nx}251}$  at room temperature show perfect reversibility, i.e. any molecular process related to the elongation and relaxation of the polypeptide chain must be fast on the time-scale of the experiment. Room temperature is below the temperature of hydrophobic folding,  $T_t$ , for  $(\text{GVGVP})_{\text{nx}251}$ , the behavior below  $T_t$  can therefore be termed ideal elasticity, with entropic elasticity as one contribution. From measurements in bulk and solution, the following additional contributions were conjectured:

- Weis-Fogh and Andersen [154] suggested that hydration of hydrophobic side chains of the protein, which become exposed to solvent on extension, would be responsible for the stretch-induced decrease in entropy.
- Hovee and Flory [155] supposed that the alignment of chains in a network of random chains is the major contribution to the observed elasticity.
- Chang and Urry [146] supposed that damping of internal chain dynamics on extension is a major reason for the elasticity in these elastomers.

Luan et al. [156] compared elastomers in water and in 30% ethylene glycol and found no experimental basis for believing that solvent entropy change contributed to elastomeric force, which opposes the first conjecture. The single molecule experiments make the second conjecture quite unlikely, as a comparison of single molecule and bulk elastic moduli show no considerable differences: [113] From the slope in the purely entropic (gaussian) part of the single molecule force-extension traces (below 50 pN) a single chain elastic modulus,  $E$ , was derived under the assumption of a random coil state ( $E = 5.7 \cdot 10^4 \text{ N m}^{-2}$ ) and a  $\beta$ -spiral structure ( $E = 1.2 \cdot 10^6 \text{ N m}^{-2}$ ). They are a factor of three lower and a factor of seven and a half higher than the macroscopic value ( $E = 1.6 \cdot 10^5 \text{ N m}^{-2}$ ). The values are even closer together, if it is considered that in a macroscopic crosslinked sample the  $\beta$ -spirals would be randomly orientated with respect to the direction of extension. Finally, low-frequency motions provide an abundant and ready source of entropy decrease on extension. [113] This would not differ much in bulk and single molecule samples, which makes the damping of internal chain dynamics on extension a likely additional contribution.

The origin of the deviations from this ideal elastic behavior observed in the force-extension traces above  $T_t$  (e.g. for  $(\text{GVGIP})_{\text{nx}260}$  at room temperature) somehow resemble the force-

extension curves obtained on freshly cleaved abalone shell, where the nature of the involved forces could not be clearly revealed. [157] The data obtained here also does not allow for a completely convincing explanation, but the model for the inverse temperature transition given in Section 4.5.2, combined with the triple-helix formation (Figure 3.3) and the following two assumptions is a likely explanation for the three features in the force-extension traces of (GVGIP)<sub>nx260</sub>:

- The molecules have to be able to form triple-helices in order to undergo an inverse temperature transition, i. e. a single strand cannot fold onto itself.
- A triple-strand has to be able to dissolve into single strands to undergo an inverse temperature transition, i. e. a triple-strand will never show ideal elasticity.

The hysteresis (above  $T_i$ ) in the force-extension traces can even be explained without the above assumptions by hydrophobic interactions, which are in general supposed to guide the folding of most polypeptides. The irregular shape, which differs from trace to trace, suggests that no unique stable native state is reached at the time scale of the experiment. Probably because of a rough folding energy landscape with many 'trapped states'. In addition the very fast 'refolding' reveals some fast processes. These observations might be caused by unspecific hydrophobic interactions in between strands but could also be caused by a hydrophobic collapse into a molten globule (which can have either no well developed secondary structure, or may be a helical liquid crystalline molten globule), [158] a misfolded state or any other collapsed structure. [159] The suggestion that hydrophobic hydration is a major component in the folding of the investigated peptides is further supported by the observation that the hysteresis disappears below  $T_i$ , which is consistent with the theory of the inverse temperature transition (Section 4.5.2).

With the above assumption the creep or slip observed in consecutive force-extension traces (Figure 6.5) might be caused by the following scenario: Just one or two molecules of the triple-helix are attached to the cantilever, these molecules slip some nanometer along the other one or two strands in every extension-relaxation cycle. Otherwise the creep would have to be explained by a slip of the extended molecule along the surface or the AFM tip, but this was not observed in such a continuous way in experiments with the (GVGVP)<sub>nx251</sub>.

From the available data it is impossible to relate the rate dependent deviation in the backward traces of (GVGIP)<sub>nx260</sub> (Figure 6.6b) to a specific folding process, there are just too many possibilities: It could be an effect of a single folded chain (folding of  $\beta$ -turns), an interaction in between triple-strands (similar to the overstretch transition in DNA [160]) or a solvent effect (like observed for PEG [161]). But in any case it does not disagree with the above assumptions.

Finally, the construction of a molecular machine like sketched in Figure 6.1 from the investigated polypeptides shall be discussed. A prerequisite for such a machine is to be able to drive the inverse temperature transition in a controlled way. In bulk, many means of manipulating  $T_t$  of polypeptides, and with this driving reversible hydrophobic contraction and expansion, were demonstrated. [11] The first single molecule stretching experiments on  $(\text{GVGVP})_{n \times 251}$  and  $(\text{GVGIP})_{n \times 260}$  at room temperature looked as if this could be repeated on the single molecule level: An additional  $\text{CH}_2$  group in each pentamer of  $(\text{GVGIP})_{n \times 260}$  resulted in a completely different force-extension behavior, which seemed to resemble a hydrophobically folded structure. But finally, neither  $(\text{GVGVP})_{n \times 251}$  nor  $(\text{GVGIP})_{n \times 260}$  could be driven from force-extension traces with hysteresis to traces showing ideal elasticity or vice versa in any experiment - every prepared system either showed hysteresis or reversibility. This again can be explained by the above stated assumptions. Then the peptide from the beginning is either adsorbed in a triple-helix formation or it is adsorbed as an individual single strand. As the mobility on the surface is considerably reduced it stabilizes both states. Therefore, even under conditions favoring triple-helix formation the separated single strands would stay separate, while triple-helices keep aggregated even below  $T_t$ . This is supported by the behavior of  $(\text{GVGIP})_{n \times 260}$  at low concentration at room temperature, and also by the conjecture of Manno et al.[162] for the dynamics of the folding transition in  $(\text{GVGVP})_{251}$ : "Smooth and progressive conformational changes promote concentration fluctuations, the related locally high concentration prompts a further, substantial conformational change ending into triple-helix formation and coacervation." (These concentration fluctuations are probably considerably reduced at a surface).

### 8.3. Polyazopeptides: Optomechanical Transition

#### 8.3.1. Length Change

Thermal effects cannot be excluded a priori as a cause for the observed length change. While any thermal energy deposited on the molecule directly would be dissipated into the bulk medium at times much faster than the time scale of our experiments, thermal effects resulting from heating of the solvent or the glass substrate have to be considered. Although the absorption of DMSO is negligible above  $\lambda = 330$  nm, a minor fraction of the pulse energy might be absorbed by the solvent which would heat up the environment of the measured polymer, thus changing the stress-strain-relation for the polymer. But independent of the excitation wavelength, this effect would lead to an increase in force at given length, or to a decrease in length at given force. In contrast, we observe a shortening at  $\lambda = 365$  nm, and a lengthening at  $\lambda = 420$  nm, which can therefore not be attributed to heating effects. The same reasoning holds for potential thermal effects due to the absorption in the glass. Therefore, the only reasonable explanation for the length change is the cis-trans isomerization of the azobenzene units in the polyazopeptide.

There is not enough data yet to relate the length change in a polyazopeptide to the number and energy of flashes applied. Nevertheless, it is possible to discuss the saturated trans and cis states and compare them to bulk experiments. The discussion refers to the traces shown in Figure 7.6 (but yields similar results with the traces from Figure 7.7). With the data given in Section 4.5.4, the fitted contour length of the polymer,  $L \approx 86.5$  nm, equals  $n \approx 46$ . Considering that effectively only 55% of the azobenzene units change their configuration upon cis-trans switching, a maximum length change of  $\Delta L_{\max} \approx 6.4$  nm could possibly be obtained by optical pumping at  $\lambda=365$  nm. The measured length change in DMSO of 2.8 nm stays well below this upper limit. The difference may reflect the fact that parts of the polymer chain are not excited by the evanescent field. More likely, it is caused by some remaining conformational freedom of the polyazopeptide backbone, so that the sum of the total length changes of the azobenzene units is not reflected in the contour length change of the polyazopeptide. Intrinsic viscosity measurements on azobenzene polymers even show very tiny effects of optical excitation on the end-end distance of the polymer coils in solution when the photoactive units were connected by flexible chain segments, [134] [135] but rigid linkers between the azobenzene moieties resulted in particularly large reversible changes of up to 60% in the viscosity. [135] In the AFM experiments, the polymer chains are fixed between tip and substrate, and stretched beyond the coil regime. This geometry is thus more comparable with photoactive bulk polymer networks, which were reported to show considerable length changes upon optical switching. [139] Altogether a considerable shortening is expected, but the remaining conformational freedom of the polypeptide backbone can well account for the reduced polyazopeptide shortening by rotations around single backbone bonds. [140]

It also has to be mentioned, that the end-end-distance of the azobenzene monomer in both configurations, as well as the energy conversion efficiency, may be affected by the solvent determining the equilibrium conformational structures (as for example in PEG the equilibrium structure at intermediate force is different in water and hexane). The data given here might thus be specific to DMSO, and may differ in other solvents.

### 8.3.2. Mechanical Stability

The cis and trans configuration were both found to be mechanically stable at all experimental pulling forces on the time scale of the experiment. This is expected for the lower energy trans configuration, as it represents the equilibrium configurational state. But according to the Bell equation (Equation 33) the lifetime of the cis configuration should be considerably reduced by a stretching force. From the data on azobenzene given in Section 4.5.4 the thermal lifetime of the cis-isomer is reduced to  $\tau_F < 100$  ms, once the projection of the stretching force on the coordinate describing the trajectory of the cis-trans transition exceeds 400 pN. This was never observed. A likely explanation for this somewhat surprisingly high stability of the cis-configuration is that the force-induced transition proceeds along a pathway nearly orthogonal

to the thermal cis-trans isomerization, which is suggested to proceed along an isomerization pathway in which the dihedral angle  $\Phi_{\text{NNC}}$  is the relevant configuration coordinate. Hence the activation barrier and thus the thermal lifetime of the cis configuration would remain almost unaltered.

A more generalized view of this effect would be that the forced transition occurs on a pathway ensemble whose width in conformation space is drastically restricted by the external force acting along the polymer backbone. Therefore, some saddles and low energy barriers, which are sampled by the thermal transition, might not be accessible for the forced transition. This would to a certain degree correspond to the conformationally locked interaction found in certain biopolymers e.g. actin filaments, which are known to withstand forces of up to 100 pN for seconds although their equilibrium constant is in the mM range.

Supposing there is such a separate mechanical pathway, these measurements allow us to set a lower bound for the lifetime,  $\tau_{o,z}$ , of the cis-state when restricted to this path along the stretching coordinate,  $z$ . With Equation 33 and the observation that a molecule can be held in the all-cis state at forces of about 500 pN for many seconds, it is estimated as  $\tau_{o,z} \approx 3 \cdot 10^{13}$  s. The lifetime of a state,  $\tau_o$ , is correlated with the energy barrier of the escape path,  $\Delta G^*$ , by  $\tau_o = (1/\nu_o) \exp(\Delta G^*/k_B T)$  (Equation 32). If  $\nu_o$  is assumed to be independent of the pathway, the energy barrier  $\Delta G_\phi^*$  along the configurational coordinate,  $\Phi_{\text{NNC}}$ , and the energy barrier  $\Delta G_z^*$  along the stretching coordinate,  $z$ , are related by

$$\Delta G_z^* = \Delta G_\phi^* + k_B T \cdot \ln(\tau_{o,z} / \tau_{o,\phi}) . \quad (59)$$

Thus,  $\Delta G_z^* \approx 62 k_B T$ , i.e. the energy barrier is increased by approximately 18  $k_B T$  when the molecule's escape path is restricted to the stretching coordinate. However, the assumption that  $\nu_o$  is independent of the pathway is quite crude: In Kramers theory for example  $\nu_o = D / l_c l_{ts}$  (Section 4.3.1), where not only the viscous damping (described by  $D$ ) but also the shape of the ground and transition state (described by the lengths  $l_c$  and  $l_{ts}$ ) are likely changed by an applied force. [76] Our finding of the high stability of the cis-state against an external force may also reflect these effects.

### 8.3.3. Optomechanical Cycles, Molecular Machines and Motors

In the introduction the following definitions for molecular machines and motors have been given: "A machine is a device that converts energy from one form into another in a cyclic way. The specific machine, which converts a 'fuel' into mechanical work in repeated cycles, shall be termed 'motor'." Molecular machines commonly are polymers that do so. In the cycles shown in Figure 7.8 clearly optical excitation was transformed into mechanical work and this change was detected. If this can be termed a motor is best discussed by comparing it

to the Otto-Cycle, which will illuminate the advantages and shortcomings of the investigated single molecule system.

In Figure 8.7a and 8.7b the pressure-volume diagram of an Otto-Cycle and the optomechanical single-molecule cycle of a polyazopeptide are sketched. Taking the force for pressure and the extension for negative volume, these two cycles are comparable:

At point one the valve is closed (the polymer attached) and the piston compresses the air (the cantilever extends the molecule) to point two, which also slightly raised the temperature. Then the combustion of the gasoline increases the temperature and pressure drastically to point three. (A  $\lambda = 365$  nm pulse is applied which contracts the polymer. The energy thereof is partly delivered to the cantilever and the other part stored in the molecule - with a stiffer cantilever, this amount increases and the Otto-Cycle is approached.) In the next step, the piston is expanded adiabatically, performing work. (The molecule is relaxed and the remaining work is performed). Finally, the exhaust is released, which corresponds to the lengthening of the molecule with a  $\lambda = 420$  nm pulses.

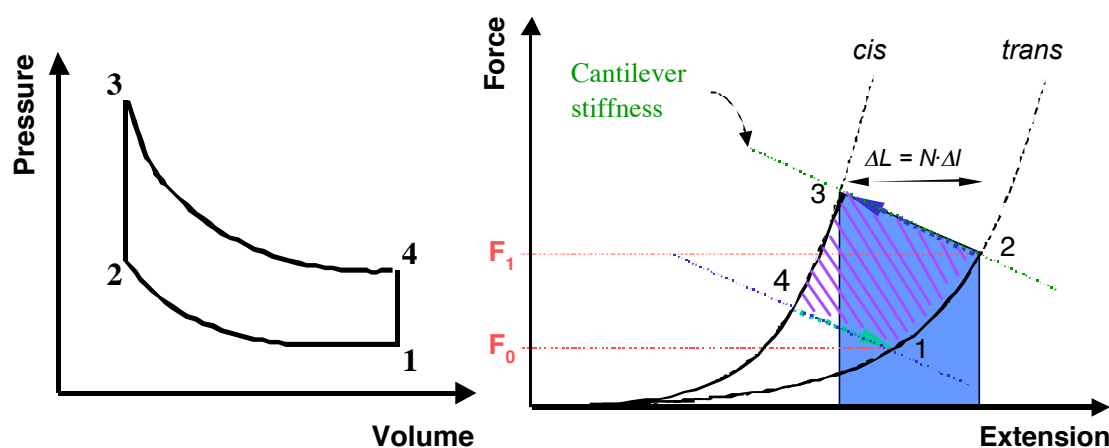


**Figure 8.7:** a) Pressure-Volume diagram for an Otto-cycle. b) Single-molecule operating cycle, based on a polymer consisting of repeating segments exhibiting a reversible transition from a short (cis) to an extended (trans) configuration, and vice versa. Blue area: mechanical work delivered during the optical contraction. Hatched area: total mechanical work per cycle.

The major achievement in this experiment is that the nanoscopic mechanical change can be interfaced, stored and quantified macroscopically, which allows to estimate the efficiency of the optomechanical energy conversion:

With the given quantum efficiencies for the cis-trans transition of about 0.5 and the trans-cis transition of about 0.1, roughly 120 photons (or an optical energy of  $6.6 \cdot 10^{-17}$  J) would be required to switch all 10 azobenzene units in the azobenzene of Figure 7.8a. The overall energy conversion efficiency for this extremely simple optomechanical motor is thus  $\eta \approx 7.5 \cdot 10^{-4}$ . [30] The efficiency of the optomechanical contraction, the key step in the cycle, can be

---

estimated by assuming that the energy of a single photon  $E_{\text{exc}} = 5.5 \cdot 10^{-19} \text{ J}$  ( $\lambda = 365 \text{ nm}$ ) is used to perform the mechanical work  $W_{\text{mech}} \approx 0.22 \text{ nm} \cdot 205 \text{ pN} \approx 4.5 \cdot 10^{-20} \text{ J}$  by contracting a single azobenzene unit against the external force. In our configuration, which is far from being optimized, we measured an upper limit of  $\eta_{\text{max}} \approx 0.1$ .

## 9. Outlook

In the following some possible future theoretical and technical developments related to this work are given. Some of them are likely to be achieved in the near future, while others might forever stay a dream:

- The investigation of theoretical models for the fitting of single molecule force-extension data showed that especially in the high force regime discretization effects <sup>[8]</sup> play a major role, but also stretching and bending fluctuations. <sup>[7]</sup> This will lead to fit-functions which will reproduce experimental data better, especially in the high force regime accessible with the AFM, and with fewer fit parameters (preliminary results for a carbon backbone are discussed in Section 8.1). <sup>[8]</sup>
- The OSF-theory describes the stiffening of polyelectrolytes with increasing charge or decreasing counter ion concentration with a constant additive term to the 'zero charge' persistence length,  $l_0$ . The single molecule measurements performed here, show that a force dependent persistence length <sup>[7]</sup> describes the experimental data better, but still not perfectly. A combination with the discretization effects <sup>[8]</sup> might further improve the fits.
- The theory for the desorption of charged polymers from solid charged substrates is still far from being complete. Especially the 'zero charge' contribution is still under discussion. The results presented here and further experiments will stimulate new theoretical approaches.
- The combination of single molecule force spectroscopy and optical excitation gives access to data which cannot be obtained by other means. It will and already has stimulated theoretical approaches and simulations on optomechanical coupling and excited states. Especially force and (excitation) energy dependent length changes will allow to test theoretical approaches and calculations. Further, it should be possible to probe the force dependent energy landscape of the excited state by wavelength dependent spectroscopy.
- Reversible molecular switches will be of great importance for all kind of future nano-devices and computers. Single light addressable molecules might become an alternative to the extensively investigated DNA approach. The technical application of single molecule motors is still in the far future, but if they are constructed, optomechanical systems are likely to be utilized besides electronic systems. Light is fast, easily addressable, can be used in most ambients and has no waste problem.

- The assembly of functional units on the nanometer scale will become more and more important. The systems investigated in this thesis could be a basis for a 'grab and release' technology: Both, the reversible switching of azobenzene and the reversible manipulation of surface adhesion could be utilized to grab and release single functional polymers. Together with the nanometer position sensitivity of an AFM this would allow for a molecular assembly. The same principle could enable the production of a molecular toolbox. Tools with an 'azobenzene handle' or variable surface adhesion properties could be grabbed, positioned and released with nanometer accuracy.
- It should be most fascinating to study hydrophobic vicinity effects on the strength and lifetime of ionic charges in aqueous systems, a fundamental problem closely related to the still unsolved protein folding mystery. Among the materials scientists, it is expected that the investigation of this apparently simple question at the level of individual polymer molecules might help to design further improved surface coatings, lubricants or other high performance colloids.
- The coupling of light into an AFM experiment could also be utilized to increase the temperature or release chemicals. Light flashes could for example release ions from caged compounds or activate ion receptors to bind ions. With compounds containing the functional azobenzene unit (e.g. an EDTA-like azobenzene) this should even be possible in a reversible way. [163] [126]

Specially designed functional synthetic polymers could be the basis for many of the above discussed light directed jobs. Of course, synthetic polymers are still far away from the almost perfect, self-healing, high-efficiency, adaptable biological machines – but they can be designed, controlled and now also interfaced to the macroscopic world.

## 10. Apendices

### 10.1. Details of the Coupling Chemistry

#### 10.1.1. Surface Preparations

Glass microscope slides (25x75x1 mm, Sigma, Deisenhofen, Germany) and flint glass microscope slides (F-2, 25x71x1 mm, Schott Glas Mainz, Hellma Optik GmbH Jena, Germany) were cleaned prior to each experiment by sonicating for 10 minutes in Hellmanex solution (Hellma, Mühlheim, Germany), and twice for 10 minutes in MilliQ water (Deionized water which is further purified using a MilliQ plus system with  $\sigma = 18.2 \text{ M}\Omega\text{cm}$ ).

In order to obtain aminoreactive surfaces the cleaned microscope slides were put in a 5 vol% solution of (3-glycidyloxypropyl)trimethoxysilane (Aldrich, Deisenhofen, Germany) in isopropanol for one hour. The substrates were then kept in an oven at 90°C for half an hour, followed by successive rinsing with isopropanol. Increased hydrophobicity of the substrates was observed in contact angle measurements after silanization. Park Thermomicroscope Cantilevers (Sunnyvale CA, USA) were used as obtained. They were made aminoreactive by putting them for 10 s in (3-glycidyloxypropyl)trimethoxysilane and rinsing in toluene and water followed by baking at 90°C for 30 minutes. The silanes should covalently bind to the silica surface and crosslinks upon baking, which gives a dense aminoreactive film on the surface (Figure 10.1).

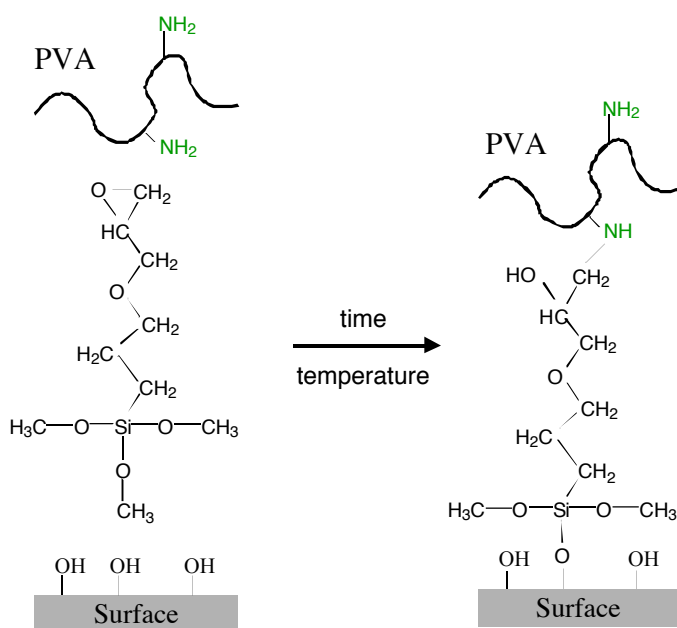


**Figure 10.1:** Surface hydroxy functions (naturally present on silica substrates as well as on silicon nitride AFM tips) are converted to amino-reactive epoxy functions via silanization. Chemical reaction with amino functions of PVA yields  $\beta$ -hydroxyalkylamine function.

Amino groups were introduced on microscope slides by putting few drops of N'-[3-(trimethoxysilyl)propyl]-diethylene-triamine (Aldrich) onto the slides, which were then

placed in a 90 °C oven for 15 minutes. Afterwards they were rinsed with ethanol followed by water and then placed in 90° C hot water for 30 minutes and rinsed again with cold water.

When gold coated surfaces were needed, cleaned glass microscope slides and Park Thermomicroscope Lever were coated with 5 nm CrNi (80:20) and 30-40 nm gold in a homebuilt evaporation-chamber. In some cases Olympus Bio-Levers (Olympus, Tokyo, Japan) were used as obtained. These cantilevers are completely gold coated, very small and soft. The spring constant for the two different beam sizes on the Olympus Bio-Lever chips are given by the manufacturer as 0.006 N/m and 0.027 N/m, respectively.

Hydrophobized glass was obtained by etching a cleaned glass slide for 10 minutes in KOH (1 M) and rinsing it with MilliQ water. Then it was exposed to dimethyldichlorsilane vapor for 10 minutes.

### 10.1.2. Coupling of the Molecules

Polyvinylamine (PVA) was attached to the substrates by incubating a small region of the surface with a few drops of an aqueous polymer solution ( $0.2 \text{ mg}\cdot\text{ml}^{-1}$ ) for 30 minutes, followed by successive rinsing with MilliQ water. This procedure was used for both, physisorption of the polymers onto the negatively charged glass substrate, as well as for covalent binding of the amino groups to aminoreactive supports. The PVA was then covalently bound to the aminoreactive cantilever within the experiment (as shown by the high rupture forces in the elasticity experiments). In some preliminary experiments the molecules were covalently attached to the cantilever prior to the experiment and then brought into contact with a clean surface. This approach was continued and optimized by Jöstl in his Diploma thesis. <sup>[10]</sup> All experiments were conducted in solutions of 1:1 electrolytes (NaCl) at room temperature ( $\sim 21^\circ\text{C}$ ), unless otherwise specified.

Polypeptides were measured with gold coated cantilevers on gold substrates. Self-assembled mixed 'mono'-layers were usually used to suppress nonspecific adhesion. For the preparation of these layers, quantities of 1 mg of the polypentapeptides and 0.5 mg methoxy-PEG-thiol (Sharewater Corporation, Huntsville, US,  $M_w \sim 5000$ ) were dissolved in 1 ml MilliQ water prior to each experiment.<sup>18</sup> 20  $\mu\text{l}$  of this solution were incubated on the gold-coated slide for about 30 minutes at  $3^\circ\text{C}$  or for 5 minutes at room temperature and then rinsed with MilliQ water.

---

<sup>18</sup> The peptides are stable infinitely, whether dry or in water, as long as the temperature is below  $60^\circ\text{C}$  (due to a very slow racemization) and as long as there is no organism that finds it and begins to degrade it. As this cannot be excluded, the recommendation is to keep the material as a dry powder until just before use, and to make up fresh solutions for each experiment (personal e-mail from D. Urry 27.11.99).

For the covalent attachment of the azobenzene containing polypeptide a stepwise approach was utilized. The polymer chains were coupled to the probe tip by first physisorbing them for 90 minutes to gold coated cantilevers in dimethylsulfoxide (DMSO, formula:  $C_2H_6OS$ ) solution, followed by deprotecting the thiol group using 5% trifluoroacetic acid in dichloromethane ( $CH_2Cl_2$ ) for 30 minutes. The proximity of the deprotected thiol groups to the gold surface resulted in chemisorption of the polypeptides to the gold-coated tip via the formation of a covalent gold-thiol bond. Having mounted a polymer modified cantilever chip in the force spectrometer, the C-termini of the polypeptides (carboxy groups) were activated by the addition of excess amounts of *N*-hydroxysuccinimide (NHS) and 1-ethyl-3-(3-dimethylaminopropyl) carbodiimide (EDC) (NHS and EDC in 1:1 molar ratio) in DMSO to promote the formation of a peptide bond with the amino groups on the aminofunctionalized glass slide surface.

## 10.2. Details of the Instrumental Setup

The principle of single molecule force spectroscopy is described in several publications, for reviews see [24] [25] [9]. The experiments in this thesis were performed on three different AFMs:

- A homebuilt instrument, which was constructed by Prof. Matthias Rief in 1996 and is described in detail in [161].
- A molecular force probe (MFP) from AsylumResearch (Santa Barbara, CA, USA), which is commercial available and described in detail at "www.asylumresearch.com".
- A homebuilt instrument, which was built by Alexander Schemmel and is described in [164].

The sample stage of the instrument built by Schemmel was redesigned in order to couple optical excitation in total internal reflection geometry into the glass microscope slide, to keep all stray light from the proximity of the cantilever and to de-couple all vibrations of the flashlamp from the AFM. A Xenon-flashlamp JML-C1 (Rapp OptoElectronic, Hamburg, D, "www.rapp-opto.com") was used as a light source. The two wavelength ranges necessary to switch the investigated polyazopeptides were obtained by the following filter sets:

- For the lengthening of the polymer a GG 420 colorglass filter (Itos GmbH, Mainz) was used, the transmission for wavelength smaller than 400 nm is less than  $10^{-5}$  while it is more than 90% for wavelength larger than 450 nm. In addition, a colorglass BG12 (Schott, Mainz) blocked more than 90% at frequencies higher than 525 nm. The maximum energy of a flash with this filter set was measured by a thermal power meter (Spectra Physics, model 407A) to  $E_{\max} = 100$  mJ. In the following, pulses with this filter set will be referred to by ' $\lambda = 420$  nm pulses'.
- For the shortening of the polymers a 365 nm bandpass filter with a band half width of 12.2 nm was used (Itos GmbH, Mainz, UVDAD T47,2%), also in combination with the colorglass BG12 (see above). With this filter set a maximum pulse energy of  $E_{\max} = 10$  mJ was measured. This filter set will be referred to by ' $\lambda = 365$  nm pulses'.

The filtered light was then focused onto the polished edge of a flint glass microscope slide (transmission at  $\lambda = 365$  nm and  $d = 10$  mm: 0.967) in total internal reflection geometry. All measurements were performed in dimethylsulfoxide (refractive index  $n_D = 1.48$ ).

### 10.3. Data Acquisition

It turned out that the following strategy was the best to obtain force profiles of just single polymer strands: The AFM tip is brought into contact with the substrate for some time to 'pick up' one or several surface bound polymer molecules. Depending on the nature of the tip-polymer interaction several milliseconds up to minutes are needed to achieve sufficient binding. Then, the cantilever is retracted to a distance at which nonspecific adhesion is no longer observed.<sup>19</sup> In successive retraction-approaching cycles the distance range is continuously increased, while avoiding contact between the tip and additional polymer strands at the substrate surface. The detachment of polymer chains from the AFM tip is reflected by sharp peaks consisting of their elastic response followed by a sudden drop in the force when the chain detaches. After their detachment, the elastic response of these shorter polymer strands will thus no longer be observed in successive cycles, such that eventually only one polymer chain will remain between tip and substrate. The force profile of this last remaining strand may then be taken repeatedly until rupture. After the eventual detachment of the investigated polymer strand, the full distance range has to be probed in order to exclude the presence of any longer strands. A reliable test for single molecules can only be done after the rupture of the molecule. Assuming that in the probed force regime the measured stretching force is a function of the relative extension of the polymer chain, i.e.  $F \sim f(R_z/L)$  – like in the FJC and WLC-model, all force traces originating from single polymer chains should superimpose when scaled to the same contour length. In turn, the superposition of the force traces serves as a criteria for the identification of single polymer strands.

For the optomechanical experiments, a computer with a National Instrument card (PCI-Mio-16XE-10) and the NIDAQ Tools from WaveMetrics (Lake Oswego, USA) was used to stream data continuously in addition to the usual data acquisition. This enabled to correct for tiny long term (up to an hour) drifts in the deflection and the piezo signal.

---

<sup>19</sup> At short distances, strong adhesive forces may dominate the interaction profile, and although they may contain many details of single molecule events, they are usually too complex to be analyzed in detail. It may include contributions from the stretching of several polymer strands, the desorption of the polymer strands from substrate and/or cantilever, from covalent bond rupture of short strands, as well as forces resulting from interchain aggregation and entanglements. While these adhesive interactions may yield important information about local surface properties averaged over several  $\text{nm}^2$ , [165] [166] in single molecule stretching experiments the minimization of unspecific adhesion is highly desired in order to extract as many details of single polymer elasticity as possible.

## 10.4. Calibration of Spring Constants

The spring constants for the cantilevers given by the manufacturer are for many applications not accurate enough, therefore different methods to measure the spring constant of an individual cantilever were developed. The most common and in our lab utilized method is the thermal method, which measures the power spectrum of the cantilever's thermal oscillations. This is then either related to the thermal energy by the equipartition theorem <sup>[167]</sup> or by fitting a damped harmonic oscillator model to the thermal power spectrum. <sup>[168]</sup> A recent study by Lèvy and Maaloum <sup>[169]</sup> found as expected more than 10% deviation from the spring constant values given by the manufacturer, while the spring constants determined by different thermal methods varied by less than 10 %. A comparison of the added-mass method and the thermal method yields an about 20% difference between these methods. <sup>[170] [171]</sup>

To measure the deflection,  $x$ , of a cantilever the most commonly used optical lever method was utilized in all experiments. The sensitivity of the optical lever can be characterized by the 'inverse optical lever sensitivity' (InvOLS), where  $x = \text{InvOLS} \cdot \Delta V$  with the differential voltage  $\Delta V$  measured by a position sensitive detector. The InvOLS is usually quantified by bringing the cantilever into contact with a rigid surface and then moving it a known distance. The slope of the resulting cantilever deflection vs. distance yields the InvOLS. The optical lever sensitivity measured with this method from the constant-compliance region of a deflection-piezopath curve is not exactly the correct InvOLS to use. This is because the shape of an oscillating cantilever (power spectrum) and one bending due to a constant force (InvOLS) are slightly different. <sup>[172]</sup> The data is corrected to reflect this like described by Butt. <sup>[167]</sup>

It is reasonable to give an error of 10% for the determined spring constants, if consistently one method is used and if the power spectrum is taken at approximately the same distance away from the surface for all cantilevers.

## 10.5. Abbreviations

AFM	-	atomic force microscopy
AMBP	-	(4-amino)phenylazobenzoic acid
ATP	-	adenosine triphosphate
DC	-	discrete chain
DMSO	-	dimethylsulfoxide
DNA	-	desoxyribonucleic acid
EDTA	-	ethylene-diamine-tetra-acetate
FJC	-	freely jointed chain
GC	-	guanidinium chloride
InvOLS	-	inverse optical lever sensitivity
LCST	-	lower critical solution temperature
MD	-	molecular dynamics
OSF	-	Odijk, Skolnick, Fixman
PBS	-	phosphate buffered saline
PEG	-	polyethyleneglycol
PNIPAM	-	poly(N-isopropylacrylamide)
PVA	-	polyvinylamine
RNA	-	ribonucleic acid
SDS	-	sodium dodecyl sulfate
SEM	-	scanning electron microscopy
SFA	-	surface force apparatus
SMFS	-	single molecule force spectroscopy
TEM	-	transmission electron microscopy
TIR	-	total internal reflection
WLC	-	worm-like chain

## 11. Literature

- 1 R. P. Feynman, *There's Plenty of Room at the Bottom*, Engineering and Science **23**, 22-36 (1960).
- 2 M. A. Reed, C. Zhou, C. J. Muller, T. P. Burgin and J. M. Tour, *Conductance of a Molecular Junction*, Science **278**, 252-254 (1997).
- 3 W. Liang, M. P. Shores, M. Bockrath, J. R. Long and H. Park, *Kondo resonance in a single-molecule transistor*, Nature **417**, 725-9. (2002).
- 4 J. Park, A. N. Pasupathy, J. I. Goldsmith, C. Chang, Y. Yaish, J. R. Petta, M. Rinkoski, J. P. Sethna, H. D. Abruna, P. L. McEuen and D. C. Ralph, *Coulomb blockade and the Kondo effect in single-atom transistors*, Nature **417**, 722-5. (2002).
- 5 Y. Wada, M. Tsukada, M. Fujihira, K. Matsushige, T. Ogawa, M. Haga and S. Tanaka, *Prospects and Problems of Single Molecule Information Devices*, Jpn. J. Appl. Phys. **39**, 3835-3849 (2000).
- 6 T. Hugel, M. Grosholz, H. Clausen-Schaumann, A. Pfau, H. Gaub and M. Seitz, *Elasticity of single polyelectrolyte chains and their desorption from solid supports studied by AFM based single molecule force spectroscopy*, Macromolecules **34**, 1039-1047 (2001).
- 7 R. R. Netz, *Strongly Stretched Semiflexible Extensible Polyelectrolytes and DNA*, Macromolecules **34**, 7522-7529 (2001).
- 8 L. Livadaru, R. R. Netz and H. J. Kreuzer, *Stretching Response of Discrete Semiflexible Polymers*, Macromolecules **submitted**, (2002).
- 9 T. Hugel and M. Seitz, *The Study of Molecular Interactions by AFM Force Spectroscopy*, Macromol. Rapid Commun. **22**, 989-1016 (2001).
- 10 W. Jöstl, *Untersuchung der Polymerdesorption von geladenen Oberflächen mit Einzelmolekülspektroskopie*, Diplom, Ludwig-Maximilians-Universität München (2002).
- 11 D. W. Urry, *Physical chemistry of biological free energy transduction as demonstrated by elastic protein-based polymers*, J. Phys. Chem. B **101**, 11007-11028 (1997).
- 12 H. Rau, *Photochromism: Molecules and Systems*, Elsevier, Amsterdam (1990).
- 13 T. Hugel, N. B. Holland, A. Cattani, L. Moroder, M. Seitz and H. E. Gaub, *Single-Molecule Optomechanical Cycle*, Science **296**, 1103 (2002).
- 14 J. F. Stoddart, *Molecular Machines*, Accounts of chemical research **34**, 410 (2001).
- 15 B. F. Erlanger, , Annu. Rev. Biochem. **45**, 267 (1976).
- 16 G. S. Kumar and D. C. Neckers, *Photochemistry of Azobenzene-Containing Polymers*, Chemical Review **89**, 1915-1925 (1989).
- 17 A. D. Mehta, M. Rief, J. A. Spudich, D. A. Smith and R. M. Simmons, *Single-Molecule Biomechanics with Optical Methods*, Science **283**, 1689-1695 (1999).

- 18 V. Balzani, A. Credi, F. M. Raymo and J. F. Stoddart, *Artificial molecular machines*, *Angew. Chem. Int. Ed.* **39**, 3348 (2000).
- 19 D. W. Urry, *Molecular Machines - How Motion and Other Functions Of Living Organisms Can Result From Reversible Chemical Changes*, *Angew. Chem.* **105**, 859-883; *Angew. Chem. Intl. Ed.* **1993**, 32, 819-841 (1993).
- 20 G. Binnig, C. F. Quate and C. Gerber, *Atomic force microscope*, *Phys. Rev. Lett.* **56**, 930 (1986).
- 21 M. B. Viani, T. E. Schaffer, G. T. Paloczi, L. I. Pietrasanta, B. L. Smith, J. B. Thompson, M. Richter, M. Rief, H. E. Gaub, K. W. Plaxco, A. N. Cleland, H. G. Hansma and P. K. Hansma, *Fast imaging and fast force spectroscopy of single biopolymers with a new atomic force microscope designed for small cantilevers*, *Rev. Scientific Instruments* **70**, 4300-4303 (1999).
- 22 T. Schäffer, *Force spectroscopy with a large dynamic range using small cantilevers and an array detector*, *Journal of applied physics* **91**, 4739-4746 (2002).
- 23 M. Rief, M. Gautel, F. Oesterhelt, J. M. Fernandez and H. E. Gaub, *Reversible unfolding of individual titin Ig-domains by AFM*, *Science* **276**, 1109-1112 (1997).
- 24 A. Janshoff, M. Neitzert, Y. Oberdörfer and H. Fuchs, *Kraftspektroskopie an molekularen Systemen - Einzelmolekülspektroskopie an Polymeren und Biomolekülen (Force Spectroscopy of Molecular Systems - Single Molecule Spectroscopy of Polymers and Biomolecules)*, *Angew. Chem.* **112**, 3346-3374 (2000).
- 25 H. Clausen-Schaumann, M. Seitz, R. Krautbauer and H. Gaub, *Force spectroscopy with single bio-molecules*, *Curr. Op. Chem. Biol.* **4**, 524-530 (2000).
- 26 R. Krautbauer, L. H. Pope, T. E. Schrader, S. Allen and H. E. Gaub, *Discriminating small molecule DNA binding modes by single molecule force spectroscopy*, *FEBS Letters* **510**, 154-158 (2002).
- 27 T. Odijk, *Polyelectrolytes near the Rod Limit*, *J. Polym. Sci.* **15**, 477-483 (1977).
- 28 J. Skolnick and M. Fixman, *Electrostatic Persistence Length of a Wormlike Polyelectrolyte*, *Macromolecules* **10**, 944-948 (1977).
- 29 R. R. Netz and D. Andelman, *Adsorbed and Grafted Polymers at Equilibrium*, Marcel Dekker, Inc., New York (2000).
- 30 N. B. Holland, T. Hugel, G. Neuert, A. Cattani-Scholz, C. Renner, D. Oesterhelt, L. Moroder, M. Seitz and H. E. Gaub, *Single Molecule Force Spectroscopy of Azobenzene Polymers: Switching Elasticity of Single Photochromic Macromolecules*, *Macromolecules* **submitted**, (2002).
- 31 S. B. Smith, L. Finzi and C. Bustamante, *Direct mechanical measurements of the elasticity of single DNA molecules by using magnetic beads*, *Science* **258**, 1122-1126 (1992).
- 32 A. Ashkin, K. Schütze, J. M. Dziedzic, U. Euteneuer and M. Schliwa, *Force generation of organelle transport measured in vivo by an infrared laser trap*, *Nature* **348**, 346-348 (1990).
- 33 A. Kishino and T. Yanagida, *Force measurements by micromanipulation of a single actin filament by glass needles*, *Nature* **334**, 74-76 (1988).

- 34 E. Evans, K. Ritchie and R. Merkel, *Sensitive force technique to probe molecular adhesion and structural linkages at biological interfaces*, Biophys. J. **68**, 2580-2587 (1995).
- 35 M. Grandbois, M. Beyer, M. Rief, H. Clausen-Schaumann and H. E. Gaub, *How Strong is a Covalent Bond ?*, Science **283**, 1727-1730 (1999).
- 36 D. Leckband and J. Israelachvili, *Intermolecular Forces in Biology*, Quarterly Reviews of Biophysics **34**, 105-267 (2001).
- 37 D. W. Urry, *Five axioms for the functional design of peptide-based polymers as molecular machines and materials: principle of macromolecular assemblies*, Biopolymers (Peptide Science) **47**, 167-178 (1998).
- 38 C. H. Luan and D. W. Urry, *Elastic, Plastic and Hydrogel Protein-based Polymers*, Oxford University Press, Oxford (2002).
- 39 D. Urry, *personal e-mail* (2000).
- 40 J. C. Rodriguez-Cabello, M. Alonso, M. I. Diez, M. I. Caballero and M. M. Herguedas, *Structural investigation of the poly(pentapeptide) of elastin, poly(GVGVP), in the solid state.*, Macromol. Chem. Phys. **200**, 1831-1838 (1999).
- 41 R. Behrendt, M. Schenk, H. J. Musiol and L. Moroder, *Photomodulation of conformational states. Synthesis of cyclic peptides with backbone-azobenzene moieties*, J. Pept. Sci. **5**, 519-529 (1999).
- 42 H. J. Kreuzer, S. H. Payne and I. Livaradu, *Stretching a macromolecule in an atomic force microscope: statistical mechanical analysis*, Biophys. J. **80**, 2505-2514 (2001).
- 43 H. J. Kreuzer and S. H. Payne, *Stretching a macromolecule in an atomic force microscope: statistical mechanical analysis*, Phys. Rev. E **63**, 021906 (2001).
- 44 American Chemical Society and G. D. Chemiker, *Hermann Staudinger Begründer der Polymerwissenschaften*, Broschüre zum Internationalen Historischen Meilenstein der Chemie in Freiburg **April**, (1999).
- 45 T. L. Hill, *An Introduction to Statistical Thermodynamics*, Dover Publications, New York (1986).
- 46 P. J. Flory, *Statistical Mechanics of Chain Molecules*, Hanser, München (1988).
- 47 G. Strobl, *The Physics of Polymers*, Springer, Berlin (1997).
- 48 M. Doi and S. F. Edwards, *The Theory of Polymer Dynamics*, Oxford University Press, Oxford (1998).
- 49 O. Kratky and G. Porod, *Röntgenuntersuchung gelöster Fadenmoleküle*, Rec. Trav. Chim. **68**, 1106 (1949).
- 50 G. U. Lee, L. A. Chris and R. J. Colton, *Direct measurement of the forces between complementary strands of DNA*, Science **266**, 771-773 (1994).
- 51 T. J. Senden, J. M. di Meglio and P. Auroy, *Anomalous adhesion in adsorbed polymer layers*, Eur. Phys. J. B **3**, 211-216 (1998).

- 52 C. Ortiz and G. Hadziioannou, *Entropic Elasticity of Single Polymer Chains of Poly(methacrylic acid) Measured by Atomic Force Microscopy*, *Macromolecules* **32**, 780-787 (1999).
- 53 M. Ullner and C. E. Woodward, *Orientalional Correlation Function and Persistence Lengths of Flexible Polyelectrolytes*, *Macromolecules* **35**, 1437-1445 (2002).
- 54 A. Y. Grosberg, A. R. Khokhlov and A. I. Grosberg, *Statistical Physics of Macromolecules*, Springer Verlag, 1994).
- 55 L. D. Landau and J. M. Lifschitz, *Lehrbuch der theoretischen Physik*, Akademie Verlag Berlin, 1979).
- 56 M. Fixman and J. Kovac, *Polymer conformational statistics. III. Modified Gaussian models of stiff chains.*, *Journal of Chemical Physics* **58**, 1564-1568 (1973).
- 57 J. Kovac and C. G. Crabb, *Modified Gaussian Model for Rubber Elasticity. 2. The Wormlike Chain*, *Macromolecules* **15**, 537-541 (1982).
- 58 C. Bustamante, J. F. Marko, E. D. Siggia and S. Smith, *Entropic Elasticity of  $\lambda$ -Phage DNA*, *Science* **265**, 1599-1600 (1994).
- 59 J. F. Marko and E. D. Siggia, *Stretching DNA*, *Macromolecules* **28**, 8759-8770 (1995).
- 60 M. D. Wang, H. Yin, R. Landick, J. Gelles and S. M. Block, *Stretching DNA with Optical Tweezers*, *Biophys. J.* **72**, 1335-1346 (1997).
- 61 C. Bouchiat, M. D. Wang, J.-F. Allemand, T. Strick, S. M. Block and V. Croquette, *Estimating the persistence length of a worm-like chain molecule from force-extension measurements*, *Biophys. J.* **76**, 409-413 (1999).
- 62 J. Kyte, *Structure in Protein Chemistry*, Garland Publishing, New York (1995).
- 63 B. D. Ratner, A. S. Hoffman, F. J. Schoen and J. E. Lemons, *Biomaterials Science*, Academic Press, San Diego (1996).
- 64 H. Dautzenberg, W. Jaeger, J. Kötzt, B. Philipp, C. Seidel and D. Stscherbina, *Polyelectrolytes*, Carl Hanser Verlag, Munich (1994).
- 65 J. Israelachvili, *Intermolecular and Surface Forces*, Academic Press Ltd., London (1991).
- 66 G. S. Manning, *Limiting Laws and Counterion Condensation in Polyelectrolyte Solutions I. Colligative Properties*, *Journal of Chemical Physics* **51**, 924 (1969).
- 67 H. Mattoussi, S. O'Donohue and F. E. Karasz, *Polyion conformation and second virial coefficient dependences on the ionic strength for flexible polyelectrolyte solutions*, *Macromolecules* **25**, 743-749 (1992).
- 68 G. Maret and G. Weill, *Magnetic Birefringence Study of the Electrostatic and Intrinsic Persistence Length of DNA*, *Biopolymers* **22**, 2727-2744 (1983).
- 69 R. R. Netz and H. Orland, *Variational theory for a single polyelectrolyte chain*, *The European Physical Journal B* **8**, 81-98 (1999).
- 70 A. V. Dobrynin, A. Deshkovski and M. Rubinstein, *Adsorption of Polyelectrolytes at Oppositely Charged Surfaces*, *Macromolecules* **34**, 3421-3436 (2001).

- 71 A. R. Khokhlov and K. A. Khachaturian, *On the Theory of Weakly Charged Polyelectrolytes*, *Polymer* **23**, 1742 (1982).
- 72 J. L. Barrat and J. F. Joanny, *Persistence Length of Polyelectrolyte Chains*, *Europhys. Lett.* **24**, 333-338 (1993).
- 73 H. Li, B. Liu, X. Zhang, C. Gao, J. Shen and G. Zou, *Single-molecule force spectroscopy on poly(acrylic acid) by AFM*, *Langmuir* **15**, 2120-2124 (1999).
- 74 E.-L. Florin, V. T. Moy and H. E. Gaub, *Adhesive forces between individual ligand-receptor pairs.*, *Science* **264**, 415-417 (1994).
- 75 G. I. Bell, *Models for the specific adhesion of cells to cells*, *Science* **200**, 618-627 (1978).
- 76 E. Evans and K. Ritchie, *Dynamic Strength of Molecular Adhesion Bonds*, *Biophys. J.* **72**, 1541-1555 (1997).
- 77 R. Merkel, P. Nassoy, A. Leung, K. Ritchie and E. Evans, *Energy landscapes of receptor-ligand bonds explored with dynamic force spectroscopy*, *Nature* **397**, 50-53 (1999).
- 78 M. Balsera, S. Stepaniants, S. Izrailev, Y. Oono and K. Schulten, *Reconstructing potential energy functions from simulated force-induced unbinding processes*, *Biophys. J.* **73**, 1281-1287 (1997).
- 79 B. Heymann and H. Grubmüller, *Dynamic Force Spectroscopy of Molecular Adhesion Bonds*, *Phys. Rev. Lett.* **84**, 6126-6129 (2000).
- 80 E. Evans, *Looking inside molecular bonds at biological interfaces with dynamic force spectroscopy*, *Biophys. Chem.* **82**, 83-97 (1999).
- 81 S. A. Arrhenius, *On the Reaction Velocity of the Inversion of Cane Sugar by Acids*, *Zeitschrift für Physikalische Chemie* **4**, 226 (1889).
- 82 P. Hanggi, P. Talkner and M. Borkovec, *Reaction-rate theory: fifty years after Kramers*, *Rev. Mod. Phys.* **62**, 251-342 (1990).
- 83 H. A. Kramers, *Brownian motion in a field of force and the diffusion model of chemical reactions*, *Physica* **7**, 284-304 (1940).
- 84 E. Evans and P. Williams, *Dynamic Force Spectroscopy: I. Single Bonds*, Springer-Verlag, Berlin (2002).
- 85 E. Evans and F. Ludwig, *Dynamic strengths of molecular anchoring and material cohesion in fluid biomembranes*, *J. Phys.: Condens. Matter* **12**, A315-A320 (2000).
- 86 E. Evans, *Probing the relation between force-lifetime-and chemistry in single molecular bonds*, *Annu. Rev. Biophys. Biomol. Struct.* **30**, 105-128 (2001).
- 87 D. A. Simson, M. Strigl, M. Hohenadl and R. Merkel, *Statistical Breakage of Single Protein A-IgG Bonds Reveals Crossover from Spontaneous to Force-Induced Bond Dissociation*, *Physical Review Letters* **83**, 652-655 (1999).
- 88 U. Seifert, *Rupture of Multiple Parallel Molecular Bonds under Dynamic Loading*, *Physical Review Letters* **84**, 2750-2753 (2000).

- 89 B. Haupt, J. Ennis and E. M. Sevick, *The detachment of a polymer chain from a weakly adsorbing surface using an AFM tip*, *Langmuir* **15**, 3886-3892 (1999).
- 90 U. Dammer, M. Hegner, D. Anselmetti, P. Wagner, M. Dreier, W. Huber and H.-J. Güntherodt, *Specific antigen / antibody interactions measured by atomic force microscopy*, *Biophys. J.* **70**, 2437-2441 (1996).
- 91 M. Ludwig, W. Dettmann and H. E. Gaub, *AFM imaging contrast based on molecular recognition*, *Biophys. J.* **72**, 445-448 (1997).
- 92 F. Kienberger, G. Kada, H. J. Gruber, V. P. Pastushenko, C. Riener, M. Trieb, H. G. Knaus, H. G. Schindler and P. Hinterdorfer, *Recognition Force Spectroscopy Studies of the NTA-His6 Bond*, *Single Mol.* **1**, 59 (2000).
- 93 D. Y. C. Chan and R. G. Horn, *The drainage of thin liquid films between solid surfaces*, *J. Chem. Phys.* **83**, 5311-5324 (1985).
- 94 M. K. Beyer, *The mechanical strength of a covalent bond calculated by density functional theory*, *J. Chem. Phys.* **112**, 7307-7312 (2000).
- 95 T. E. Fisher, A. F. Oberhauser, M. Carrion-Vazquez, P. E. Marszalek and J. M. Fernandez, *The study of protein mechanics with the atomic force microscope*, *Trends in Biochemical Sciences* **24**, 379-384 (1999).
- 96 M. Conti, Y. Bustanji, F. Giuseppe, P. Ferruti, S. Stefoni and B. Samori, *The Desorption Process of Macromolecules Adsorbed on Interfaces: The Force Spectroscopy Approach*, *ChemPhysChem* **10**, 610-613 (2001).
- 97 M. Rief, H. Clausen-Schaumann and H. E. Gaub, *Sequence dependent mechanics of single DNA-molecules*, *Nature Struct. Biol.* **6**, 346-349 (1999).
- 98 I. Borukhov, D. Andelman and H. Orland, *Scaling Laws of Polyelectrolyte Adsorption*, *Macromolecules* **31**, 1665-1671 (1998).
- 99 R. R. Netz and J. F. Joanny, *Complexation Behavior of Polyampholytes and Charged Objects*, *Macromolecules* **31**, 5123-5141 (1998).
- 100 A. G. Moreira and R. R. Netz, *Strong-Coupling Theory for Counter-Ion Distributions*, *Europhysics Letter* **52**, 705-711 (2000).
- 101 L. Bergström, *Hamaker Constants of Inorganic Materials*, *Adv. Colloid Interface Sci.* **70**, 125-169 (1997).
- 102 H. C. Hamaker, *The London-Van der Waals Attraction between Spherical Particles*, *Physica* **4**, 1058-1072 (1937).
- 103 R. R. Netz and J.-F. Joanny, *Adsorption of Semiflexible Polyelectrolytes on Charged Planar Surfaces: Charge Compensation, Charge Reversal, and Multilayer Formation*, *Macromolecules* **32**, 9013-9025 (1999).
- 104 X. Châtellier, T. J. Senden, J. F. Joanny and J. M. di Meglio, *Detachment of a single polyelectrolyte chain adsorbed on a charged surface*, *Europhys. Lett.* **41**, 303-308 (1998).
- 105 H. Römer and T. Filk, *Statistische Mechanik*, VCH, Weinheim (1994).
- 106 F. Merzel and J. C. Smith, *Is the first hydration shell of lysozyme of higher density than bulk water?*, *PNAS* **99**, 5378-5383 (2002).

- 107 D. Svergun, S. Richard, M. H. Koch, Z. Sayers, S. Kuprin and G. Zaccai, *Protein hydration in solution: Experimental observation by x-ray and neutron scattering*, Proc. Natl. Acad. Sci USA **95**, 2267-2272 (1998).
- 108 S. K. Pal, J. Peon and A. H. Zewail, *Biological water at the protein surface: Dynamical solvation probed directly with femtosecond resolution*, PNAS **99**, 1763-1768 (2002).
- 109 O. Teschke, G. Ceotto and E. F. de Souza, *Interfacial water dielectric-permittivity-profile measurements using atomic force microscopy*, Physical Review E **64**, 011605 (2001).
- 110 D. Bulone, V. Martorana, P. L. Biagio and M. B. Palma-Vittorelli, *Effects of electric charges on hydrophobic forces. II.*, Physical Review E **62**, 6799-6809 (2000).
- 111 A. Chandra, *Effects of Ion Atmosphere on Hydrogen-Bond Dynamics in Aqueous Electrolyte Solutions*, Physical Review Letters **85**, 768-771 (2000).
- 112 A. Bakk, J. S. Hoye and A. Hansen, *Apolar and Polar Solvation Thermodynamics Related to the Protein Unfolding Process*, Biophysical Journal **82**, 713-719 (2002).
- 113 D. W. Urry, T. Hugel, M. Seitz, H. E. Gaub, L. Sheiba, J. Dea, J. Xu and T. Parker, *Elastin: a representative ideal protein elastomer*, Phil. Trans. R. Soc. Lond. B Biol. Sci. **357**, 169-84. (2002).
- 114 G. Bokias and Y. Mylonas, *Association of Positively Charged Copolymers Based on N-Isopropylacrylamide with Hydrophobically Modified Poly(sodium acrylate) in Water*, Macromolecules **34**, 885-889 (2000).
- 115 R. Ballardini, V. Balzani, A. Credi, M. T. Gandolfi and M. Venturi, *Artificial Molecular-Level Machines: Which Energy To Make them Work?*, Acc. Chem. Res. **34**, 445-455 (2001).
- 116 C. H. Brown, *Photochromism*, Wiley-Interscience, New York (1971).
- 117 M. Irie, *Photoreactive Materials for Ultrahigh-Density Optical Memory*, Elsevier, Amsterdam (1994).
- 118 B. L. Feringa, W. F. Jager and B. de Lange, *Organic materials for reversible optical data storage*, Tetrahedron **49**, 8267-8310 (1993).
- 119 N. Tamai and H. Miyasaka, *Ultrafast Dynamics of Photochromic Systems*, Chem. Rev. **100**, 1875 (2000).
- 120 Bergmann and Schaefer, *Lehrbuch der Experimentalphysik - Optik*, Walter de Gruyter, Berlin - New York (1993).
- 121 H. Haken and H. C. Wolf, *Molekülphysik und Quantenchemie*, Springer-Verlag, Berlin Heidelberg (1997).
- 122 C. Renner, R. Behrendt, S. Spürlein, J. Wachtveitl and L. Moroder, *Photomodulation of Conformational States. I. Mono- and bicyclic Peptides with (4-Amino)phenylazobenzoic Acid as Backbone Constituent*, Biopolymers **54**, 489-500 (2000).
- 123 S. Spörlein, *Femtosekunden-Spektroskopie schnellster Strukturänderungen in Peptid-Chromophor-Komplexen*, Dissertation, Ludwig-Maximilians-Universität München (2001).

- 124 W. Demtröder, *Experimentalphysik - Atome, Moleküle und Festkörper*, Springer-Verlag, Berlin, Heidelberg, New York (1996).
- 125 G. S. Hartley, *The Cis-form of Azobenzene*, *Nature* **140**, 281 (1937).
- 126 S. Shinkai and O. Manabe, *Photocontrol of ion extraction and ion transport by photofunctional crown ethers*, *Topics Curr. Chem.* **121**, 67-104 (1984).
- 127 I. Willner, *Photoswitchable biomaterials: en route to optobioelectronic systems*, *Acc. Chem. Res.* **30**, 347-356 (1997).
- 128 L. Ulysse, J. Cubillos and J. Chmielewski, *Photoregulation of cyclic peptide conformation*, *J. Am. Chem. Soc.* **117**, 8466-8467 (1995).
- 129 H. Asanuma, T. Ito, T. Yoshida, X. Liang and M. Komiyama, *Photoregulation of the Formation and Dissociation of a DNA Duplex by Using the cis-trans Isomerization of Azobenzene*, *Angew. Chem. Int. Ed.* **38**, 2393-2395 (1999).
- 130 M. Irie, *Photoresponsive polymers*, *Adv. Polym. Sci* **94**, 27-67 (1990).
- 131 F. Vögtle, *Supramolecular Chemistry*, Wiley, New York (1991).
- 132 F. Würthner and J. Rebek Jr., *Photoresponsive synthetic receptors: binding properties and photocontrol of catalytic activity*, *J. Chem. Soc. Perkin Trans. 2* , 1727-1734 (1995).
- 133 A. Archut, G. C. Azzellini, V. Balzani, L. De Cola and F. Vögtle, *Toward photoswitchable dendritic hosts. Interaction between azobenzene-functionalized dendrimers and eosin*, *J. Am. Chem. Soc.* **120**, 12187-12191 (1998).
- 134 H. S. Blair, H. I. Pogue and E. Riordan, *Photoresponsive effects in azo polymers*, *Polymer* **21**, 1195 (1980).
- 135 M. Irie, Y. Hirano, S. Hashimoto and K. Hayashi, *Photoresponsive polymers. 2. Reversible solution viscosity change of polyamides having azobenzene residues in the main chain*, *Macromolecules* **14**, 262 (1981).
- 136 L. A. Strzegowski, M. B. Martinez, D. C. Gowda, D. W. Urry and D. A. Tirrell, *Photomodulation Of the Inverse Temperature Transition Of a Modified Elastin Poly(Pentapeptide)*, *J. Am. Chem. Soc.* **116**, 813-814 (1994).
- 137 F. Lagungé Labarthe, J. L. Bruneel, T. Buffeteau, C. Sourisseau, M. R. Huber, S. J. Zilker and T. Bieringer, *Photoinduced orientations of azobenzene chromophores in two distinct holographic diffraction gratings as studied by polarized Raman confocal microspectrometry*, *PhysChemChemPhys* **2**, 5154-5167 (2000).
- 138 B. M. Schulz, M. R. Huber, T. Bieringer, G. Krausch and S. J. Zilker, *Length-scale dependence of surface relief gratings in azobenzene side-chain polymers*, *Synth. Metals* **124**, 155-157 (2001).
- 139 H. Finkelmann, E. Nishikawa, G. G. Pereira and M. Warner, *A new opto-mechanical effect in solids*, *Phys. Rev. Lett.* **87**, 015501-015504 (2001).
- 140 C. Renner, J. Cramer, R. Behrendt and L. Moroder, *Photomodulation of Conformational States. II. Mono- and bicyclic Peptides with (4-Amino)phenylazobenzoic Acid as Backbone Constituent*, *Biopolymers* **54**, 501-514 (2000).

- 141 R. Behrendt, C. Renner, M. Schenk, F. Wang, J. Wachtveitl, D. Oesterhelt and L. Moroder, *Photomodulation of the Conformation of Cyclic Peptides with Azobenzene Moieties in the Peptide Backbone*, *Angew. Chem. Intl. Ed.* **38**, 2771-2773 (1999).
- 142 T. Nägele, R. Hoche, W. Zinth and J. Wachtveitl, *Femtosecond Photoisomerization of cis-azobenzene*, *Chem. Phys. Lett.* **272**, 489 (1997).
- 143 S. Spörlein, H. Carstens, H. Satzger, C. Renner, R. Behrendt, L. Moroder, P. Tavan, W. Zinth and J. Wachtveitl, *Ultrafast spectroscopy reveals subnanosecond peptide conformational dynamics and validates molecular dynamics simulation*, *Proc Natl Acad Sci U S A* **99**, 7998-8002. (2002).
- 144 S. Monti, G. Orlandi and P. Palmiere, *Features of the Photochemically Active State Surfaces of Azobenzene*, *Chemical Physics* **71**, 87-99 (1982).
- 145 H. Rau, *Further evidence for rotation in the  $\pi, \pi^*$  and the inversion in the  $n, \pi^*$  photoisomerization of azobenzenes*, *Journal of Photochemistry* **26**, 221-225 (1984).
- 146 D. K. Chang and D. W. Urry, *Polypentapeptide Of Elastin - Damping Of Internal Chain Dynamics On Extension*, *J. Comput. Chem.* **10**, 850-855 (1989).
- 147 Z. R. Wasserman and F. R. Salemme, *A molecular dynamics investigation of the elastomeric restoring force in elastin*, *Biopolymers* **29**, 1613-1631 (1990).
- 148 L. Cannavacciuolo, C. Sommer, J. S. Pedersen and P. Schurtenberger, *Size, flexibility and scattering functions of semiflexible polyelectrolytes with excluded volume effects: Monte Carlo simulations and neutron scattering experiments.*, *Physical Review E* **62**, 5409 (2000).
- 149 P. E. Marszalek, H. Lu, H. B. Li, M. Carrion-Vazquez, A. F. Oberhauser, K. Schulten and J. M. Fernandez, *Mechanical unfolding intermediates in titin modules*, *Nature* **402**, 100-103 (1999).
- 150 G. Vigil, Z. Xu, S. Steinberg and J. Israelachvili, *Interactions of Silica Surfaces*, *J. Colloid Interf. Sci.* **165**, 367-385 (1994).
- 151 M. Radmacher, *Spontane Bildung von planaren Bilayern auf Festkörperoberflächen aus der Vesikelfase*, Diplom, LMU (1990).
- 152 E. Poptoshev, M. W. Rutland and P. M. Claesson, *Surface Forces in Aqueous Polyvinylamine Solutions*, *Langmuir* **15**, 7789-7794 (1999).
- 153 P. Hinterdorfer, W. Baumgartner, H. J. Gruber, K. Schilcher and H. Schindler, *Detection and localization of individual antibody-antigen recognition events by atomic force microscopy*, *Proc. Natl. Acad. Sci. USA* **93**, 3477-3481 (1996).
- 154 T. Weis-Fogh and S. O. Andersen, *New molecular model for the long-range elasticity of elastin*, *Nature* **227**, 718-721 (1970).
- 155 C. A. J. Hoeve and P. J. Flory, *Elastic properties of elastin*, *Biopolymers* **13**, 677-686 (1974).
- 156 C.-H. Luan, J. Jaggard, R. D. Harris and D. W. Urry, *On the source of entropic elastomeric force in polypeptides and proteins: backbone configurational vs side chain solvational entropy.*, *Int. J. Quant. Chem. Quant. Biol. Symp.* **16**, 235-244 (1989).

- 157 B. L. Smith, T. E. Schaffer, M. Viani, J. B. Thompson, N. A. Frederick, J. Kindt, A. Belcher, G. D. Stucky, D. E. Morse and P. K. Hansma, *Molecular mechanistic origin of the toughness of natural adhesives, fibres and composites*, *Nature* **399**, 761-763 (1999).
- 158 J. N. Onuchic, Z. Luthey-Schulten and G. Wolynes, *Theory of Protein Folding: The Energy Landscape Perspective*, *Annu. Rev. Phys. Chem.* **48**, 545-600 (1997).
- 159 D. K. Klimov and D. Thirumalai, *Factors Governing the Foldability of Proteins*, Wiley-Liss, Inc., New York (1996).
- 160 M. C. Williams and I. Rouzina, *Force spectroscopy of single DNA and RNA molecules*, *Current Opinion in Structural Biology* **12**, 330-336 (2002).
- 161 F. Oesterhelt, M. Rief and H. E. Gaub, *Single molecule force spectroscopy by AFM indicates helical structure of Poly(ethylene-glycol) in water*, *New J. Phys.* **1**, 6.1-6.11 (1999).
- 162 M. Manno, A. Emanuele, V. Martorana, P. L. San Biagio, M. B. Palma-Vittorelli, D. T. McPherson, J. Xu, T. M. Parker and D. W. Urry, *Interaction of Processes on Different Length Scales in a Bioelastomer Capable of Performing Energy Conversion*, *Biopolymers* **59**, 51-64 (2001).
- 163 M. Blank, L. M. Soo, N. H. Wassermann and B. F. Erlanger, *Photoregulated Ion Binding*, *Science* **214**, 70-72 (1981).
- 164 A. Schemmel, *Kraftspektroskopie an einzelnen Molekülen zur Untersuchung von Proteinfaltung*, Promotion, LMU (1998).
- 165 A. Noy, D. V. Vezenov and C. M. Lieber, *Chemical force microscopy*, *Annual Rev. Mater. Sci.* **27**, 381-421 (1997).
- 166 H. Schönherr, Z. Hruska and G. J. Vansco, *Toward high resolution mapping of functional group distribution at surface-treated polymers by AFM using modified tips*, *Macromolecules* **33**, 4532-4537 (2000).
- 167 H. J. Butt and M. Jaschke, *Calculation of thermal noise in atomic force microscopy*, *Nanotechnology* **6**, 1-7 (1995).
- 168 J. E. Sader, I. Larson, P. Mulvaney and L. R. White, *Method for the calibration of atomic force microscope cantilevers*, *Rev. Sci. Instrum.* **66**, 3789-3797 (1995).
- 169 R. Levy and M. Maaloum, *Measuring the spring constant of atomic force microscope cantilevers: thermal fluctuations and other methods*, *Nanotechnology* **13**, 33-37 (2002).
- 170 D. Walters, J. Cleveland, N. H. Thomson, P. K. Hansma, M. A. Wendman, G. Gurley and V. Elings, *Short Cantilevers for Atomic Force Microscopy*, *The Review of Scientific Instruments* **67**, 3583 (1996).
- 171 R. Proksch and J. Cleveland, *Spring Constant Note*, <http://www.asylumresearch.com/springconstant.asp> (2002).
- 172 J. L. Hutter and J. Bechhoefer, *Calibration Of Atomic-Force Microscope Tips*, *Review of Scientific Instruments* **64**, 186 (1993).

### **Parts of this Work are Published in**

- 1) T. Hugel, M. Grosholz, H. Clausen-Schaumann, A. Pfau, H. Gaub, M. Seitz, *Macromolecules* **34**, 1039 (2001)  
*"Elasticity of Single Polyelectrolyte Chains and their desorption from solid supports studied by AFM based Single Molecule Force Spectroscopy"*
- 2) T. Hugel, M. Seitz, *Macromol. Rapid Commun.* **22**, 1 (2001)  
*"The Study of Molecular Interactions by AFM Force Spectroscopy"*
- 3) D. W. Urry, T. Hugel, M. Seitz, H. E. Gaub, L. Sheiba, J. Dea, J. Xu and T. Parker, *Phil. Trans. R. Soc. Lond. B* **357**, 1418: 169-184 Feb 28 (2002)  
*"Elastin: a Representative Ideal Protein Elastomer"*
- 4) M. Seitz, T. Hugel, N. B. Holland, H.E. Gaub,  
*Nanotechnology toward the Organic Photonics*,  
Ed.: H. Sasabe, GOOTech Ltd. Chitose, Japan (2002)  
*"Single Molecule Force Spectroscopy by AFM-Related Techniques"*
- 5) T. Hugel, N. B. Holland, A. Cattani, L. Moroder, M. Seitz, H. E. Gaub,  
*Science* **296**, 5570, 1103 (2002)  
*"Single-Molecule Optomechanical Cycle"*
- 6) N.B. Holland, T. Hugel, G. Neuert, D. Oesterhelt, L. Moroder, M. Seitz,  
H.E. Gaub, *Macromolecules*, submitted  
*"Single Molecule Force Spectroscopy of Azobenzene Polymers: Switching Elasticity of Single Photochromic Macromolecules"*
- 7) M. Seitz, T. Hugel, H. E. Gaub, *Spektrum der Wissenschaft* **10**, 14 (2002)  
*"Ein lichtgetriebener Molekülmotor"*

## Thanks

Finally, I say thank you very much to everyone who contributed to the success of this thesis, especially:

- to Dr. Nolan B. Holland who was always a great comrade: Especially with all the azopeptide experiments, Igor-programming and improvement of the English in this PhD-thesis, but also in hiking and belief,
- to the whole Gaub group which provided a great atmosphere and support, especially:
  - Angelika Kardinal for the excellent managing of the chemistry lab,
  - Gregor Neuert for the very good teamwork,
  - Ingo Schwaiger for great discussions about science, philosophy and life,
  - Martin Benoit for the help with every technical or electronics problem,
  - Rupert Krautbauer for valuable tips and discussions concerning experiments and the PhD-thesis, but also politics, sports and beer,
  - Anabel, Anki, Bernhard, Christian, Clara, Claudia, Ferdi, Johnny, Larissa, Max, Michael and the 'Alumni' Albert, Hauke, Janosch, Hilde, Maria, Michael, Sina, Tobias, Wenke for their help in all the little daily things and the great working atmosphere,
- to my Diploma student Willi Jöstl for uncountable measurements and their evaluation, good discussions and all the care for our MFP,
- to Dr. Carsten Sönnichsen and the whole Feldmann group for their help with everything concerning optical instrumentation and the great soccer games,
- to Alexander Hoch and Jürgen Aust from the mechanical workshop for building all the little mechanical parts to improve the AFM and optics setups,
- to Josef Wieser and Christian Holopirek from the electronics workshop for building the electronics to improve the AFM and optics setup,
- to Dr. Jason Cleveland and Asylum Research for the excellent support and their great hospitality,
- to Dr. Andreas Pfau for providing the polyvinylamine samples,
- to Dr. Anna Cattani from the group of Prof. Luis Moroder for providing the azopeptide samples,
- to Prof. Dr. Wolfgang Zinth, Dr. Helmut Grubmüller and Prof. Dr. Evan Evans for helpful discussion,
- to Prof. Dr. Dan Urry for teaching the secrets of hydrophobicity and the inverse temperature transition and for providing the polypeptide samples,
- to Prof. Dr. Roland Netz for many helpful discussions and fit formulas that can be easily applied by experimental physicists,
- to Prof. Dr. Matthias Rief for the support on any AFM problems, helpful discussions about physics in general and for always asking the right questions,
- to **Dr. Markus Seitz** for the excellent support and great ideas not only concerning chemistry topics,
- to **Prof. Dr. Hermann Gaub** for the great opportunity to research at his chair for applied physics, for helpful discussions with many new ideas, for the large freedom and 'Red Beauty',
- to Daniela for the title page and the great comprehension and patience for and with me ...

---

## Lebenslauf

Name: Thorsten Hugel  
Geboren: 1. Mai 1973 in Konstanz  
Nationalität: deutsch

### Schule:

1979-1983 Grundschule Wollmatingen  
1983-1992 Gymnasium der Geschwister-Scholl-Schule Konstanz  
Mai 1992 Abitur

### Zivildienst:

1992-1993 Zivildienst bei den Krankenanstalten Konstanz

### Studium:

1993-1999 Physikstudium an der Albert-Ludwigs-Universität Freiburg  
1995-1996 Physikstudium an der *University of Bristol* (GB)  
Okt. 1999 Diplom Physik: "*Lamellenbildung in teilkristallinen Polymeren*"  
(Auszeichnung für das beste Diplom 1999)  
2000-2003 Promotion an der LMU München bei Prof. Gaub (Angewandte Physik)  
(<http://www.biophysik.physik.uni-muenchen.de/staff/hugel.html>)